THE UNIVERSITY OF ALBERTA

Mass Spectrometric Investigation of Gas Phase Hydration Equilibria Involving

(a) Hydration of the Halide Negative Ions

(b) Hydration of the Hydroxide, Nitrogen Dioxide and Oxygen Negative Ions

(c) Hydration of the Proton

by

Mohammed Reza Arshadi

A THESIS

SUBMITTED TO THE FACULTY OF GRADUATE STUDIES

IN PARTIAL FULFILMENT OF THE REQUIREMENTS FOR THE DEGREE

OF DOCTOR OF PHILOSOPHY

Department of Chemistry

Edmonton, Alberta

Fall, 1969

UNIVERSITY OF ALBERTA

FACULTY OF GRADUATE STUDIES

The undersigned certify that they have read, and recommend to the Faculty of Graduate Studies for acceptance, a thesis entitled MASS SPECTROMETRIC INVESTIGATION OF THE GAS PHASE HYDRATION EQUILIBRIA (a) Hydration of the Halide Negative Ions, (b) Hydration of the Hydroxide, Nitrogen Dioxide and Oxygen Negative Ions, (c) Hydration of the Proton submitted by Mohammed Reza Arshadi in partial fulfilment of the requirements for the degree of Doctor of Philosophy.

P. Kebarle
.....
Supervisor

.....

.....

.....

.....

.....
External Examiner

Date August 26, 1969.

ABSTRACT

The gas phase hydration of the halide negative ions was studied by means of a specially designed mass spectrometer which is capable of operating at an ion source pressure as high as 10 torr. By the determination of the equilibrium constants for the general reaction (1)

(1) $$X^-(H_2O)_{n-1} + H_2O \rightleftharpoons X^-(H_2O)_n$$

at various temperatures the thermodynamic values of $\Delta H^\circ_{n-1,n}$, $\Delta G^\circ_{n-1,n}$ and $\Delta S^\circ_{n-1,n}$ were determined. The values of n, the number of water molecules around the negative ion, ranged from 1 to 5 for F^-; 1 to 4 for Cl^- and Br^-; and 1 to 3 for I^-. In addition to the halide negative ions, the gas phase hydration of O_2^-, OD^- and NO_2^- was also studied. The $\Delta H^\circ_{n-1,n}$, $\Delta G^\circ_{n-1,n}$, $\Delta S^\circ_{n-1,n}$ were determined for OD^- with n=1 to n=5 and for O_2^- with n=1 to n=3. However, the study of the $NO_2^-(H_2O)_n$ was carried out at only one temperature (292°K), therefore, only $\Delta G^\circ_{n-1,n_{292}}$ with n from 2 to 4 could be calculated.

A theoretical calculation of the potential energies of cluster $X^-(H_2O)_n$ is presented. This calculation was based on the various electrostatic energies involved between the central ion and the ligand molecules as well as those among the ligand molecules. A qualitative agreement was observed between the potential energies $\Delta E_{n-1,n}$

calculated and $\Delta H^{\circ}_{n-1,n}$ obtained experimentally. The entropy values, $\Delta S_{0,1}$ for reaction (1) were calculated theoretically and are compared with the experimental values.

From the results of this work and the study of the gas phase hydration energies carried out by other workers in this laboratory, a comparison is made between the hydration of the positive and negative ions. Our studies indicate that the initial hydration steps are more favorable for positive ions. However, as more water molecules are added to the clusters, negative ion hydration becomes more favorable. The trend in our data supports the single ion hydration energies obtained from the Randles free energies of hydration.

ACKNOWLEDGEMENTS

Sincere appreciation and gratitude is due Dr. P. Kebarle for his kind guidance and advice. The co-operation of Dr. J. Scarborough who worked jointly with the author in the study of the gas phase hydration of proton is also acknowledged.

I wish to thank Dr. R. Yamdagni for programming the theoretical calculations, Mr. William Paisley for his technical assistance during the study of I^- hydration and other members of the mass spectrometry group for their valuable suggestions during the course of this study.

The encouragement and understanding of my wife, Mehri, is sincerely appreciated. Her care in typing the manuscript was invaluable.

I am grateful for the financial assistance rendered by the University of Alberta during the academic year and support by the Canadian National Research Council during the summer months.

TABLE OF CONTENTS

Page

Page

LIST OF FIGURES

LIST OF TABLES

INTRODUCTION

1.1 Scope of Present Study

The present work is mostly concerned with the study of the attachment reactions between the halide negative ions and water molecules in the vapour phase. This investigation was carried out in the ion source of a specially designed mass spectrometer. The temperature of the ion source could be varied from room temperature (25°C) to 500°C. The equilibrium constants for the attachment reactions of the type:

$$
\begin{aligned}
& X^-_g + H_2O_{(g)} = X^-(H_2O)_{(g)} \\
& X^-(H_2O)_g + H_2O_{(g)} = X^-(H_2O)_{2(g)} \\
& \vdots \\
& X^-(H_2O)_{n-1} + H_2O_g = X^-(H_2O)_n
\end{aligned}
\qquad (1\text{-}1)
$$

were determined, at different ion source temperatures, by the following relation:

$$
K_{n-1,n} = \frac{P_{X^-(H_2O)_n}}{P_{X^-(H_2O)_{n-1}}} \cdot \frac{1}{P_{H_2O}} \qquad (1\text{-}2)
$$

where $P_{X^-(H_2O)_{n-1}}$ is the pressure of the reacting ion and $P_{X^-(H_2O)_n}$ that of the product. P_{H_2O} is the partial pressure of water in the ion source. The pressure ratio of the ions was taken as equal to the ratio of the intensities

of the respective ions, recorded by the mass spectrometer. The standard free energy of the reactions (1-1) can be calculated by the following equation:

$$\Delta G^\circ_{n-1,n} = -RT \log_e K_{n-1,n}$$

where R is the universal gas constant, T is the absolute temperature and $K_{n-1,n}$ is equilibrium constant. From the study of the equilibrium constant at various temperatures, $\Delta H_{n-1,n}$ could be calculated and $\Delta S^\circ_{n-1,n}$ was determined from

$$\Delta G^\circ_{n-1,n} = \Delta H^\circ_{n-1,n} - T\Delta S^\circ_{n-1,n}$$

In addition to halide negatives the O_2^-, OD^- and NO_2^- also were studied and their thermodynamic properties $\Delta G^\circ_{n-1,n}$, $\Delta H^\circ_{n-1,n}$ and $\Delta S^\circ_{n-1,n}$ were determined similarly.

1.2 Production of Negative Ions

Negative ions are produced in the ion source of the mass spectrometer ordinarily by two distinct processes: (A) electron capture and (B) ion pair production.

A. Electron Capture Process

When a beam of electrons or some other ionizing media such as alpha particles or protons are passed through a gaseous medium, collisions between the gas molecules and the electron beams will take place. These collisions can result in the ionization of some of the gaseous molecules. This process can be represented as

$$e + RX = RX^+ + 2e$$

The secondary electrons produced by the above process can undergo further collisions and subsequently ionize more molecules. Finally when these secondary electrons have lost most of their energy and have become thermalized, some of them may be captured by the gas molecules. The molecular negative ion which is formed can be stablized either by radiating its excess energy or by losing it through collisions with other molecules (third body collision)

$$\begin{aligned} RX + e &= [RX^-]^* \\ [RX^-]^* + M &= RX^- + M \end{aligned} \qquad (1\text{-}3)$$

The appearance potential (the minimum electronic energy for production of the ion) of the ion RX^- is

$$AP(RX^-) = EE + EA(RX)$$

where EE is the excess energy of RX^- and EA(RX) is the electron affinity of RX. As it is observed from equation (1-3), the rate of formation of the negative ion RX^- depends on the availability of a third body, M, thus, initially it will be proportional to the pressure of the gas. However, as the gas pressure is increased a value would be reached above which the rate will become pressure independent. It can be shown (1) that this critical value is the pressure at which the average time, t_s, taken by the excited ion $[RX^-]^*$ to transfer its excess energy to another

molecule, becomes equal to the average life time, t_d, of the ion against dissociation.

If the negative ion RX^- could not stablize itself either through collisions with other molecules or emission of radiation, it would return to its original state RX, by releasing the captured electron, or dissociate to a negative ion X^- and a free radical R

(1-4) $$[RX^-] = R + X^-$$

The appearance potential of X^- by process (1-4) is given by

(1-5) $$AP(X^-) = D(R-X) + EA(A) + EE$$

D(R-X) is dissociation energy of RX, EA(A) electron affinity of X and EE is the excess energy. The bond dissociation energy D(R-X) for most molecules is about 3 to 5 eV and the electron affinities for most atoms are between 1.5 to 3.5 eV, thus $AP(X^-)$ is in the range of 0.5 to 4 eV.

B. Pair Production

Negative ions can also be produced by an ion pair production such as

(1-6) $$RX + e = R^+ + X^- + e$$

In this process the electron serves simply as a source of energy, therefore, other ionizing media such as alpha particles or protons can also initiate this process.

In the ion pair process, the molecule RX, through absorption of energy from the ionizing media, is raised to an excited state [RX]* and then dissociates into a positive and a negative ion

$$[RX]^* = R^+ + X^-$$

The ions R^+ and X^- can be either in their normal ground state or in an excited state. This process differs from the dissociative attachment in the products of the dissociation as well as the effect of the energy of the ionizing electron. The dissociative capture of an electron can only take place if the electron energy is within a narrow range, usually from 0.5 to 5 eV (1). Ion pair production on the other hand is not restricted to a small energy range, as long as the ionizing media has an energy equal or greater than the appearance potential of X^-, the process (1-6) can take place. The appearance potential of X^-, $AP(X^-)$ for the ion pair production is given as

$$(1\text{-}7) \qquad AP(X^-) = D(R\text{-}X) + I(R) + EA(A) + EE$$

where I(R) is the ionization potential of R and other terms have been defined previously. Again a rough estimate of appearance potential $AP(X^-)$ can be made by applying the data given in dissociative attachment process (1-5) and noticing that the first ionization potentials of most atoms lie between 6 and 15 eV. Thus, equation (1-7) would give

a value of 6 to 13 eV for $AP(X^-)$.

1.3 A Survey of the Previous Work

The knowledge of the existence of the ions, composed of clusters or group of molecules, in the gas phase dates back to the beginning of this century. Rutherford and Thomson (2) discovered that the mobilities of the ions were lower than the values predicted by the kinetic theory. They attributed this deviation to the formation of the ion clusters. Thus the ion cluster theory was born. According to this theory the charge on the ion would attract the neutral molecules so strongly that a bond is formed between the central ion and the surrounding molecules. As the result of this bonding, there will be an increase in the mass and the size of the ions, which will cause a decrease of the ion mobility. The condition for the stability of these clusters was set as follows (2): Since a cluster is subjected to repeated collisions with the gas molecules, it could be stable only if its potential energy were greater than thermal energy. The potential energy of the central ion - ligands system is the result of the polarization interaction between an ion and a neutral molecules. Mathematically this is expressed (3) by:

$$\frac{(D-1)e^2}{12\pi Pr^4} > 1$$

here D is the diffusion constant of the gas, r is the

distance of the closest approach of the ion and neutral molecule, P is pressure of the gas and e in the electronic charge.

A second theory, to explain the discrepancy between the theoretical and the experimental values of ion mobility, was put forward by Sutherland and Wellisch (2) independently. This theory which later on became known as "small ion theory" assumes that the increased size of the clustered ions is not the major factor in retarding the ionic motion through the gas, but the motion is retarded by momentum transfer as the result of the electrical forces between the ions and neutral molecules. Although it is the general belief today that the polarization scattering is mostly responsible for the lowering of the mobility (4), ions do form clusters when the conditions are right. Munson and Hoselitz, for instance, have obtained evidence of the attachment of inert gas atoms to lithium ion. They have shown (5) that, the clusters $Li^+(Xe)_n$ and $Li^+(Kr)_n$ are formed at room temperature with values of n ranging from one to two. Munson and Tyndall in their experimental measurements of the mobility of alkali ions (6) also observed evidence of formation of $Li^+(H_2O)_n$ with n as large as six at room temperature.

Although, there were some studies of the gas phase cluster formation made in early 1930, by mass spec-

tographic method (7), the vigorous work on this subject did not start until early 1960. In the following a brief review of the recent works is given.

A. Hydration of Proton

The system $H^+(H_2O)_n$ has been studied by a number of investigators. Beckey (8), for instance, observed cluster $H^+(H_2O)_n$ up to n=10. Furthermore he obtained the value of 4 Kcal/mole for ΔH_{1-2} and ΔH_{2-3}. Knewstubb and Sugden (9) in a mass spectrometric study of ionization in flame, observed the ion H_3O^+ as well as NH_4^+ and NO^+. The first two of these also occurred in hydrated form up to 4 molecules of H_2O.

They concluded that these hydrated ions were formed, to a large extent, in the cooler part of the flame system. In a later study, Knewstubb and Tickner (10) observed the $H_3O^+(H_2O)_n$ from n=0 to n=6 in glow discharges. They concluded that their results indicated an exceptional stability of the ion $H_3O^+(H_2O)_3$ and stated that there might be two hydration shells for H_3O^+ the first one containing three molecules of water. This, however, is in contradiction with what was observed in this laboratory. The hydration of proton was studied here in an alpha irradiated ion source by J. Scarborough and this author and in a proton beam mass spectrometer by S. K. Searles and A. Zolla (11). Our results, which will be presented in a

later chapter, did not indicate any discontinuity in exothermicity of the reaction

$$H^+(H_2O)_{n-1} + H_2O \longrightarrow H^+(H_2O)_n$$

which is essential for the theory for the exceptional stability of the ion $H_3O^+(H_2O)_3$. More recently the $H^+(H_2O)_n$ system was also investigated by F. H. Field (12) and his results are in excellent agreement with Kebarle et al (11). A. Good and D. Durden and P. Kebarle (13) have made a kinetic study of hydration of proton. Employing a quadrupole mass spectrometer, they have determined the rate constants for the forward reactions

$$H^+(H_2O)_{n-1} + H_2O \xrightarrow{N_2} H^+(H_2O)_n$$

for n=2 to n=4. With the aid of the equilibrium constant determined previously (11), they were able to calculate also the rate constant of the reverse reactions.

B. O_{2n}^+ Clusters

Yang and Conway (14) (15) have studied mass spectrometrically the system

$$O_{2n}^+ + O_2 \longrightarrow O_{2n+2}^+$$

for n=1 to 4. They found that the higher clusters are too unstable to be the dominant species of the series O_{2n+2}^+ in the lower region of the ionosphere. From a plot of the

equilibrium constant, K_p versus $\frac{1}{T}$ they determined the $\Delta H°$ for the above reactions. Their results are as follows

$$O_2^+ + O_2 \longrightarrow O_4^+ \qquad \Delta H°_{2-4} = -9.7 \text{ Kcal/mole}$$

$$O_4^+ + O_2 \longrightarrow O_6^+ \qquad \Delta H°_{4-6} = -6.7 \text{ Kcal/mole}$$

$$O_6^+ + O_2 \longrightarrow O_8^+ \qquad \Delta H°_{6-8} = -2.8 \text{ Kcal/mole}$$

$$O_8^+ + O_2 \longrightarrow O_{10}^+ \qquad \Delta H°_{8-10} = -2.1 \text{ Kcal/mole}$$

The reaction $O_2^+ + O_2 \longrightarrow O_4^+$ has also been studied by D. Durden, P. Kebarle and A. Good (16) over a temperature range of 295-350°K. These authors' value for ΔH_{2-4} is in good agreement with the result obtained by Yang and Conway.

C. N_4^+ Clusters

The attachment reaction

$$N_2^+ + N_2 \longrightarrow N_4^+$$

has been studied extensively (17, 18, 19). Varney (19) studied the extent of the dissociation of N_4^+, from the change of ion mobility with variation of the field strength to the pressure radio (E/P°), in a drift field tube. He calculated the equilibrium constant for the above reaction. By relating the ion temperature, T_i, to the field strength

$$T_i = T_{gas} + \Theta \, E/P°$$

where Θ is a constant; from a plot of the equilibrium constants versus $1/T_i$ he estimated a value of 0.50 eV for the

dissociation energy, $D(N_2-N_2^+)$.

D. $N_2O_2^+$ System

Equilibrium constant for the reaction

$$O_2^+ + N_2 \longrightarrow N_2O_2^+$$

have been determined mass spectrometrically by Janik and Conway (20). On the basis of the observed value of -5.6 Kcal/mole for $\Delta H_{reac.}$, they have concluded that the equilibrium ratio of the [60]/[32] peak could not be $[(NO)_2^+]/[O_2^+)]$. According to these authors the reaction

$$N_2^+ O_2^+ \longrightarrow (NO_2)_2^+$$

is endothermic by 22 + $D(NO-NO^+)$ Kcal.

E. O_4^- System

Conway and Nesbitt (21) have studied the formation of O_4^- in 6-12 torr of O_2 gas irradiated by 2-ci tritium source with the subsequent mass analysis. From the equilibrium constants for reaction

$$O_2^- + O_2 \longrightarrow O_4^-$$

it was deduced that ΔH°_{298} = -13.55 Kcal/mole. Voshall, Pack and Phelps (22), on the basis of the negative ion mobilities in pure O_2 near 80°K concluded that $D(O_2-O_2^-) = 1.4\pm0.5$ Kcal/mole. This value has been questioned by Conway and Nesbitt on the ground of the uncertainty involved in the calculation and non-equilibrium conditions in the system.

F. Gas Phase Hydration of Alkali Ions

The gas phase hydration of alkali metals have been studied in this laboratory by S. K. Searles, I. Dzidic and P. Kebarle (24,35). The alkali metal ions were produced by thermoionic emission from a platinum filament which was located in a housing attached to the ion source. These ions were hydrated by drifting through the water vapour which was present in the ion source as well as the filament housing. The equilibrium constants for reaction

$$(1\text{-}8) \qquad M^+(H_2O)_{n-1} + H_2O \rightleftharpoons M^+(H_2O)_n$$

were determined at different temperature and thus $\Delta H°$, $\Delta G°$, $\Delta S°$ were obtained by the method explained earlier. These authors have also calculated, semi-empirically, the hydration energies of formation of these clusters by considering the net electrostatical forces involved and obtained relatively good agreement between the calculated and experimentally determined values of the heat of hydration of the reaction (1-8).

G. $NH_4^+(NH_3)_n$

The study of $NH_4^+(NH_3)_n$ system was also undertaken in this laboratory extensively (25,35) and the thermodynamic values for the reactions:

$$NH_4^+(NH_3)_{n-1} + NH_3 \rightleftharpoons NH_4^+(NH_3)_n$$

have been determined.

In addition to the works cited above, there have been a number of other studies of ion-cluster formation,

both here in this laboratory and by other investigators, which cannot be dealt with in more detail here. Among these are the competitive solvation of protons by H_2O and CH_3OH (26), of NH_4^+ by NH_3 and H_2O (25) and flowing afterglow kinetic study of N_n^+ where n=6 to 9 at 82°K (32).

1.4 Purposes of the $X^-(H_2O)_n$ Study

As can be seen from the above discussion, most of the previous work dealt with positive ion clusters. The present study was undertaken to obtain some comparative data for negative ion clusters and thus complement the gas solvation studies which have been taking place in this laboratory for the past few years. The choice of hydration of the halide negative ions was somewhat natural. Water is the most common solvent and halide ions have been the subject of interest in physical chemistry throughout the years. Moreover, the relative ease of production of halide negative ions in the ion source of a mass spectrometer makes them a good steppingstone for further study of other negative ion-solvent interactions.

1.5 Application of Mass Spectrometric Study of Ion Clusters

Before leaving this chapter, it is appropriate to mention in a few words about the importance of ion cluster studies and their applications in the other fields of chemistry and physics. The role of clusters in

ion mobility work has already been mentioned. The importance of ion clusters in radiation chemistry was realized already a few decades ago when Lind (27) put forward his theory about ion molecule complexes. According to Lind's theory, an ion can attract one or two molecules through induced polarization and hold them until neutralized by an oppositely charged ion. The heat of neutralization and the close proximity of ions and attached molecules would promote chemical reaction, polymerization, decomposition etc. Later on this theory was over-shadowed by the free radical theory of Eyring, Hirschfelder and Taylor (28). The E. H. T. Theory postulates that the reaction of single ions and free radicals and molecules is more probable than large ion cluster reaction. The products of the neutralization of ions or ion clusters and also the products of dissociation of excited molecules may be free radicals or atoms which can initiate chain reactions and thus improve the yield (27).

Early in the 1950's, however, Lind's theory gained additional support when it was shown, by mass spectrometric work that long lived complex ions are formed by ions and neutral molecules (29). Recently, in a study of the radiolysis of ethanol vapour, Bansal and Freeman (30) have attributed the decrease of acetaldehyde and hydrogen

yields with increasing dose to the scavenging of the electrons by acetaldehyde with ultimate production of $(CH_3CHO^-)_nC_2H_5OH$. Also the formation of $H^+(C_2H_5OH)_m$ and $NH_4^+(C_2H_5OH)_n$ have been postulated by the same authors.

Formation of ion clusters in the D region of the ionosphere has been confirmed by the investigation of Narcisi and Bailey (31). In experiments carried out by rocketborne quadrupole mass spectrometers, they have observed heavy positive ions with mass numbers greater than 45 amu. Some of these ions have been attributed to hydrate ion clusters. Also they have reported that the cluster $H_3O^+(H_2O)$ appeared to be a dominant positive ion at an altitude of 60 to 80 Km. The "D region simulation" flowing afterglow experiment by Ferguson et al (32) have proved the formation of the hydrated clusters $H_3O^+(H_2O)_n$, in the ionosphere, with n as large as 6. Primary negative ions also may form clusters with neutral molecules in D region. Formation of clusters such as $O_2^-(H_2O)_n$, $NO^-(H_2O)$ and CO_4^- have been postulated (33). The diurnal variation in the electron density of D regions has been attributed to certain negative ion molecule reactions including cluster formation (33). Thus we can conclude that the importance of the process of ion-cluster formation cannot be overemphasized, if a full understanding of the chemical composition of the

ionosphere and the ion molecule reaction involved and the related phenomena is desired.

Another interesting application of cluster ions has been recently considered by Doyle and Caldwell (34). According to these authors, the removal of certain molecular contaminants from manned space cabin atmosphere can be accomplished by injection of some stable ions into the contaminated atmosphere and allowing them to react with the polar contaminants to form stable clusters. These clusters can then be collected at an appropriate electrodes. The only theoretical complication involved is the competition of innocuous polar constituents of the atmosphere, especially water vapour, with the contaminants to form the clusters. Therefore, only certain compounds such as alcohols, amines and acids are collectable by this method. One way which has been suggested (34) is to remove most of the water vapour and then inject the ions. Alternately, since the mixture of the ions, water vapour, and oxygen constitutes an oxidizing atmosphere, an attempt can be made to fragment or oxidize those neutral molecular species that would not be able to compete in clustering reactions to the polar species that could be clustered.

2 EXPERIMENTAL

2.1 General Description

The gas phase solvation study by means of a mass spectrometer involves the production of the solvated species X^-A_n, X^-A_{n+1}, etc. in a field free ion source and the measurement of their relative concentrations. The clusters, X^-A_n, are produced by the interaction of some ionizing media such as an electron beam or alpha particles with suitable compound containing X, in the presence of a polar compound A. The measurement is performed by bleeding a sample of the gas into the main vacuum chamber of the mass spectrometer. There, the ions present in the gas are captured, accelerated by the electric field of the mass spectrometer and then mass analyzed. After mass analysis the ion current is amplified and detected.

Certain modifications have to be made in a conventional mass spectrometer in order to make it applicable for solvation studies. Most of these modifications apply to the ion source of the mass spectrometer. In order to assure the achievement of equilibrium in the ion source, the ion source has to be able to handle pressures of the order of 5 to 10 torr. This condition, in turn, requires that the electron beam, which is used for ionizing the gas, must be generated in the region outside of the ion source. It is also necessary that the attachment reactions be carried

out in a field free region. Therefore, the repeller voltage, which is an essential part of the conventional mass spectrometer, has to be eliminated from the ion source of the mass spectrometer used in the solvation studies. In order that the high pressure of the ion source does not interfere with the performance of the mass spectrometer, a high capacity pumping speed system is required. Differential pumping between the main chamber and the mass analyser tube is also desirable.

A conventional mass spectrometer already present in this laboratory was modified for the purpose of studying the gas phase hydration of the halide negative ions. Since the investigation of the gas phase solvation of proton and a portion of the negative ions study was performed by the alpha source mass spectrometer, this instrument will be discussed in brief first.

2.2 Alpha Source Mass Spectrometer

This instrument has been in operation in this laboratory for several years, and descriptions concerning its design and construction have been given in several publications (11, 25, 26). Therefore, only those features pertinent to the present work will be discussed here.

The ion source of this instrument is shown in figure (2-1). A mixture of the carrier gas and the compounds required was passed through the ion source, where

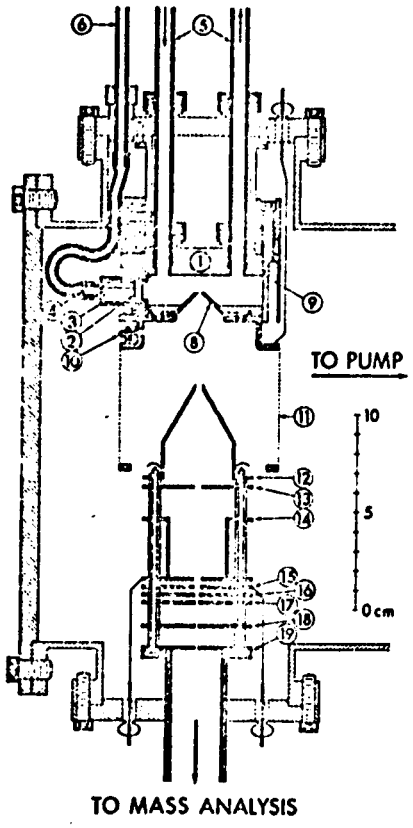

Figure 2-1: Ion Source and Electrode System: (1) Ion Source, (2) Alpha Source carrying polonium Disk, (3) Alpha Source Container with stainless Foil Window, (4) Stainless-Steel Porous Plug, (5) Gas Supply and Flow System, (6) Pressure Equalization, (7) Electrical and Thermal Insulator, (8) Cone Carrying Metal Foil Leak, (9) Heater and Thermocouple Wells, (10) Auxiliary Electron Gun, (11)-(19) Electrodes.

it was irradiated by a 200 m-C. polonium 210 source. This polonium 210 alpha source was contained in a removable compartment. The alpha rays entered the ion source through a three micron thick nickel foil, which separated the ion source from the polonium 210 compartment.

In the primary study of the halide negative ions as well as proton-water attachment reactions, all the runs were made with a continuous flow of the gaseous mixture through the ion source. The flow was used to provide gas mixing, scavenging of impurities out of ion source, and constant water pressure in the ion source. For this purpose the ion source was provided with an inlet and an outlet tubes figure (2-1, item 5). The linear flow through the ion source was approximately 20 cm/sec. This corresponded to a gas residence time in the irradiated volume of about 0.1 second. The ion residence time in the same volume was estimated to be about 1 milli-second (11), thus the gas flow could not affect the ion residence time.

The ion source could be heated by means of heater windings mounted around the ion source. The maximum working temperature of the ion source was restricted to 150°C. This was due to the direct contact of the polonium source with the ionization chamber and the fear of rapid spreading of the polonium which could occur above this temperature. The ionization chamber could also be cooled below room temperature by circulating cold nitrogen gas through the copper tubing

which was silver soldered around the ion source. Thus experiments could be performed at temperatures from -40°C to 150°C. As will be explained later, this temperature range was not wide enough for the complete study of the halide negative ions.

The gas handling plant and flow system of the alpha source mass spectrometer were identical with the electron beam mass spectrometer to be described in detail in later sections.

After being irradiated inside the ion source a part of the ion-gas mixture effused into the electrode chamber, through the ion exit leak. In order to assure that the ion cluster would not undergo any cooling due to the adiabatic expansion past the exit leak, measurements were carried out only at conditions of molecular flow i.e. at conditions where the mean free path of the gas molecules and the ion-clusters was larger than the dimension of the ion exit slit. For the pressure range used in these studies a slit of 10 microns width fulfilled this requirement. This was proven by varying the slit size and observing its effect on the distribution of the detected ion-clusters.

In the electrode chamber the ions were accelerated and mass analyzed by a 90° sector mass spectrometer. The detection of the ion current was accomplished by a Bendix M 306 electron multiplier.

2.3 Electron Beam Mass Spectrometer

The alpha source mass spectrometer had certain drawbacks which made it inadequate for the complete study of the halide negative ions. Thus while temperatures up to 500°C were required for this study, the ion source of this instrument could not be heated above 150°C without endangering the polonium 210 alpha source. Also while the work on the hydration of proton and the halide ion was undertaken by this author with the alpha mass spectrometer, a pulsed electron beam mass spectrometer for high ion pressure studies had been developed by D. A. Durden and P. Kebarle of this laboratory. This pulsed high pressure mass spectrometer has been described elsewhere (67). Since the pulsed electron beam high pressure model seemed to offer a number of advantages also for the present study, it was decided to equip a second mass spectrometer with the pulsed electron beam high pressure source. The main components of this instrument are shown in figure (2-2). They are gas handling plant, ion source, electron gun, mass analysis and detection units and high capacity vacuum system.

2.4 Gas Handling Plant

The gas handling plant is shown in figure (2-3). It consisted mainly of a large glass bulb (4 litre), with the proper valves and connections to let gas, at desirable flow rate, pass through the ion source of the mass spec-

21. Cylinder entrance

22. First cylinder

23. Second cylinder

24. Cylinder exit

25. First deflection half plate

25a. Second deflection half plate

26. Mass analysis slit flange

27. Mass analyzer tube

Figure 2-2

A. Electron Gun

1. Filament
2. Draw out
3. Extractor
4. First focussing and accelerating electrode
5. Second focussing and accelerating electrode
6. Third focussing and accelerating electrode
7. Horizontal deflection half plates
8. Vertical deflection half plates
9. Shielding cylinder

B. Ion Source

10. Copper Jacket
11. Electrostatic Shield
12. Electron entrance slit flange
13. Electron trap flange
14. Ion exit slit cone
15. Gas inlet
16. Kovar seal flange
17. Stainless steel support
18. Ceramic Spacer

C. Ion Accelerating Tower

19. First cone
20. Second cone

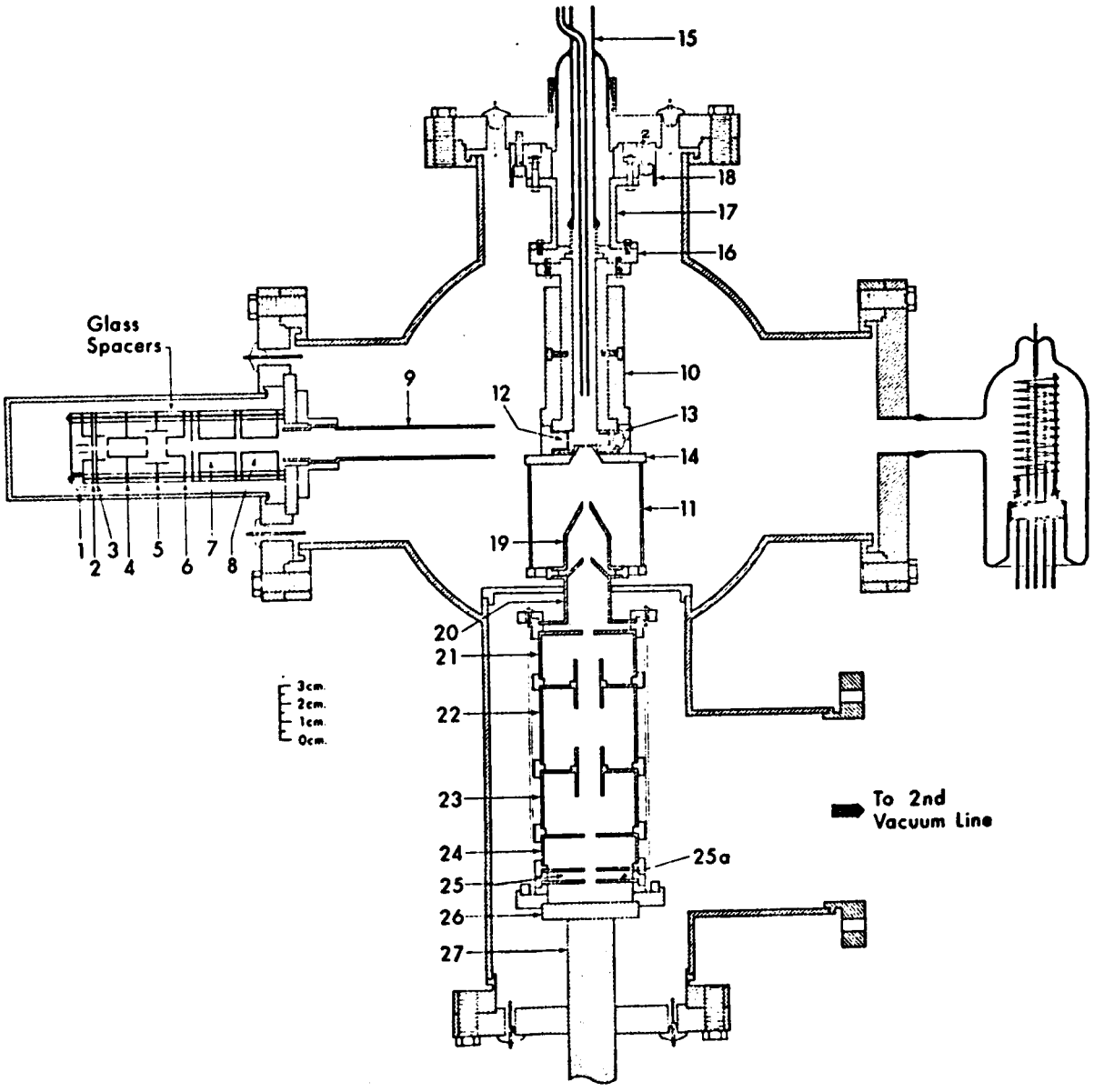

Figure 2-2: Main Components of the Electron Beam Mass Spectrometer: Ion Source, Electron Gun, Ion Accelerating Tower.

trometer. It could be evacuated by two different pumping systems. The rough pumping system was used whenever a large amount of gas was to be removed from the gas handling plant. The clean vacuum line was used for removing a small amount of gas from the ion source and the inlet system. Moreover, the clean vacuum line was also used as the flow outlet during the experiment. The flow of the carrier gas and the compounds to be investigated was conducted from the gas handling plant, through the ion source, and out through the clean vacuum line.

All the valves and the main manifold of the gas handling plant were made from stainless steel. The inside diameter of the main manifold and the glass tubing connecting the various part of the gas handling system and the ion source was about 1.5 cm. The valves were all 1/2 inch in diameter.

The pressure in the gas handling plant and the ion source was measured by an Atlas MCT manometer. This manometer was calibrated by means of a wide U tube mercury manometer and a cathetometer prior to the start of this study. The calibration was checked, during this study, from time to time to assure the accuracy of the pressure measurement. The entire gas handling plant was enclosed in an asbestos board chamber which could be thermostated up to 150°C. The inlet and outlet gas line, connecting the

gas handling plant to the ion source, could also be heated to 150°C by means of heating tape.

2.5 Electron Gun

The electron gun is shown in figure (2-4). The electrons, emitted from the filament [1] were passed through small hole (1/16 inch) at the centre of the draw out electrode [2]; then they were accelerated slightly by the field between the draw out and the extractor electrodes [3]. The major acceleration and focussing occurred by three accelerating and focussing electrodes [4,5,6]. The horizontal and the vertical deflection of the beam was obtained by the two sets of deflection half plates [7,8]. After emerging from the second set of deflection half plates, the beam passed through a shielding cylinder [9] and entered the ion source through the electron entrance slit. The electron gun was designed and constructed to operate for both positive and negative ions study. For this work when negative ions were studied and the ion source was at -2000 volts, the potential at the different electrodes were as follows: the filament was at -4000 volts, the draw out potential was about 10 to 20 volts positive with respect to the filament. The potential of the extractor plate could be varied from -4000 to -3800 volts. The first and the third focussing electrodes were at -2000 volts and the second focussing electrode potential could be varied from -4000 volts to

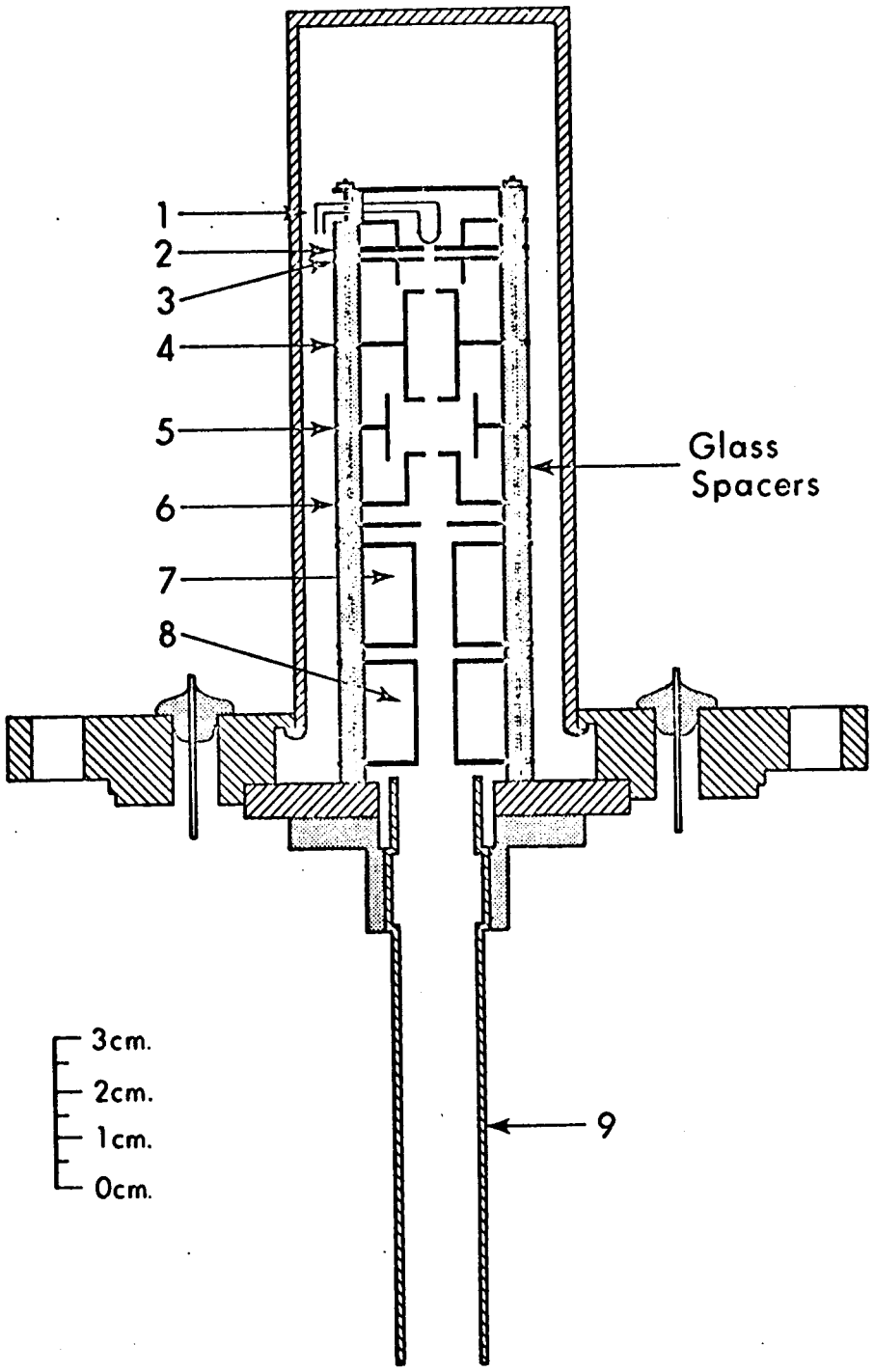

Figure 2-4: Electron Gun Numerical Legends are give on Page Opposite to Figure (2-2).

-3000 volts. The first vertical and the first horizontal half plates as well as the shielding cylinder were at the ion source potential, -2000 volts. The potential of the second vertical and horizontal deflection half plates could be independently varied from -2000 to -1800 volts. Thus, the electrons were generated at -4000 volts, accelerated by a field of 2000 volts, focussed, and entered the ion source with 2000 electron-volts energy.

To assure the proper focussing of the beam, there was a plate located in the front of the ion source entrance slit, coated with a mixture of phosphorus, sodium silicate and sodium chloride. This plate contained a 1/8 inch hole coaxial with the electron entrance slit. Prior to each experiment the electron beam was deflected out of the central hole, properly adjusted and focussed to a spot with a diameter of the order of two millimeters, then deflected back to the central hold of the plate. The total emission current from the filament was 200 micro-amps and the trap current was 1×10^{-8} ampere in an ordinary experiment.

The filament of the electron gun was heated by a direct current power supply. The voltage across the filament was two to three volts, the filament current was from 5.2 to 4.2 amperes depending on the age of the filament. The electron current was automatically controlled by using a saturable transformer filament regulator which controlled

the filament heating current through the total emission from filament. Originally, pure tungsten ribbon was used as the material for the filament. This, however, proved unsatisfactory, since the life time of the filament was very short when oxygen was used as carrier gas. Finally, a thoriated iridium filament was used. This filament proved to be very satisfactory since it was inert to both oxygen and water vapour.

In order to prevent the interference of the mass spectrometer magnetic field with the performance of the electron gun, the electron gun was equipped with a magnetic shield. The shield was made from the "Netic and Co-netic Alloys" obtained from the Magnetic Shield Division of Perfection Mica Company of Bensville, Illinois. These alloys were rolled into cylinders and were mounted on the electron gun housing.

Originally, the electron gun was designed such that the electron beam could be pulsed for ion pulsing experiments. The electron beam pulsing was to be accomplished by applying pulses from a generator to the electron deflection plates [7] or [8]. However, no pulsing experiments were attempted in this work.

2.6 Ion Source

The ion source is shown in figure (2-5). It was machined from non-magnetic stainless steel. It consisted

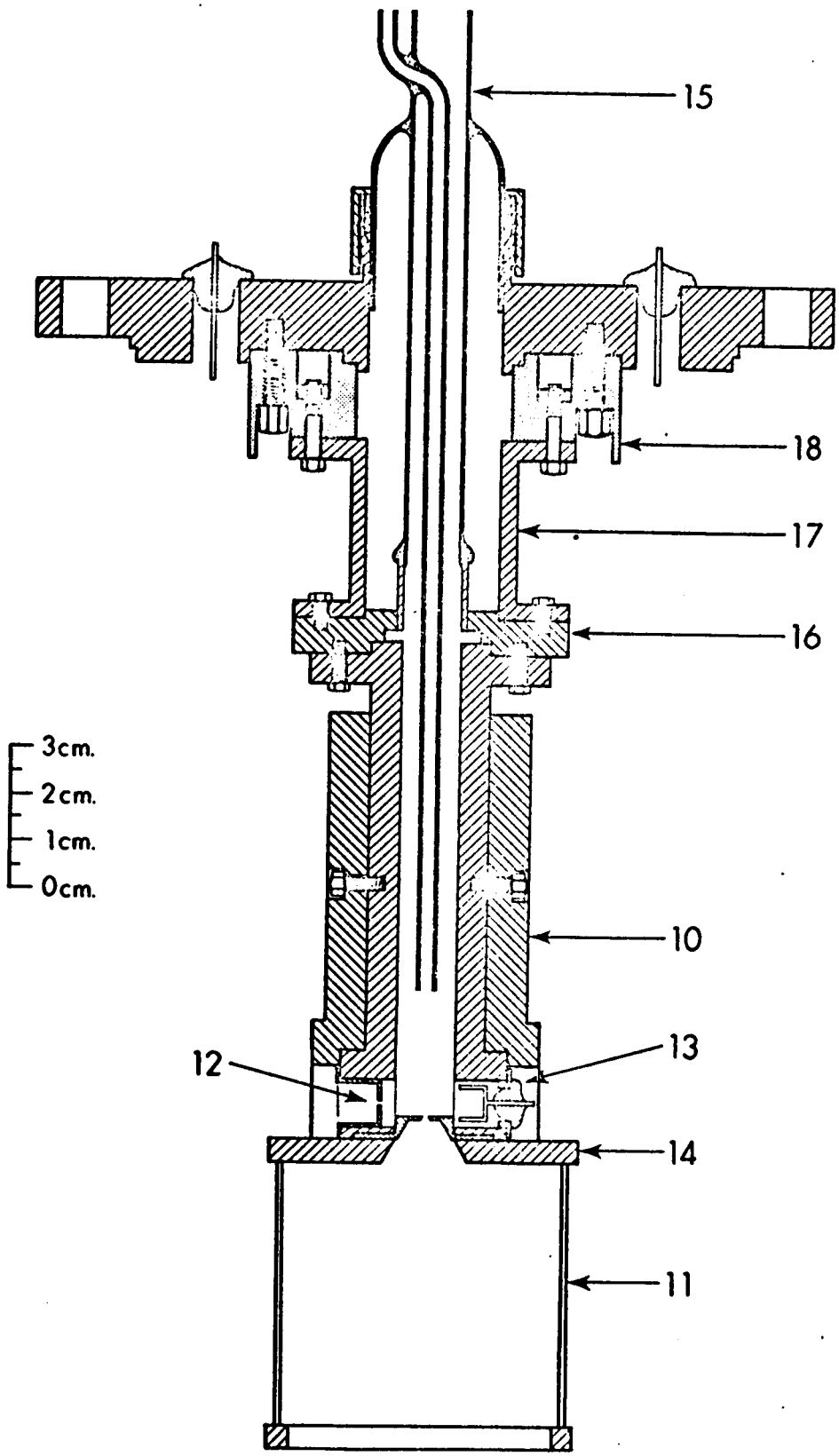

Figure 2-5: Ion Source Numerical Legends are explained in the Page Opposite to Figure (2-2).

of a cylindrical chamber with inside diameter of 1/2 inch. In the lower part of the ion source a channel was bored prependicular to the main axis of the ion source. A small flange carrying the electron entrance slit was located in one side of this channel and the electron trap flange in the other side. The electron entrance slit was welded on a "hat shaped" flange, [12] and this flange was sealed onto the ion source by four 1-72 stainless steel screws and a gold O-ring. The electron trap assembly consisted of a flange [13] which contained a kovar electrical feed through. A Faraday cup electron trap was mounted on this feed through. This cup was made of non-magnetic stainless steel. The electron trap assembly was also sealed to the ion source by four 1-72 screws and a gold O-ring. The ion exit slit was mounted on a cone [14] which in turn was bolted to the bottom of the ion source by four 1-72 stainless steel screws and sealed by a gold O-ring. Both, ion exit slit and the electron entrance slit were made by welding stainless steel razor blade edges to a circular tantalum disc which was 0.030 inch thick and contained a 2 mm centre hole. These tantalum discs were in turn spot welded to the respective cones. Both, ion exit slit and electron entrance slit were 2 mm long and 0.015 mm wide.

The connections between the ion source and the gas inlet system were provided by two concentric tubes [15].

The gas entered the ion source through the outer tubing and left the ion source through the inner tubing. The concentric tubes were sealed to a flange by a kovar seal and this flange [16] was mounted on the top of the ion source and sealed in place by a set of six screws and a gold O-ring.

For the purpose of heating, the ion source was enclosed in a heating jacket [10]. This jacket was machined from copper and it was divided into two half cylinders. Each half was secured to the ion source by means of a screw. The jacket was slotted and an electrical heater was placed in these slots. The heater consisted of 28 gauge nichrome wire inserted into fused silica insulators. There were a total of six fused silica insulators and each one had six bores. Each insulator was fitted into one of the slots on the copper jacket. The heater voltage was supplied by a variac and the temperature was controlled by manual setting of the heater voltage. The copper jacket and the heater were surrounded by a stainless steel thermal shield which was supported by two screws going through to the copper jacket. To minimize the heat lost by radiation, the entire ion source assembly was surrounded by another stainless steel radiation shield.

The temperature of the ion source was measured by means of an iron-constantan thermocouple. The thermocouple was placed in a well drilled in the wall of the ion

source to a depth of 3/8 inch, and was located next to the ion exit slit.

To provide a controlled electric field between the ion source and the first cone of the ion accelerating tower, an electrostatic shield [11] was mounted below the source. This shield was fabricated from metallic mesh of high transparency and extended from the ion exit slit cone of the ion source to the second cone of the ion accelerating tower.

The entire ion source assembly was mounted on a cylindrical stainless steel support [17] which in turn was mounted on a machined ceramic (super-mica spacer) [18]. The spacer was mounted on the vacuum chamber port flange. The electrical connections to the ion source were made by 10 electrical feed-throughs which were soldered on the port flange.

2.7 Ion Accelerating Tower

The ion accelerating tower is shown in figure (2-6). Ions diffusing out of the ion exit slit of the ion source were accelerated and focussed on the mass analyzer entrance slit by the ion accelerating tower. This stepwise acceleration of the ions was carried out by the successive electrodes of the ion accelerating tower. The approximate voltages of the ion accelerating tower electrodes are shown in table (2-1). The last electrode before mass analyzer tube consisted of two half plates. One of these half plates

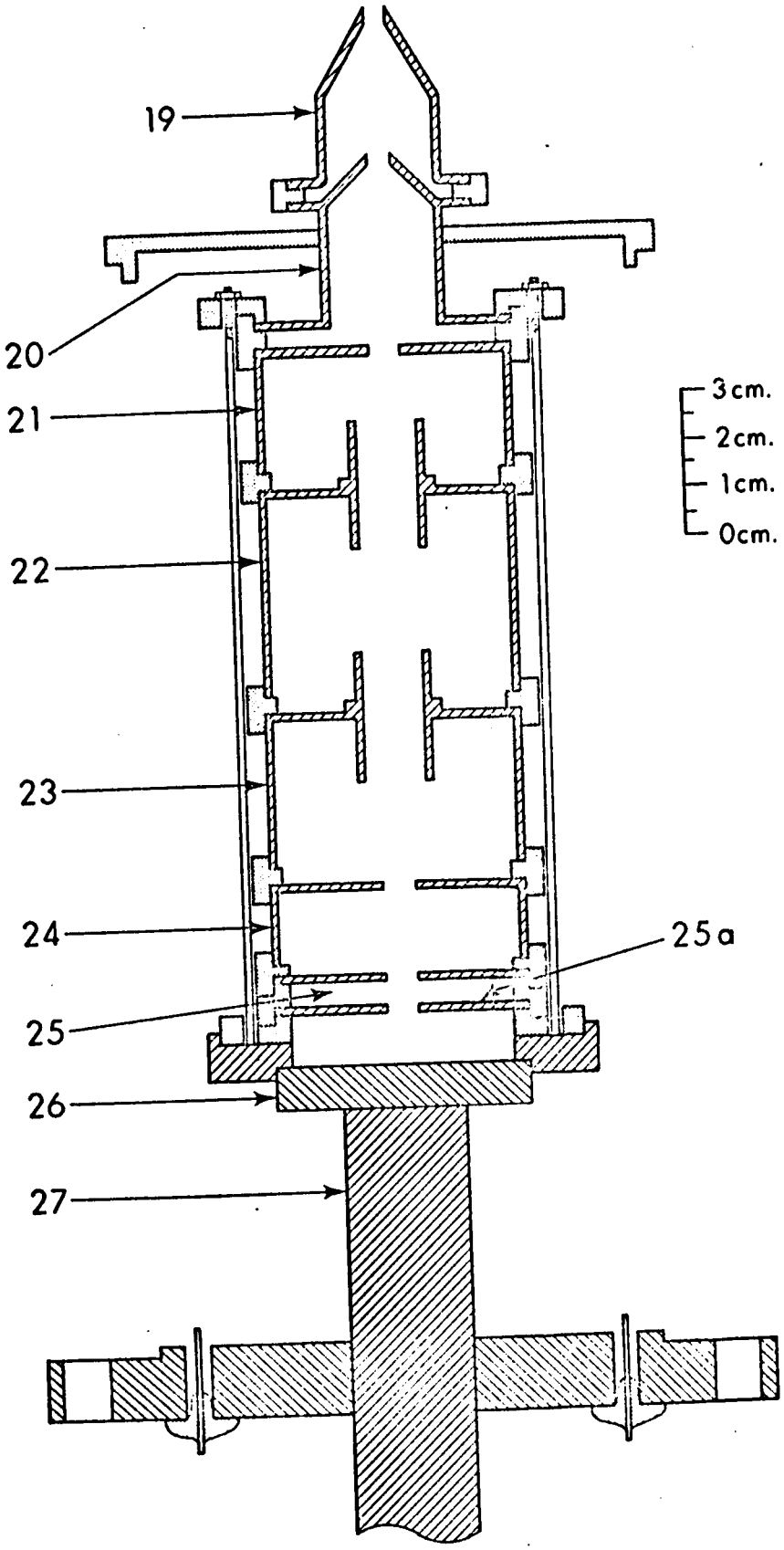

Figure 2-6: Ion Accelerating Tower. Numerical Legends are Explained on the Page Opposite to the Figure (2-2).

Table 2-1

Ion Accelerating Tower Potentials For Negative Ion Study

Electrode*	Potential, Volts
First Cone, 19	-1874
Second Cone, 20	-1702
Cylinder Entrance, 21	-1786
First Cylinder, 22	-1006
Second Cylinder, 23	-1207
Cylinder Exit, 24	-1274
First deflection half plate, 25	0
Second deflection half plate, 25a	-49

*Numbers refer to figures (2-2) and (2-6).

was at ground potential, and the potential of the other one could be varied from ground to -400 volts. It was intended to use this electrode for pulsing of the ion beam. However, the pulsing capability of the mass spectrometer is to be developed in future work in this laboratory. In the present experiments, the potential of this half plate was kept slightly negative, about -20 to -50 volts, for optimum operating condition.

2.8 Mass Analysis and Ion Current Detection

After acceleration the ions were magnetically mass analyzed in a 90°, 15 cm radius tube. Differential pumping was applied to the analyzer tube and thus the pressure in the tube was about ten times lower than that of the main vacuum chamber. Mass scanning was obtained by changing the magnetic field at a constant accelerating voltage. Mass determination was obtained by a Hall probe (manufactured by F. W. Bell Inc., Columbus, Ohio) which was located in the magnetic field just next to the analyzer tube. A constant voltage of 14 volts was applied across the primary circuit of the Hall probe and the induced voltage in the secondary circuit was measured by a Hewlett Packard digital voltmeter. Prior to these studies the Hall probe was calibrated for both positive and negative ions by working with gases which provided ions of known mass to charge ratio. Although the Hall voltage changed with room

temperature, the calibration remained valid within one mass unit for the mass range of 15 to 70 and within two mass unity for the range 70 to 200.

After mass analysis the ion current was amplified by a 17 stage secondary electron multiplier (SEM). The first dynode was slightly above ground voltage (about 50 volts), the last dynode was at +3200 volts and the SEM collector plate was at +3500 volts. The SEM output, was connected, through a capacitor, to a pulse counting system consisted of a preamplifier, amplifier, discriminator unit, manufactured by Johnston Laboratories Inc., Model PAD-1. The amplified pulses coming out of this unit were counted by a "Hamner Electronic Model N730" counter. The noise level of the counting circuit was approximately 20 counts per second. Figure (2-7) represent a plot of the counter output versus the SEM voltage.

2.9 Vacuum Chamber

The main vacuum chamber was built from 8 inch stainless steel pipe[figures (2-2) and (2-8)]. In addition to the top entrance, there were four entrances or ports provided for the chamber. To each port another piece of 4 inch stainless steel pipe was welded and each one was provided with a flange. The orientation of the different component of the mass spectrometer was as follows: the ion source was mounted on entrance [1], figure (2-8), the

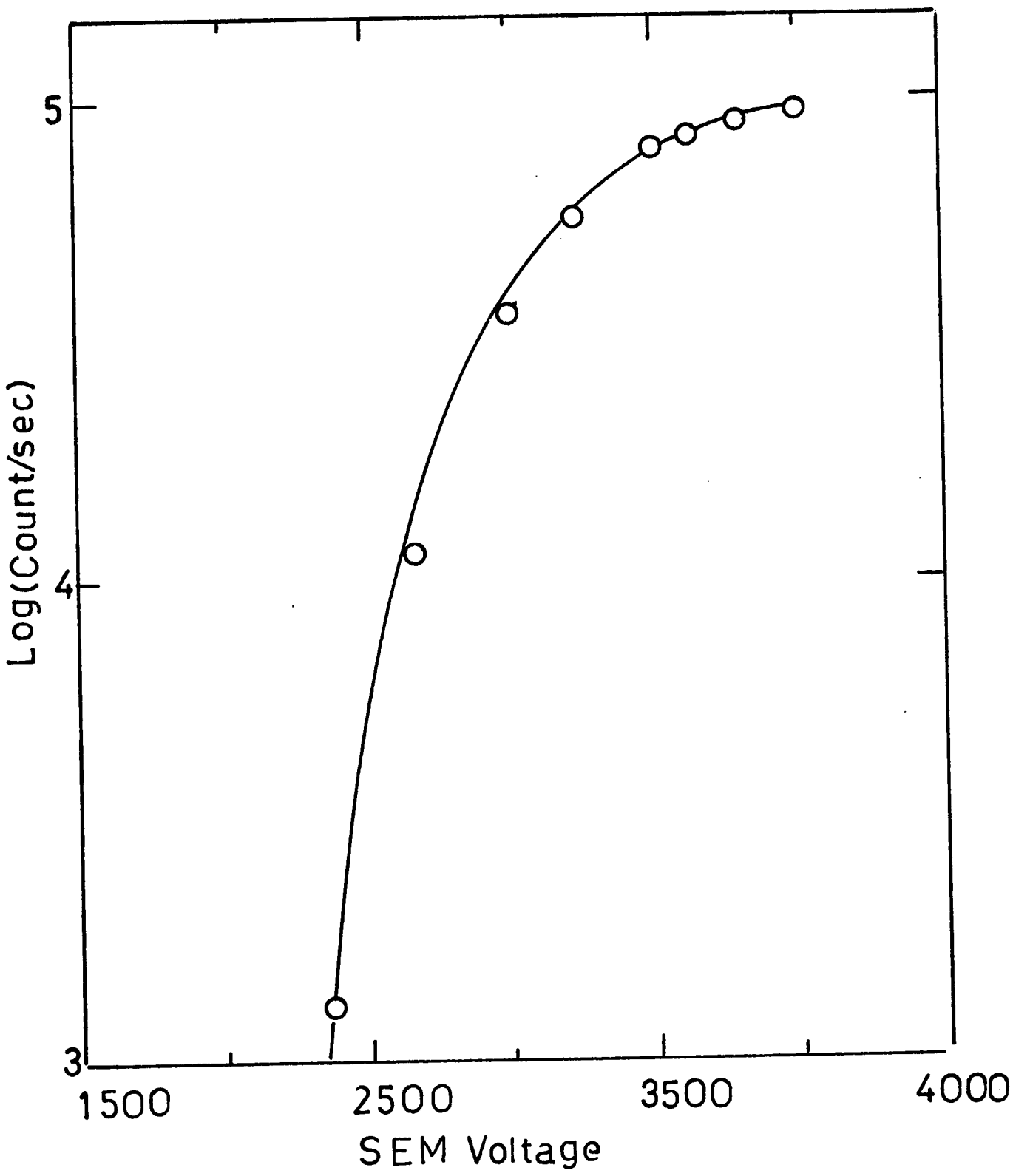

Figure 2-7: Counts/Second as a Function of Voltage Across Secondary Electron Multiplier.

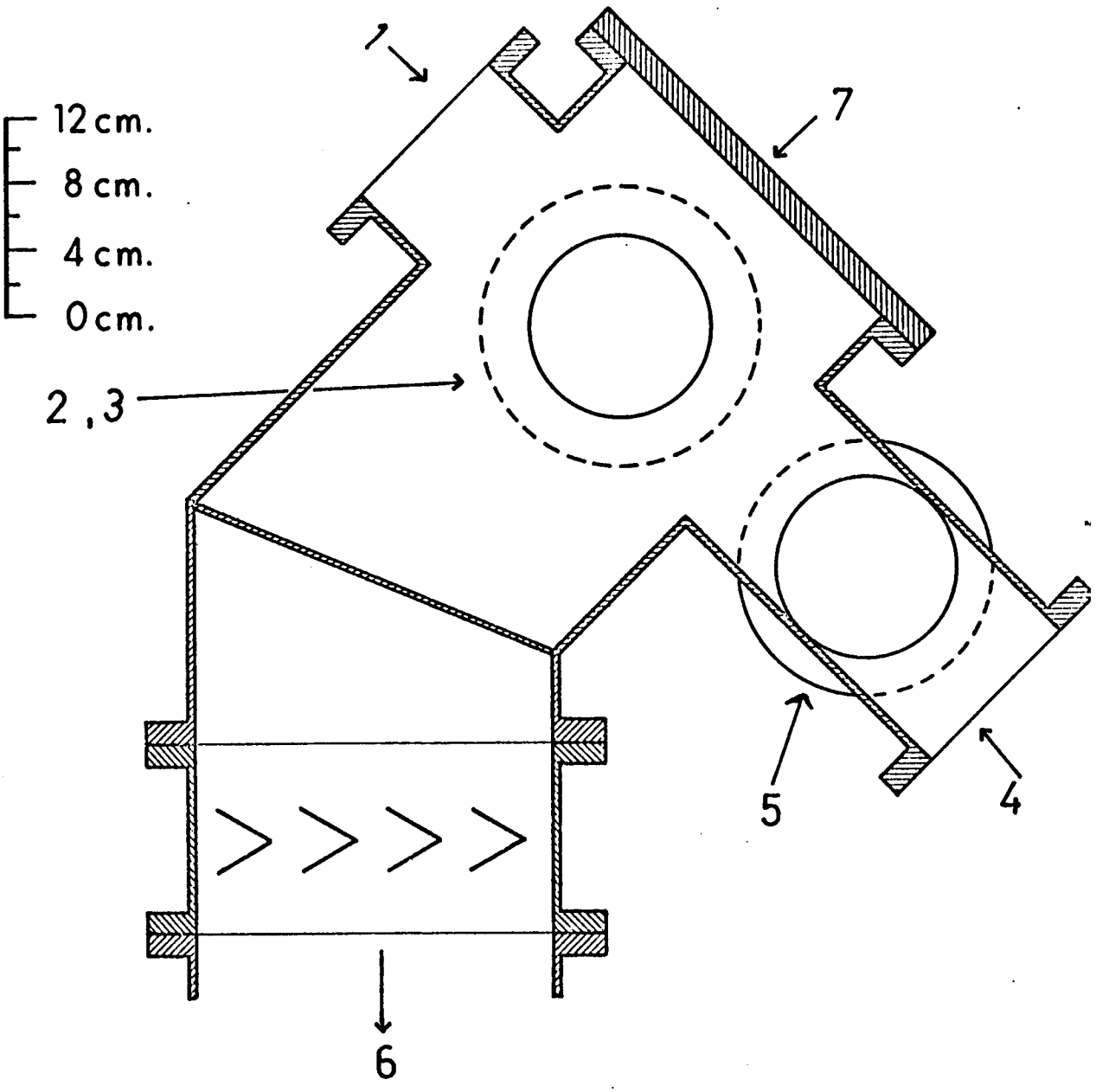

Figure 2-8: Main Vacuum Chamber, 1) Ion Source Flange, 2) Electron Gun flange, 3) Ionization Gauge, 4) Mass Analyzer Tube flange, 5) To Second Vacuum Line 6) Main Diffusion Pump, 7) The Top Entrance.

electron gun on [2] the ionization gauge on [3], and mass analyzer tube on entrance [4]. In addition to these, the 4 inch pipe on the mass analyzer side was provided with another flange, which was connected to a 4 inch "National Research Corporation" oil diffusion pump. This auxiliary vacuum line was to evacuate the mass analyzer tube and the detection part of the instrument. The top entrance of the vacuum chamber was covered with a plexiglass lead. The use of plexiglass lead instead of stainless steel was necessary for the observation and adjustment of the electron beam.

The bottom of the vacuum chamber was welded, at a 45 degree angle, to another 8 inch stainless steel pipe, figure (2-8). This port was fitted, by means of proper flanges, to the top of a water cooled optical baffle of the type 506 Chevron Cryo-baffle, manufactured by National Research Corporation.

The main vacuum chamber was pumped by a National Research Corporation "VHS6-184" diffusion pump. The pumping speed at the top of the baffle was given by manufacturer as 1100 litres/sec. The conductance of the 8 inch pipe from the baffle to the ion source exit slit was obtained from the graph in reference (69), and was also about 1100 litres/sec. The pumping speed, S, just outside of the ion exit slit can be calculated from the equation:

$$\frac{1}{S} = \frac{1}{F} + \frac{1}{S_p}$$

where S_p is the pumping speed at the top of the baffle, and F is the conductance of the 8 inch stainless steel pipe. Using the values given above for S_p and F, a value of 550 litres/sec is obtained for S. The conductance of the ion exit slit and the electron entrance slit of the ion source can be calculated from equation (2-1), if we assume molecular flow through both slits.

$$F = \frac{\bar{V}}{4} A \qquad (2\text{-}1)$$

F is the conductance of the slit, $\bar{V}$ is the average linear velocity of the gas through the slit and A is the area of the slit. For air at 300°K, $\bar{V}$ is equal to 4.70×10^4 cm/sec (68). The total area of the two slits is 6×15^4 cm^2, thus, F is calculated to be 7.0 cc/sec. From the value of the conductance of the slits, the pumping speed outside of the ion source and the ion source pressure, the pressure outside of ion source in the main vacuum chamber can be calculated by the equation:

$$S.P_{chamber} = F.P_{i.s.}$$

The calculated value for the pressure in the main vacuum chamber, when the ion source pressure was two torr, is 2.5×10^{-5}. The observed reading from the Veeco ionization gauge was 5×10^{-5} torr, which is of the same magnitude.

2.10 Experimental Procedure

The investigation of the halide negative ions

was carried out at ion source temperatures from 25 to 500°C. Whenever the experiment was to be performed at an elevated temperature, the voltage of the ion source heater was adjusted, at least, five hours in advance. Ordinarily, the ion source heater was set for the desired temperature the night before the experiment was to be carried out, so that the ion source temperature equilibrated by the morning.

For the experiments in which oxygen was used as carrier gas, the water vapour was supplied to the gas stream through a capillary by means of small bulb containing liquid water. The rate of flow of water vapour through the capillary was regulated by controlling the temperature of liquid water and thus the water vapour pressure in the bulb. This was done by placing the water container in a constant temperature bath and adjusting the temperature of the bath, for a particular partial pressure of water. The partial pressure of water in the gas stream was determined by the weight loss of the water container during the experiment and the flow rate of the carrier gas. The flow rate was determined by means of a calibrated flowmeter which was installed in the gas line. Assuming that the water-oxygen mixture obeyed the ideal gas law, the partial pressure of water is given by

$$P_{H_2O} = \frac{P_{total} \cdot W_{H_2O}}{W_{H_2O} + (W_{oxygen})18/32}$$

where P_{total} is the ion source pressure, P_{H_2O} is the partial

pressure of water, W_{H_2O} amd W_{oxygen} are the weight loss of water and the weight of oxygen passing through the ion source per unit time, respectively.

The halide compound to be studied was also added to the gas stream, through a capillary. The partial pressure of the halide compound in the ion source was adjusted to be between 30 to 100 microns. In most cases this was done by the proper selection of the capillary and having the halide compound container at room temperature. In those instances where this procedure was not applicable due to the limitation of the capillary size, the compound to be studied was cooled, by means of a mini-freezer. Most of the experiments were carried out with a carrier gas pressure of 4 torr, although pressures up to 8 torr were used in some cases.

In those experiments where no carrier gas was used, the water pressure was measured directly with t he Atlas MCT manometer. Experiments were run with water pressure of one to four torr. After the water pressure and the partial pressure of the halide compound were adjusted to the desired values, the gas stream was allowed to run through the ion source for approximately 30 minutes. After this time interval, the electron beam was turned on, adjusted and focussed properly, the ion source, SEM and magnet high voltages were also turned on and adjusted. To assure that

the emission has reached a constant value, the system was allowed to run for another fifteen minutes before a complete spectrum of the mass range pertinent to the halide ion under consideration was taken and studied. From these spectra, the equilibrium constants, for the reactions which were taken place in the ion source at that particular temperature, were determined. For each temperature, several runs were made at different partial pressures of water in the ion source. The temperature of the ion source was checked before and after each run. The variation of the ion source temperature during each run was about two degrees at the high temperature (200-500°C) and about one degree at temperatures below 200°C.

3 PRODUCTION OF IONS AND SAMPLING

3.1 Production of Halide Negative Ions

At the normal operating condition of a conventional mass spectrometer, where ionizing electrons of 50-75 eV are employed and the gas pressure is less than 10^{-4} torr, the predominant products of the electron impact ionization of a molecule, RX, are a positive ion and a secondary electron

(3-1) $$RX + e = RX^+ + 2e$$

or

(3-2) $$RX + e = R^+ + X + 2e$$

Thus the probability for production of negative ions by electron impact, through dissociative electron capture (3-3) or pair production (3-4), is generally two orders of magnitude smaller than that of positive ions (36)

(3-3) $$RX + e = R + X^-$$

(3-4) $$RX + e = R^+ + X^- + 2e$$

However, at high ion source pressure (above 1 torr), as in this work, negative ions can be produced in abundance approaching that of the positive ions by "three body" capture of the low energy or thermalized electrons

$$e_{thermalized} + RX + M = RX^- + M$$

In the first part of this work, oxygen was used

as a carrier gas. In this case the thermal electrons were captured by the oxygen molecules according to the reaction (3-5)

$$(3\text{-}5) \qquad 2O_2 + e = O_2^- + O_2$$

Then they were transferred to the halogen being studied, through negative ion molecule reactions of the type (3-6)

$$(3\text{-}6) \qquad O_2^- + RX = R + X^- + O_2$$

where RX is a suitable compound of the halogen. Reaction (3-6) can occur in the ion source of a mass spectrometer, only if the electron affinity of the halogen is greater than the sum of the electron affinity of oxygen molecule and the bond energy, D(R-X). The electron affinities of halogens are about 70-85 Kcal/mole (48) and $EA(O_2)$ = 10 Kcal/mole (38); therefore, only halogen compounds with D(R-X) below 60 Kcal/mole can be used as a source of X^-. Moreover, since the life time of the ionic species, O_2^-, is of the order of 1 to 2 milli-seconds, only fast ion molecule reactions of the type (3-6) can be used. In other words, the reaction time of (3-6) has to be short enough so that the electron transfer is completed before the ion is lost by some other processes like collisions with the walls, neutralization by positive ions, etc.

The use of carrier gas was essential for the part of this work which was carried out with the alpha source

mass spectrometer. This was due to the low sensitivity of that instrument especially for ion source pressures below 1 torr. With the electron beam mass spectrometer, where the problem of low sensitivity was no longer present, it was found more convenient to abondon the oxygen gas and use a flow of pure water vapour. In this case, although the exact process by which X^- was produced is not known, it is believed that the thermal electrons were captured by molecule RX followed by its dissociation to R and X^-.

In the following section the production of halide negative ions I^-, Br^-, Cl^- and F^- will be discussed individually. However, a more detailed discussion of reactions involved will be given after the results of this work have been presented in the next chapter.

3.1a Production of I^-

The iodide ion was produced from the compound CH_3I. This comound was supplied to the gas stream through a capillary, from a small glass container. The conductance of the capillary was so selected that the resulting pressure of methyl iodide in the ion source was about 30 to 50 microns. The methyl iodide used was Eastman Chemical reagent grade. No attempt was made to purify it any further. The spectra obtained by our instrument did not show any peaks which could be attributed to the impurities in methyl

iodide. In addition to the peaks due to $I^-(H_2O)_n$, some very small peaks were observed which could always be traced back to Cl^-. It is believed that impurities producing the chloride ion were present in our apparatus from the previous work and could not be completely removed by baking out.

3.1b Production of Br^-

The compound used in the production of bromide ion was CH_2Br_2. As in the case of CH_3I, the bromide compound was introduced into the ion source from a glass container through a capillary. By proper adjustment of the temperature of methyl dibromide container and the size of the capillary, the partial pressure of CH_2Br_2 in the ion source was regulated to be about 50 microns. The methyl dibromide used was spectroscopic grade and was obtained from Eastman Chemical.

3.1c Production of Cl^-

The chloride ion was produced by addition of CCl_4 to the oxygen stream or to the water vapour whenever oxygen was not used. The chloride ion could also be obtained from CH_3Cl or CH_2Cl_2. Some peaks corresponding to the attachments of chloride ions to CH_3Cl or CH_2Cl_2 were also observed, but the intensities of these peaks were very low in comparison to those due to $Cl^-(H_2O)_n$. This was due to the low concentration of CH_3Cl which was about

100 microns. The carbon tetrachloride used in this experiment was Eastman Chemical reagent grade.

3.1d Production of F^- and OD^-

The fluoride ion was produced by the addition of 30 to 50 microns of NF_3 to the oxygen stream. Reese and Dibeler (37) have observed the ion F^- with near 0-Volt appearance potential, in the electron impact study of NF_3. In the present study, reaction (3-7) was probably involved

$$(3\text{-}7) \qquad O_2^- + NF_3 \longrightarrow NF_2 + O_2 + F^-$$

In the study of the hydration of fluoride ions, the effect of chloride ion impurity was very serious. This was mostly due to the correspondence of the mass of $^{37}Cl^-(H_2O)_n$ with the mass of the series $F^-(H_2O)_{n+1}$. This difficulty was successfully eliminated by the use of deuterium oxide instead of water. Upon replacing of water with D_2O a new series of peaks corresponding to $OD^-(D_2O)_n$ was observed. This observation was confirmed when the ion source temperature was raised above 350°C and the peak at mass number 18 was detected. It is believed that the following process is involved in the production of OD^-:

$$F^- + D_2O \longrightarrow DF + OD^-$$

This postulate was supported by the observation of some small peaks (less than 4% of total ionization) corresponding to

$F^-(DF)_n$ and $F^-(DF)_n(D_2O)_m$. Since NF_3 was purified by fractional distillation at 150°K, it was very unlikely that the hydrogen fluoride entered into the system with nitrogen trifluoride gas. A typical spectrum of the fluoride ion study is given in table (3-1). This spectrum was taken at ion source temperature of 409°C and deuterium oxide pressure of 3.5 mm Hg. The impurities referred to in this table are Cl^-_{35}, Cl^-_{37} peaks along with some unknown peaks at mass number 26 and 43 and 62. The peak at 26 could be due to CN^-, and the one at 62 due to $OCN^-(D_2O)$. A trace of mass 42 (OCN^-) was observed later at higher ion source temperatures. The peak at mass number 43 could not be identified at all.

Referring back to series $OD^-(D_2O)_n$, it should be mentioned that the ions $OH^-(H_2O)_n$ were not observed in the study of Br^- and I^- hydration. Since the series $OH^-(H_2O)_n$ appears at the same mass numbers as $^{35}Cl^-(H_2O)_{n-1}$, it cannot be said definitely whether this series was present when the Cl^- hydration was studied or not. But the isotope ratio of $^{37}Cl^-(H_2O)_{n-1}$ to $Cl^-_{35}(H_2O)_{n-1}$ did not indicate the presence of $OH^-(H_2O)_n$.

Although the exact process of production of OD^- ion cannot be determined solely by this work, the consistency of the equilibrium constants (given in chapter 5) for attachment of OD^- to D_2O indicates that the equilibrium

Table 3-1

A typical Mass Spectrum of Fluoride Ion Hydration Study at 409°c and P_{D2O} = 3.50 mmHg

Ion	m/e	% of Total Ionization
OD^-	18	4.04
F^-	19	2.92
$OD^-(D_2O)$	38	20.6
$F^-(D_2O)$	39	56.0
$F^-(DF)$	40	1.31
$OD^-(D_2O)_2$	58	0.8
$F^-(D_2O)_2$	59	3.9
$F^-(D_2O)$ (DF)	60	0.2
$F^-(DF)_2$	61	0.90
Impurities	--	9.5

condition in our ion source was achieved.

3.2 Production of O_2^-, NO_2^-

In addition to the halide negative ions and OD^-, the hydration of the ions O_2^-, NO_2^-, was also studied. The study of the hydration of O_2^- was accomplished simply by adding known amounts of water to the oxygen stream. The major ions observed in the pure oxygen stream were $O_2^-(H_2O)_n$, although some small peaks due to the series $O^-(H_2O)_n$ and $O_3^-(H_2O)_n$ were also noticed. This observation confirmed our assumption that the majority of the negative ions produced in the ion source of both our mass spectrometers -- alpha source and electron beam system-- were due to thermal electrons with energy less than 3.5 eV, since the production of O^- requires electrons with energy higher than 3 eV (38).

In the study of NO_2^-, at first it was attempted to produce NO_2^- by the addition of nitrogen dioxide gas into the oxygen stream. However, this attempt proved unsuccessful. The series $NO_2^-(H_2O)_n$ could not be observed, but instead the series $NO_2^-(HNO_2)_n$ and $NO_2^-(HNO_3)_n$ were seen, with the $NO_2^-(HNO_2)_n$ being the major peaks. The presence of the series $NO_2^-(HNO_2)_n$ and $NO_2^-(HNO_3)_n$ could be attributed to the formation of HNO_2 and HNO_3 by the following reactions:

$$H_2O + NO_2 + NO \rightarrow 2HNO_2$$

$$2NO_2 + H_2O + 1/2\ O_2 \rightarrow 2HNO_3$$

nitrogen oxide being present as impurity in NO_2 gas. The identities of $NO_2^-(HNO)_n$ and $NO_2^-(HNO_3)_n$ were established by replacing water with D_2O and observing the resulting mass shift in the clusters. When nitrogen dioxide was purified by low temperature distillation thus removing NO, the ions $NO_2^-(HNO_2)_n$ were no longer the major series, they were overtaken by ions $NO_2^-(HNO_3)_n$. It was observed that the preferential attachment of NO_2^- to nitrous and nitric acid in place of water could occur even when no NO_2 was added to the water-oxygen stream. In this case, the only possible source of NO_2^-, HNO_3, HNO_2 was the minute quantities of these acids absorbed on the glass walls of the gas handling plant. Considering that the flow of gas through the ion source was over 300 cc/min and the partial pressure of water in the ion source was 100 microns, the equilibrium concentration ratio of nitrous and nitric acid to water could not possibly be over 10^{-3}. Thus the HNO_3 molecule attaches preferentially by a factor of at least 1000. Finally, the NO_2^- was successfully produced from $C_2H_5ONO_2$. Ethyl nitrate was added to the oxygen stream so that a partial pressure of approximately 100 microns of $C_2H_5ONO_2$ was obtained. The reaction involved was possibly

$$(3\text{-}8) \quad O_2^- + C_2H_5ONO_2 \longrightarrow NO_2^- + C_2H_5O + O_2$$

The available thermochemical data: $EA(NO_2)$ = 84 Kcal/mole

(48) $EA(O_2)$ = 10 Kcal/mole (38) and $D(C_2H_5O - NO_2)$ = 36 Kcal/mole (48)will give a value of -38 Kcal/mole for the enthalpy change of the reaction (3-8).

3.3 Ion Sampling

There are two basic assumptions made in this work, and in fact, in any other mass spectrometry study of the gas phase solvation reactions;

(a) equilibrium conditions prevail in the ion source,

(b) ion currents recorded by the mass spectrometer are proportional to the concentration of the respective ions in the ion source.

3.3a Equilibrium Condition in the Ion Source

The achievement of equilibrium in the ion source can be studied best by the investigation of the conditions of the ions from the time of their formation to the time of their departure from the ion source through the ion exit slit. After their production, in the ionization region of the ion source, some of the primary negative ions will diffuse out of this region. In their way towards the walls of the ion source where they are discharged, the primary ions will collide with the solvating molecules. Some of these collisions may result in the attachment of the ion to the neutral molecules thus forming ion-clusters. The ion-clusters can stablize themselves by giving up their

excess energy through collisions with other molecules (third body collisions). In order that equilibrium conditions prevail, this stablization of ion clusters should be achieved and all reactions involved be completed before the ion clusters diffuse out of the ion exit slit.

The time, t, necessary for the ions to travel the distance from the ionization region to the ion exit slit can be estimated by the approximate equation given below, which establishes a relationship between the time, t, required by a particle to diffuse the distance, d (39), and the diffusion coefficient, D.

(3-9) $$t \approx \frac{d^2}{2D}$$

In the present case d is the distance from the electron beam plate to the ion exit slit and is equal to 4 mm, D is the diffusion coefficient of the ions through the gas and is taken as 50 cm^2/sec (39) for an ion source pressure of one mm Hg and a temperature of 300°K. Thus, the diffusion time t is calculated to be 1.6 milli-seconds. The half life of the attachment reaction

(3-10) $$X^-(H_2O)_{n-1} + H_2O \xrightarrow{M} X^-(H_2O)_n$$

can be calculated, if we assume a value for the rate constant, K. The reaction

$$H_3O^+(H_2O)_{n-1} + H_2O \xrightarrow{N_2} H_3O + (H_2O)_n$$

has been studied by A. Good, D. Durden and P. Kebarle (13)

kinetically. They found the third order rate constants to be around 1 X 10^{-27} $cc^2/molecule^2 sec$. As an approximation, the same value can be assumed for the rate constant of the reaction (3-10). The half-life $t_{1/2}$ is then given by

$$t_{1/2} = \frac{1}{1X10^{-27}[H_2O]^2} \qquad (3\text{-}11)$$

where $[H_2O]$ is the concentration of water in the ion source, in molecules/cc. At an ion pressure of 1 mm Hg and a temperature of 298°C, the water concentration is equal to 3 X 10^{16} molecules/cc. Introducing this value, into equation (3-11), the half life comes out to about one microsecond. This is three order of magnitude smaller than the ion residence time calculated from equation (3-9).

The ion residence time calculated from equation (3-9) represents a statistical average value, thus it applies to ions with relatively high observed ion intensities. The equilibrium conditions, therefore, can be assumed only for the ions which are represented by a major peak in the spectra.

In addition to the diffusion process, the ions can be removed from the ion source by mass flow. It has been shown (35), however, that the mass flow does not become significant until about 1 mm from the exit slit. Thus starting from the electron beam, the ions are transported for the first 2 to 3 mm by diffusion and in the last one mm by mass flow.

3.3b Relation of the Ion Current to the Ion Concentration

From the time of their formation in the ion source to the time of their recording by the detection system, the ion-clusters are engaged in a number of processes. A few of these processes may discriminate against one or the other type of ions. Some of these discriminatory processes will be discussed below.

(i) Discrimination in Transport Through the Ion Source

The diffusion coefficient of an ion is inversely proportional to the square root of the mass of the ion (39). Therefore, one expects that the lighter ions would travel, through the ion source, faster and would reach the ion exit slit in a shorter interval than the heavier ions. Thus, the actual concentration of the ions with smaller mass would be less than what is represented by the recorded signal. In short, there would be a discrimination against the heavier ions by the diffusion process. However, since the average half life of the clustering reaction is short in comparison to the ion residence time of the ion, and a cluster, $X^-(H_2O)_n$, gains and loses water molecules at a fast rate; all the clusters would have the same average molecular weight and their diffusion coefficient would be equal.

(ii) Discrimination in Passage Through Exit Slit

The flow through the ion exit slit may also cause discriminations. If the width of the ion exit slit is much

larger than the mean free path of the ion cluster– water molecule collision, the condition of molecular flow would cease to exist. This will result in the cooling of the gas due to adiabatic expansion in vacuum and consequently, a trend towards heavier clusters would appear. For a slit of 10 microns, the maximum allowable pressure of the ion source is 6 mm Hg (11).

(iii) Discrimination due to Stripping Outside of Ion Source

If the pressure in the region just outside of the ion exit slit is high, some ion molecule collisions may take place in the vacuum region between the ion source exit slit and the first cone electrode. Due to the presence of the ion accelerating field, these collisions occur with kinetic energies much higher than thermal. As a result of these collisions, the heavier ion-clusters may dissociate. To avoid this handicap and also the effect of adiabatic expansion, discussed in previous section, almost all runs were made with the ion source pressure below 5 mm Hg.

(iv) Discrimination in Mass Analyzer Tube

In general, in a magnetic mass analyzer tube such as the one used in this work, any loss of ions due to elastic scattering, collisions with the wall, etc., will be the same for all ions. Consequently, we can assume that the effect of mass discrimination in the analyzer

tube was negligible.

(v) Discrimination in the Ion Current Detection System

It has been reported (40) that the emission of electrons from the cathode of the secondary electron multiplier (SEM), upon the impinging of the incoming ions, is dependent on the velocity of the ions as well as their chemical composition. Thus, the gain of the multiplier would not be the same even for two isobaric ions such as N^+ and $(CH_2)^+$ (41). The reason for this difference is that, the multi-atom ions may break up when they strike the surface of the SEM cathode and act as a group of particles instead of just one ion.

When a secondary electron multiplier is used for the counting ions, as in this work, it is the efficiency, not the gain, which is of prime concern. The efficiency is the ratio of the number of output pulses to the number of the incoming ions. Unfortunately, due to the low negative ion current (10^{-14}A), it was not possible to measure the efficiency of the electron multiplier used in this work. However, S. K. Searles, while studying (35) the positive ions $H^+(H_2O)_n$ and $NH_4^+(NH_3)_n$, determined the gain of a similar electron multiplier. He found that the maximum error introduced by the SEM discrimination in the ion-cluster measurements was about 20%. Considering the fact that the efficiency of an electron multiplier is not affected

by the factors which cause mass discrimination as much as its gain, our maximum error due to the SEM discrimination should not be over Searles' value of 20%.

4 RESULTS AND DISCUSSIONS OF HYDRATION OF HALIDE NEGATIVE IONS, X^-

4.1 Introduction and Thermodynamic Relations

After their formation, some of the halide negative ions diffuse out of the ionization region of the ion source and react with the water molecules and are converted to ion clusters, $X^-(H_2O)_n$, by the following sequence:

$$X^- + H_2O = X^-(H_2O)$$

$$X^-(H_2O) + H_2O = X^-(H_2O)_2$$

$$\vdots$$

$$X^-(H_2O)_{n-1} + H_2O = X^-(H_2O)_n$$

provided that the equilibrium is achieved in the ion source, the equilibrium constant can be calculated from

$$K_{n-1,n} = \frac{P_{X^-(H_2O)_n}}{P_{X^-(H_2O)_{n-1}} P_{H_2O}}$$

The partial pressure of H_2O, P_{H_2O} is determined by direct pressure measurement or by the weight loss of water (see chapter 2) and the ratio

$$\frac{P_{X^-(H_2O)_n}}{P_{X^-(H_2O)_{n-1}}}$$

is assumed to be the same as the ratio of the ion currents

$$\frac{I_{X^-(H_2O)_n}}{I_{X^-(H_2O)_{n-1}}}$$

Determination of the equilibrium constants, at different ion source temperatures, will result in the calculation of the thermodynamic values ΔH°, ΔG°, ΔS° for the reaction

$$(4\text{-}1) \qquad X^-(H_2O)_{n-1} + H_2O = X^-(H_2O)_n$$

$\Delta H^\circ_{n-1,n}$ is determined from the plot of the equilibrium constant, $K_{n-1,n}$, versus reciprocal of temperature (in degrees Kelvin). $\Delta G^\circ_{n-1,n}$ from

$$(4\text{-}2) \qquad \Delta G^\circ_{n-1,n} = -RT \log_e K_{n-1,n}$$

where R is the universal gas constant, $\Delta S^\circ_{n-1,n}$ is obtained from

$$(4\text{-}3) \qquad \Delta S^\circ_{n-1,n} = \frac{\Delta H^\circ_{n-1,n} - \Delta G^\circ_{n-1,n}}{T}$$

4.2 Presentation of the Results and General Discussion

The equilibrium constants obtained for the gas phase hydration of the fluoride, chloride, bromide and iodide ions are presented in figures (4-1) to (4-16). It can be seen that at any one temperature, the values of $K_{n-1,n}$ are relatively constant, over the pressure range covered. This independency of $K_{n-1,n}$ of water pressure indicates that, equilibrium conditions indeed prevailed in the ion source and no significant amounts of collisions occurred outside of the ion source.

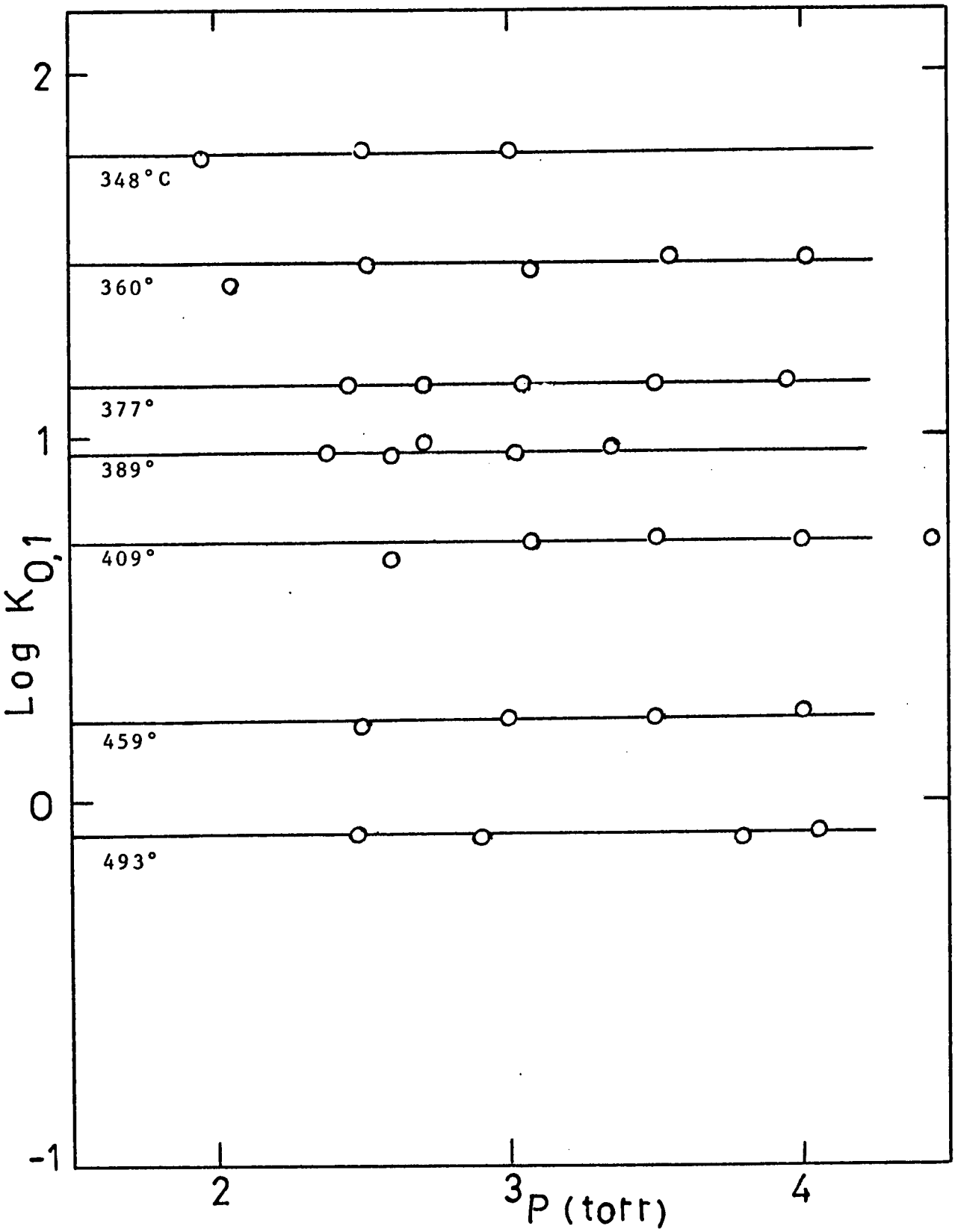

Figure 4-1: Plots of Log $K_{0,1}$ for the Gas Phase Hydration of F^-, at Various Temperatures, Versus Pressure of D_2O.

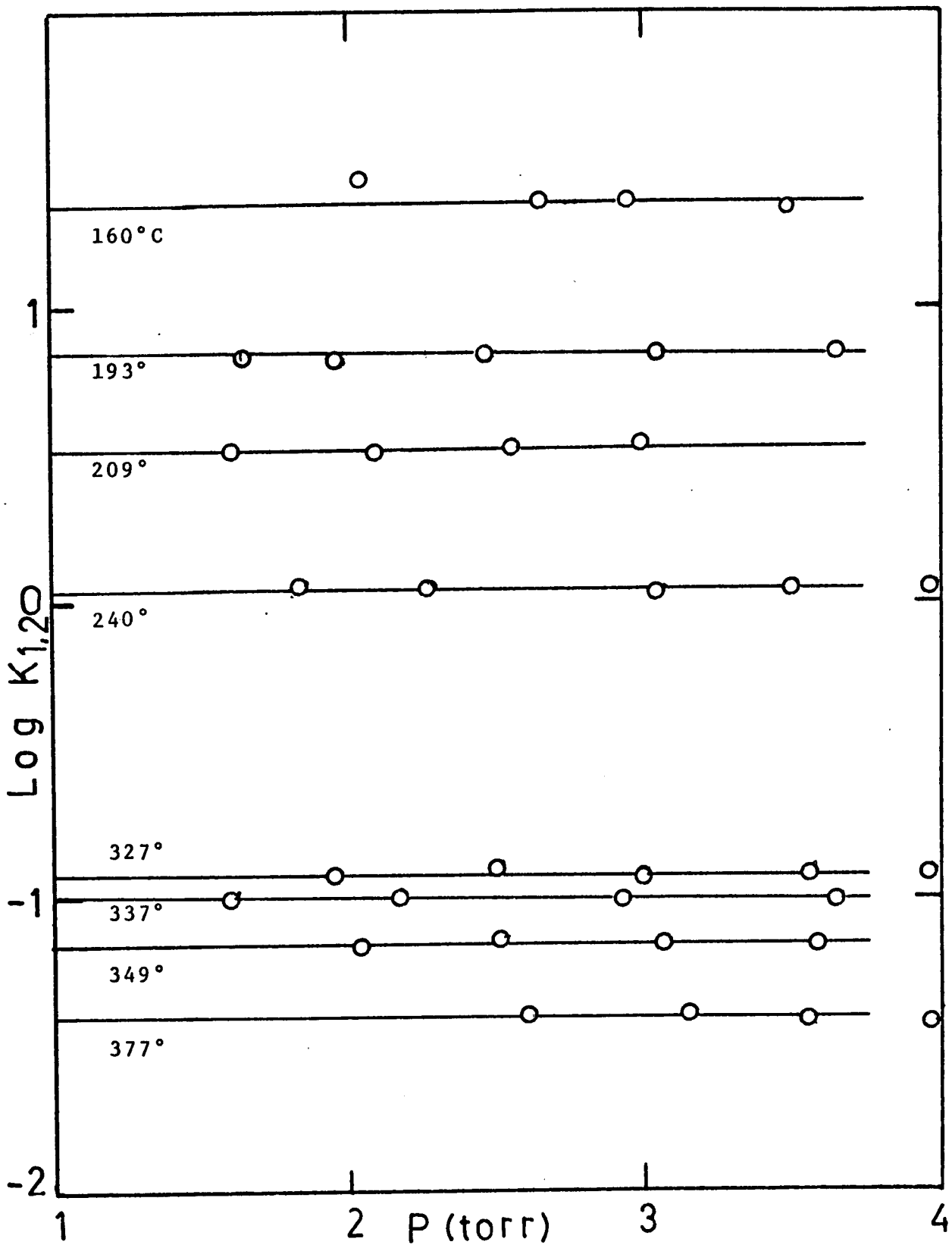

Figure 4-2: Plots of Log $K_{1,2}$ for the Gas Phase Hydration of F^-, at Various Temperatures, Versus Pressure of D_2O.

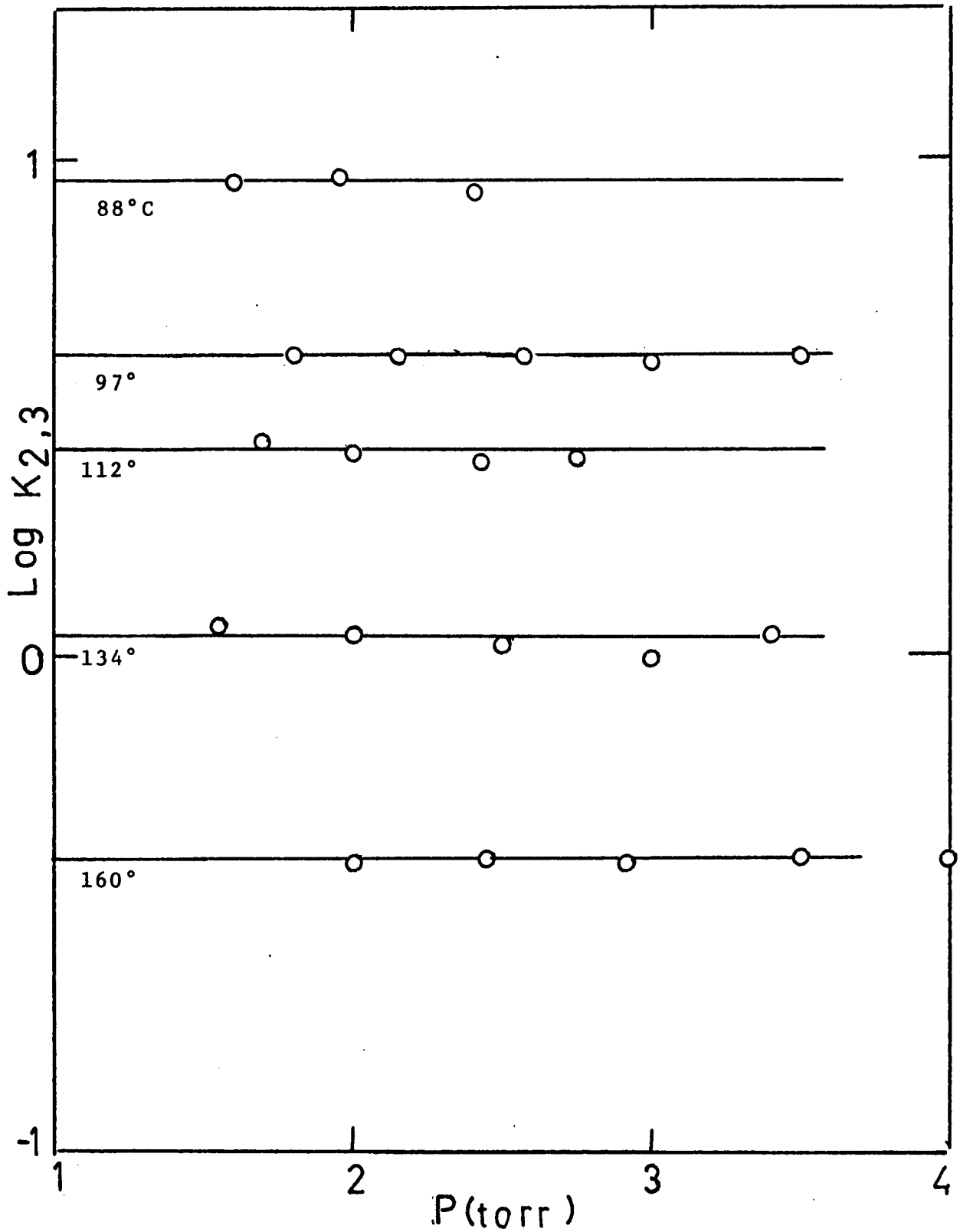

Figure 4-3: Plots of Log $K_{2,3}$ for the Gas Phase Hydration of F^-, at Various Temperatures, Versus Pressure of D_2O.

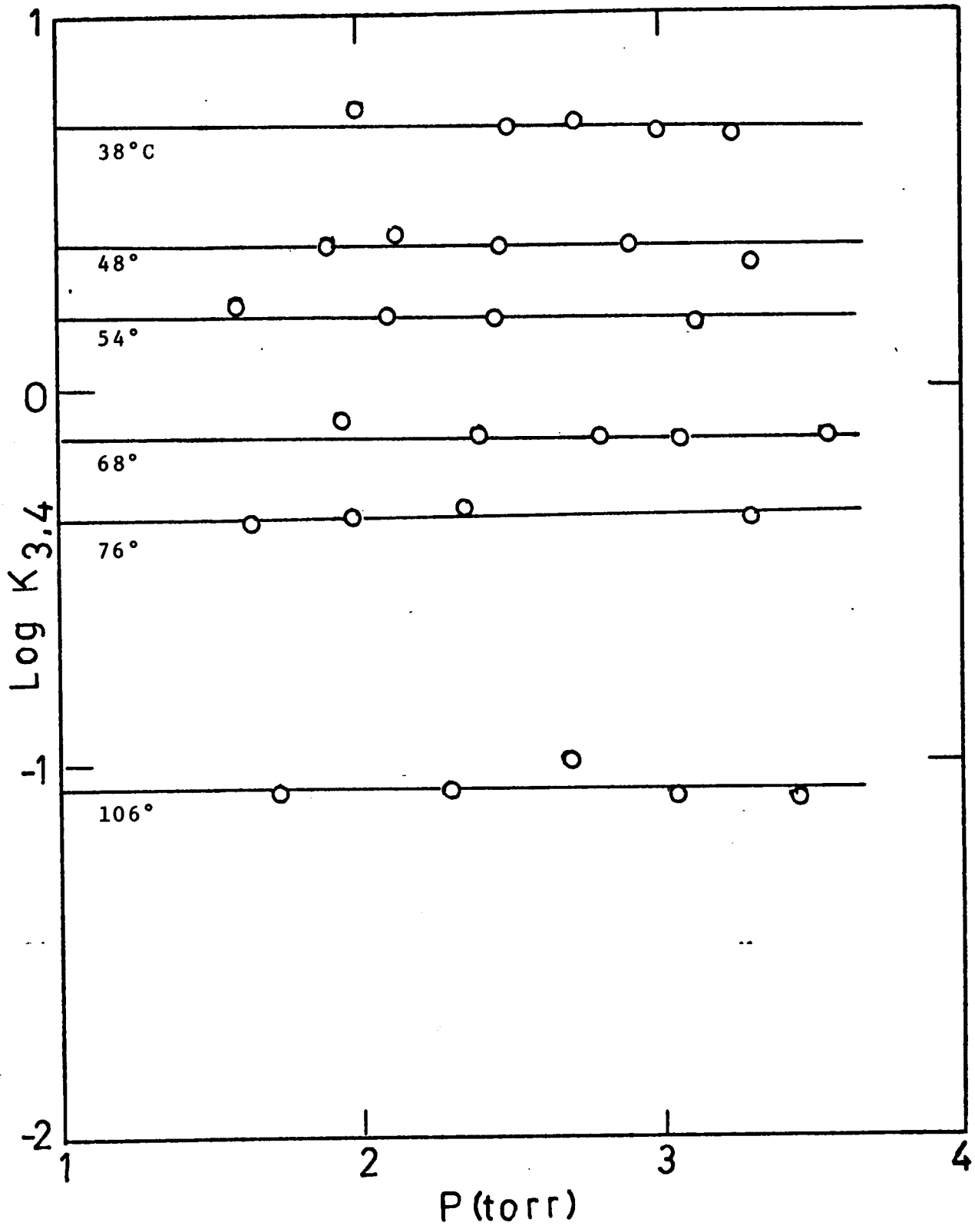

Figure 4-4: Plots of Log $K_{3,4}$ for the Gas Phase Hydration of F^-, at Various Temperatures, Versus Pressure of D_2O.

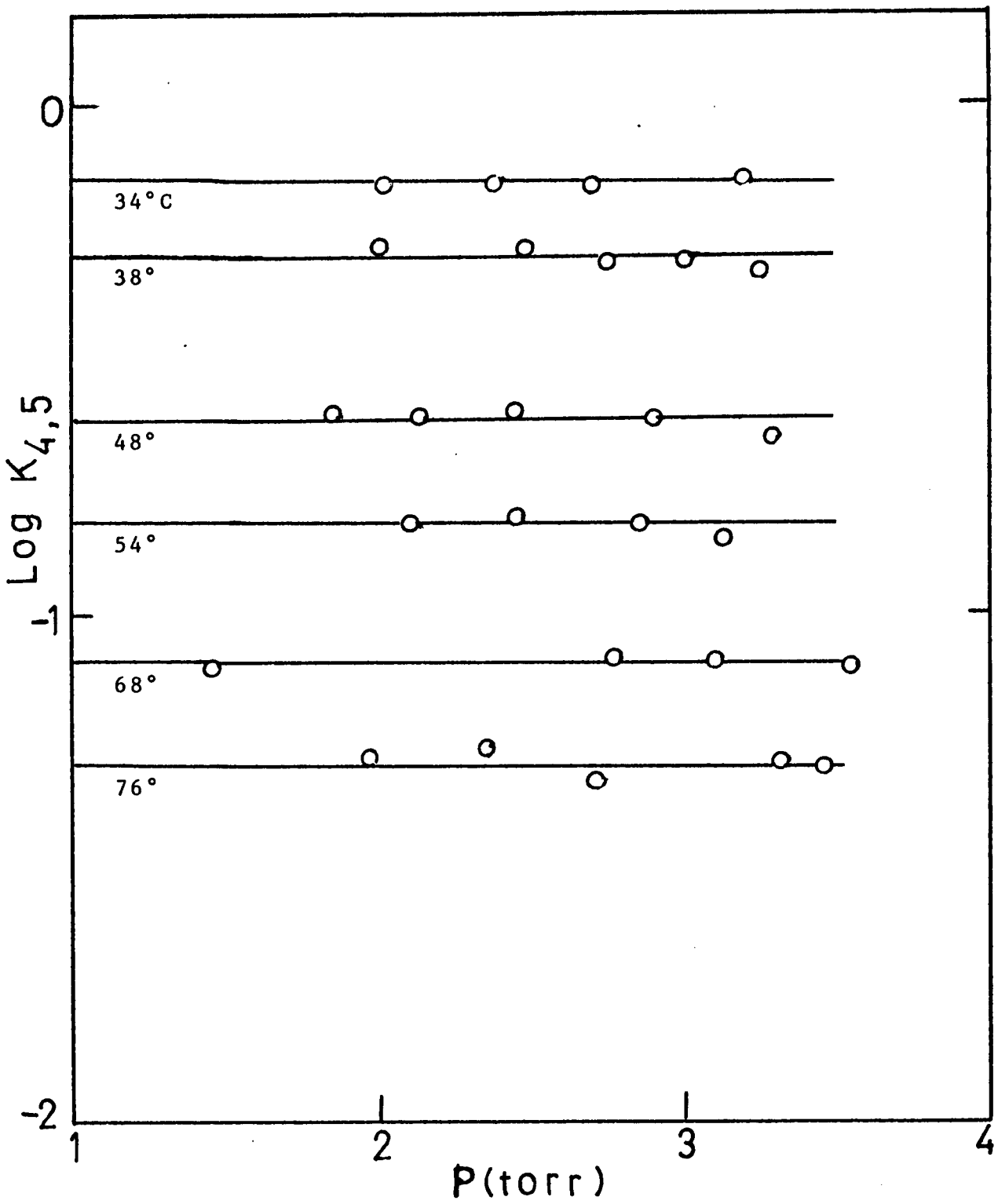

Figure 4-5: Plots of Log $K_{4,5}$ for the Gas Phase Hydration of F^-, at Various Temperatures, Versus Pressure of D_2O.

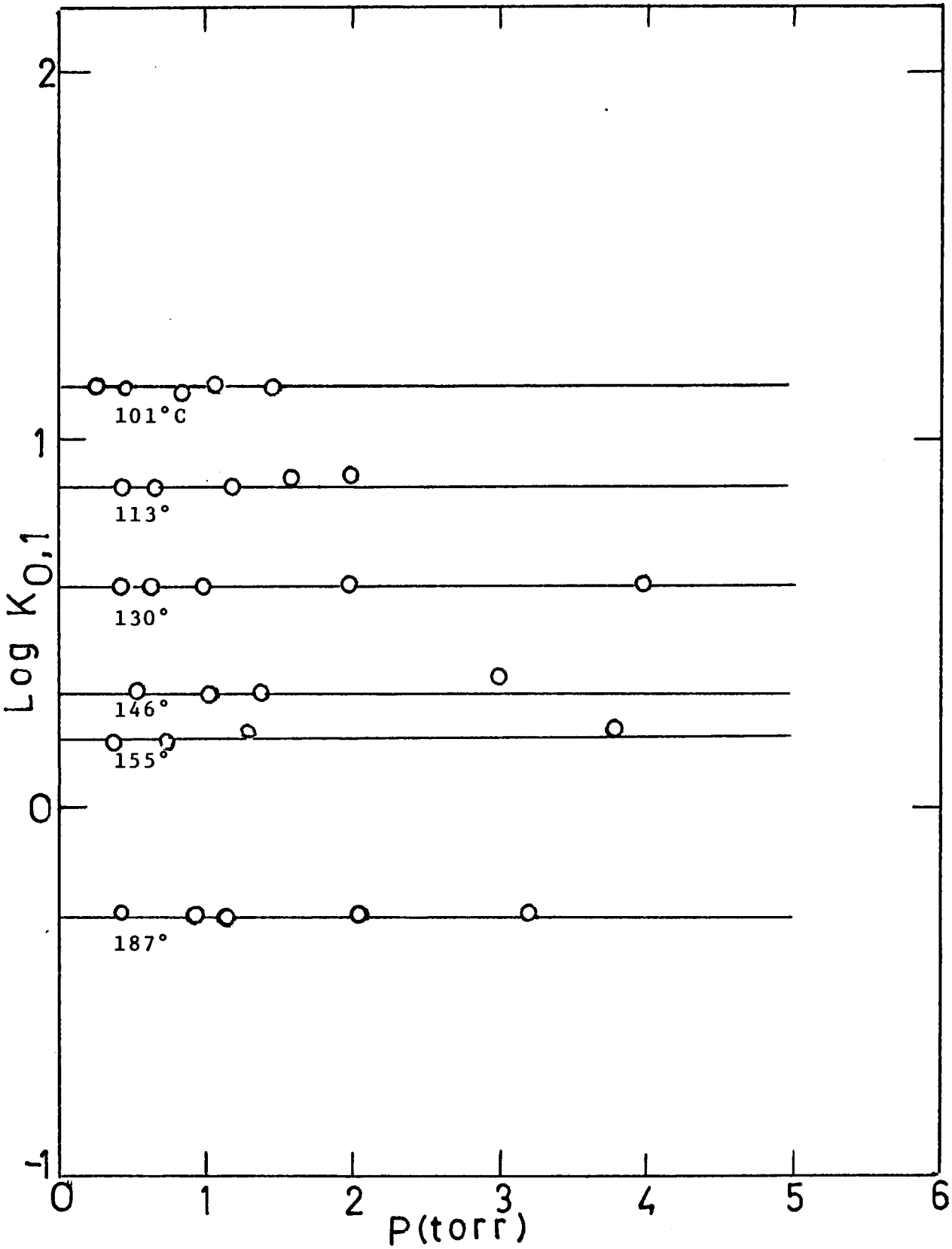

Figure 4-6: Plots of Log $K_{0,1}$ for the Gas Phase Hydration of Cl^- at Various Temperatures, Versus Pressure of H_2O.

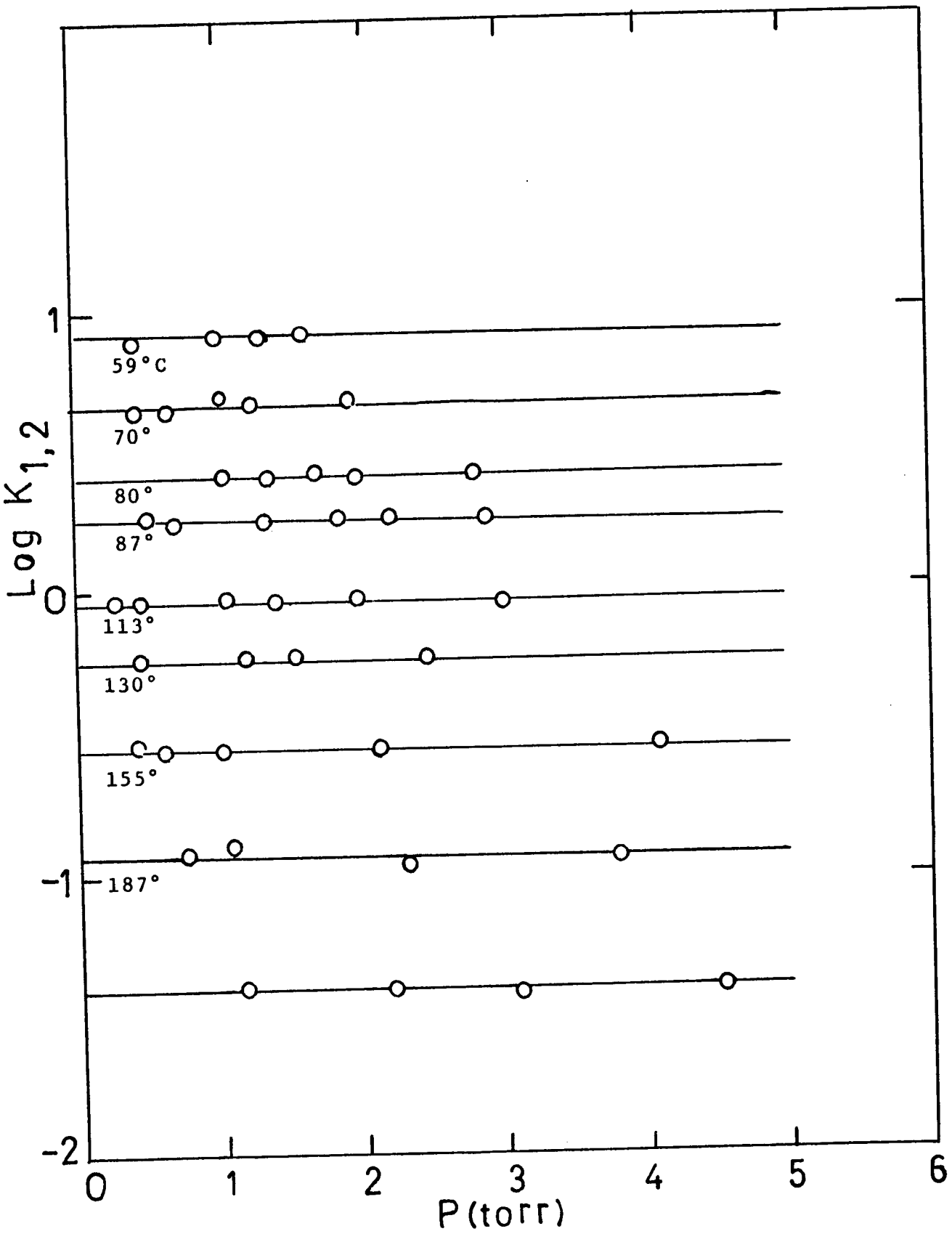

Figure 4-7: Plots of Log $K_{1,2}$ for the Gas Phase Hydration of Cl^-, at Various Temperatures, Versus Pressure of H_2O.

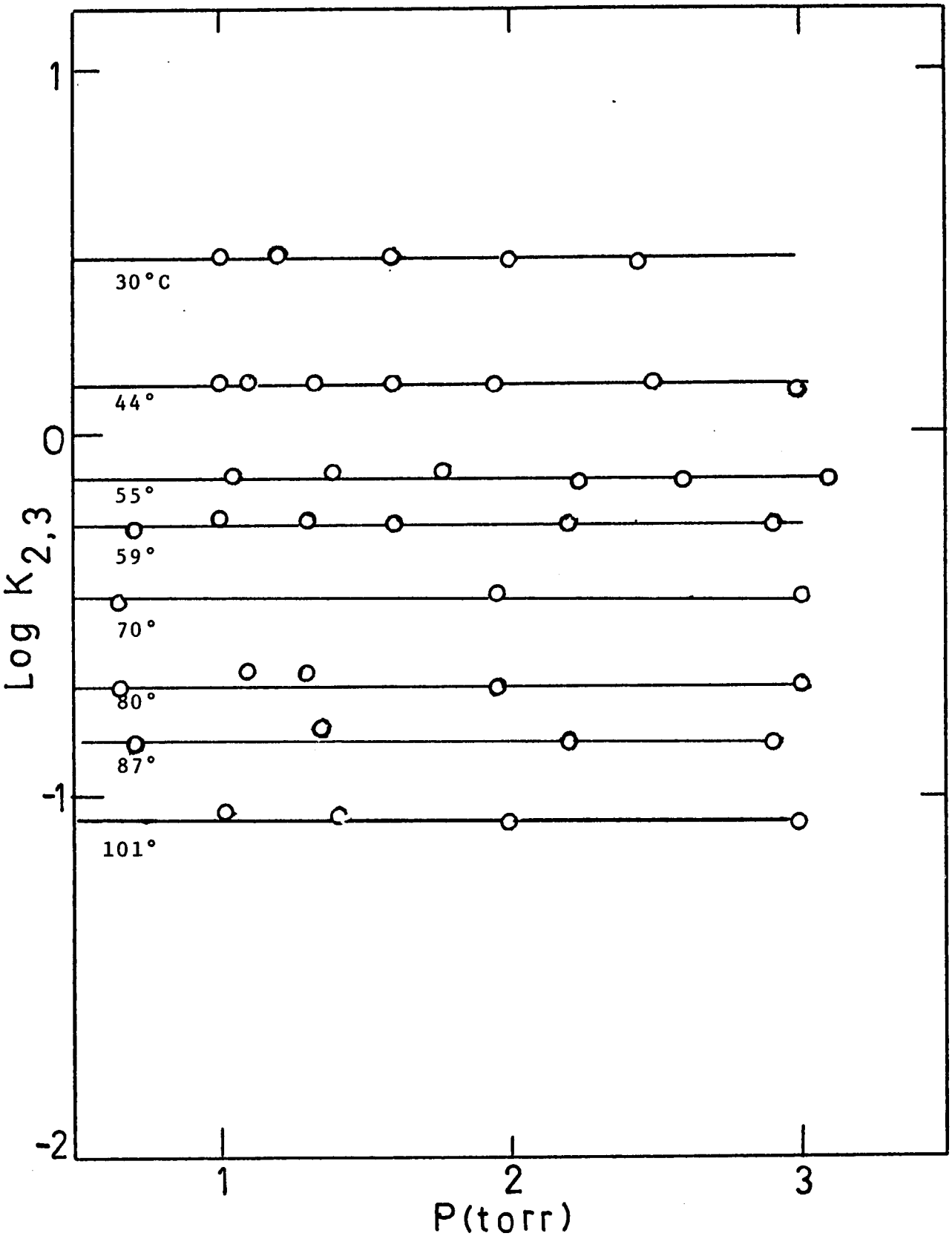

Figure 4-8: Plots of Log $K_{2,3}$ for the Gas Phase Hydration of Cl^- at Various Temperatures, Versus Pressure of H_2O.

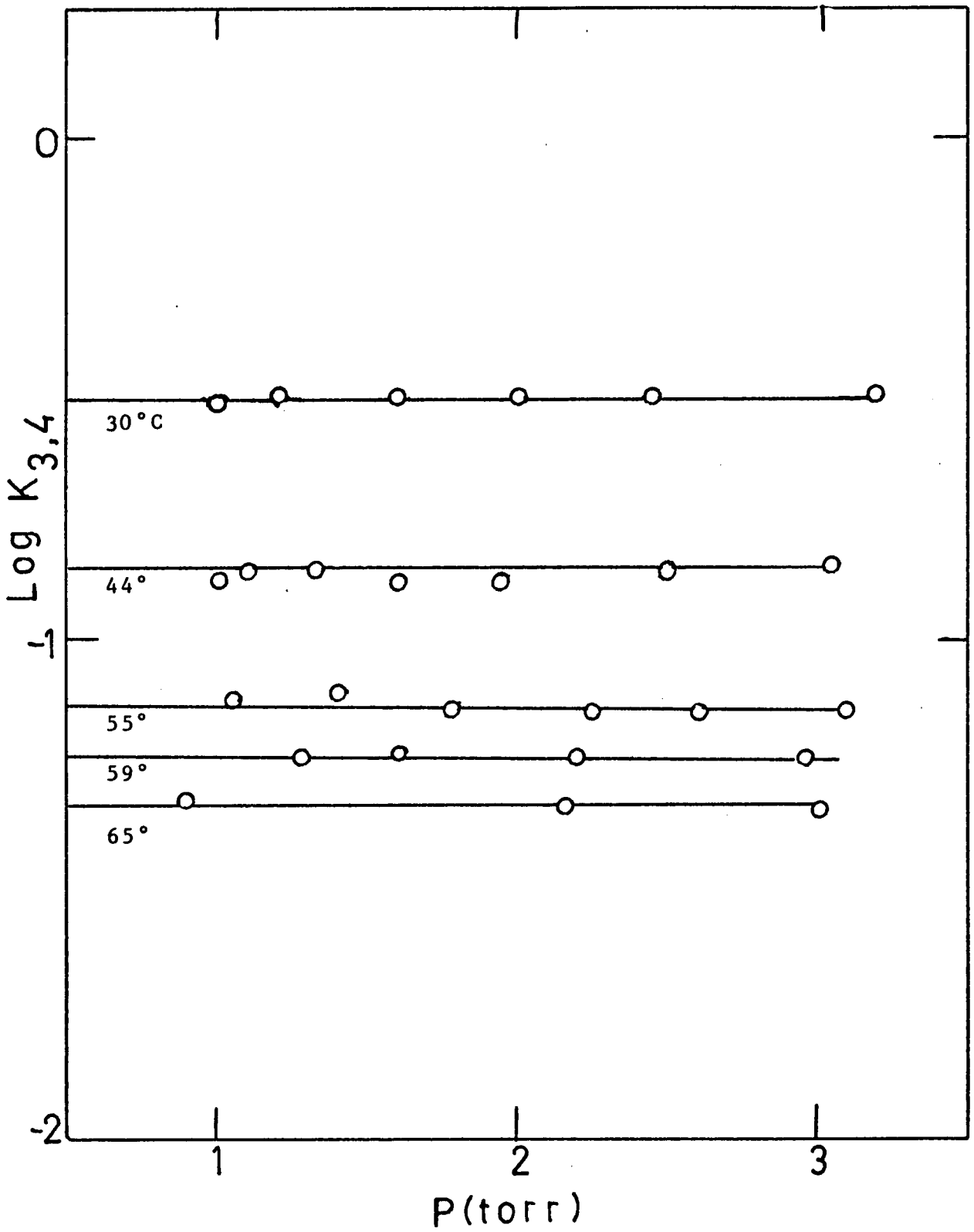

Figure 4-9: Plots of Log $K_{3,4}$ for the Gas Phase Hydration of Cl^- at Various Temperatures, Versus Pressure of H_2O.

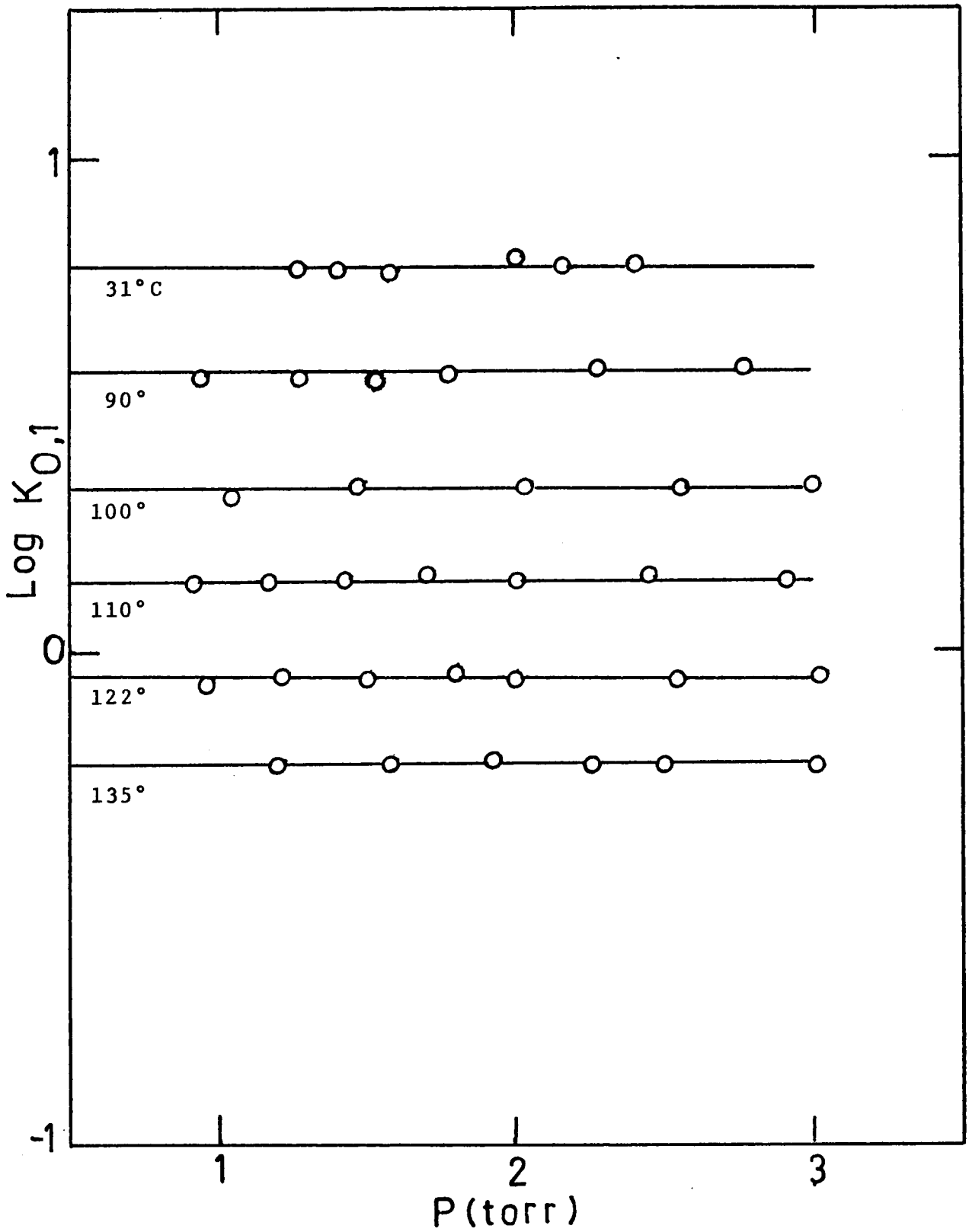

Figure 4-10: Plots of Log $K_{0,1}$ for the Gas Phase Hydration of Br^-, at Various Temperatures, Versus Pressure of H_2O.

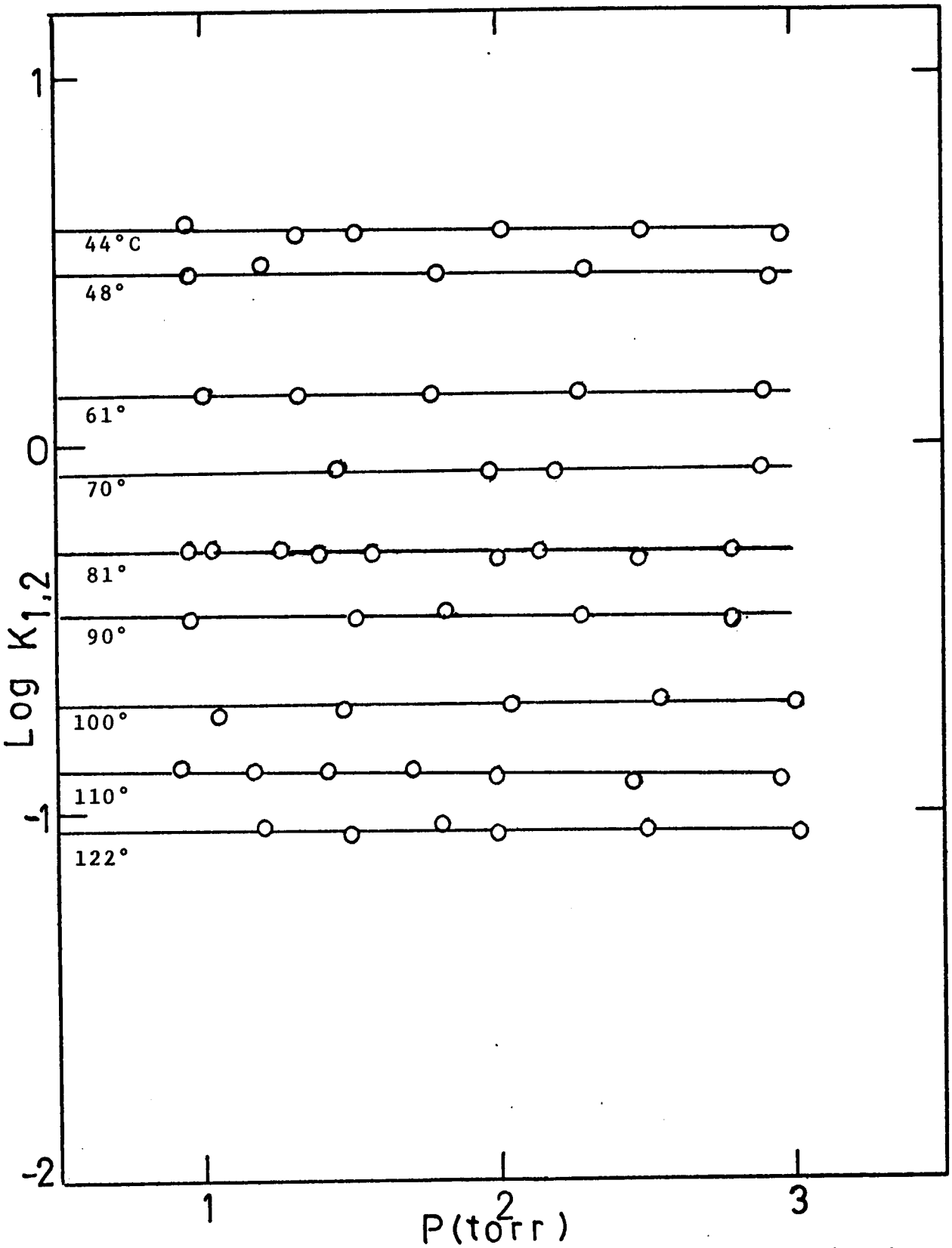

Figure 4-11: Plots of Log $K_{1,2}$ for the Gas Phase Hydration of Br^- at Various Temperatures, Versus Pressure of H_2O.

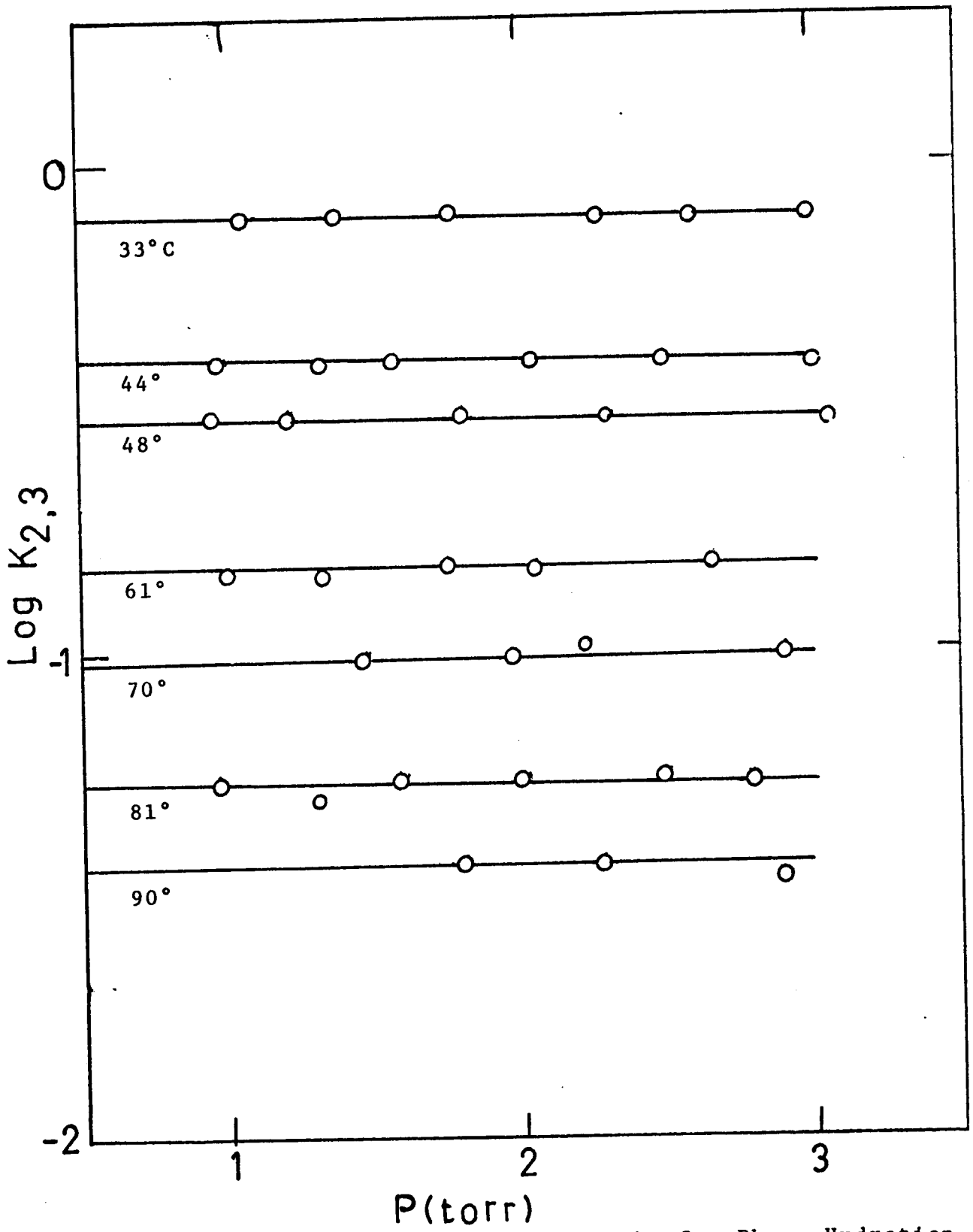

Figure 4-12: Plots of Log $K_{2,3}$ for the Gas Phase Hydration of Br^- at Various Temperatures, Versus Pressure of H_2O.

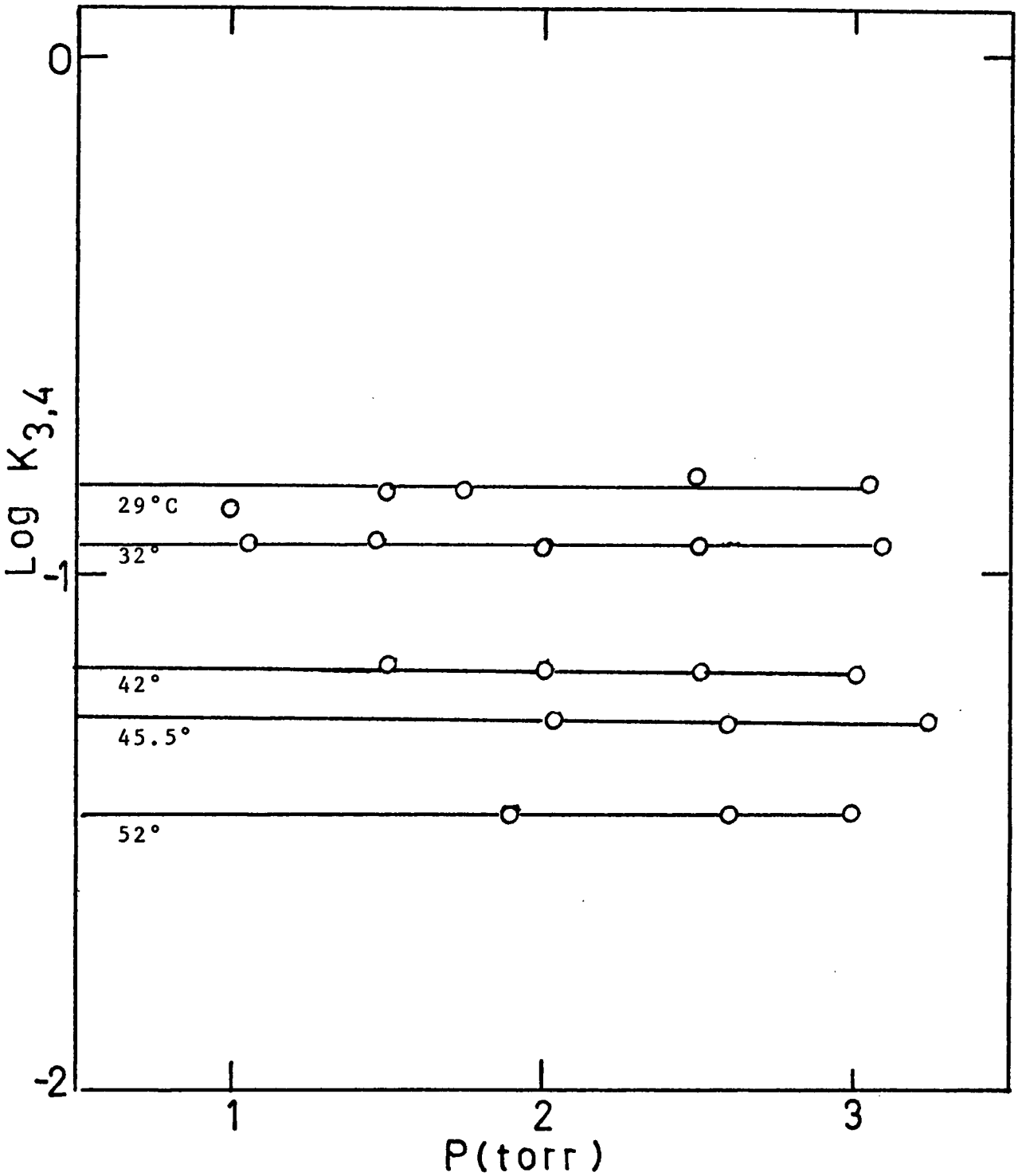

Figure 4-13: Plots of Log $K_{3,4}$ for the Gas Phase Hydration of Br^-, at Various Temperatures, Versus Pressure of H_2O.

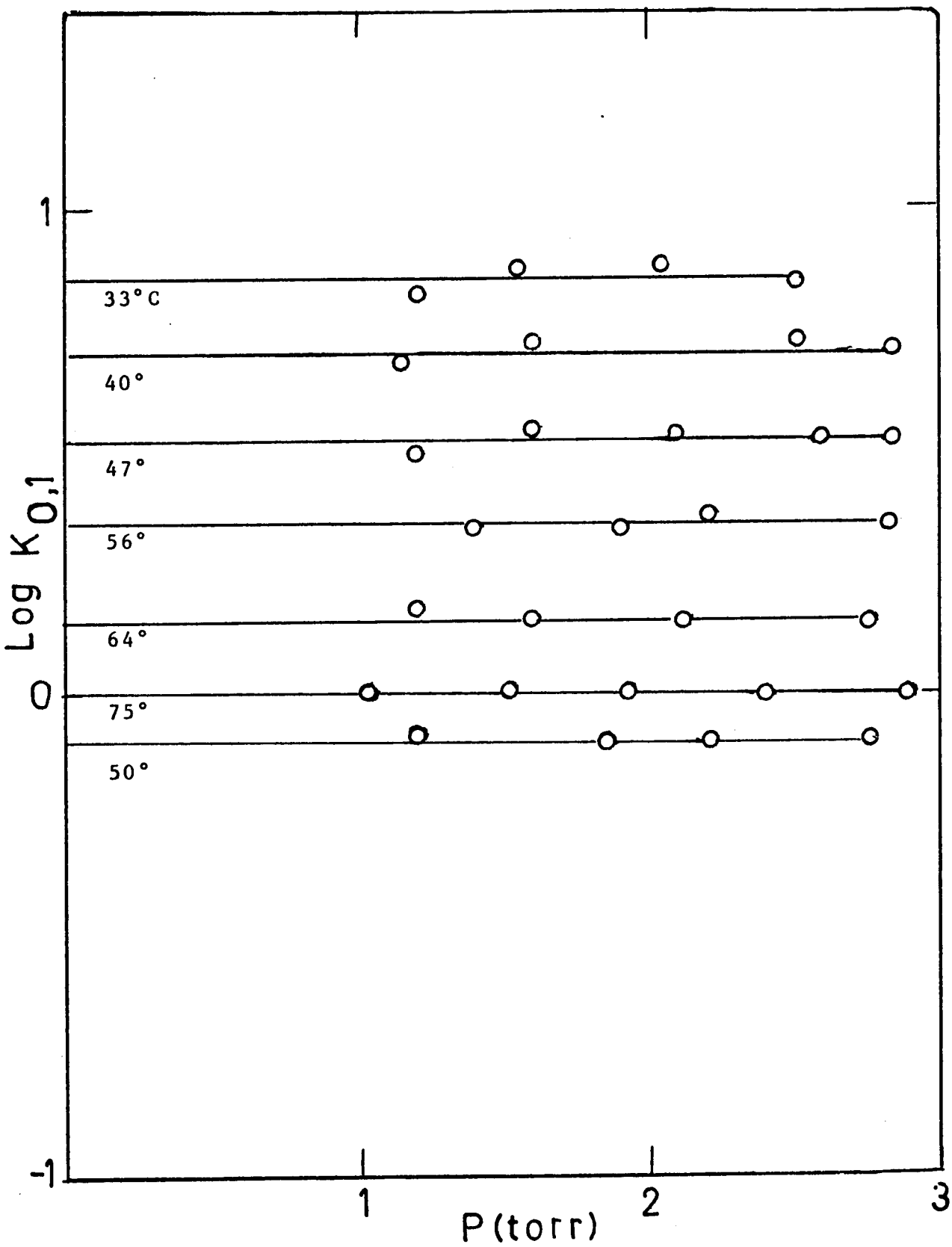

Figure 4-14: Plots of Log $K_{0,1}$ for the Gas Phase Hydration of I^-, at Various Temperatures, Versus Pressure of H_2O.

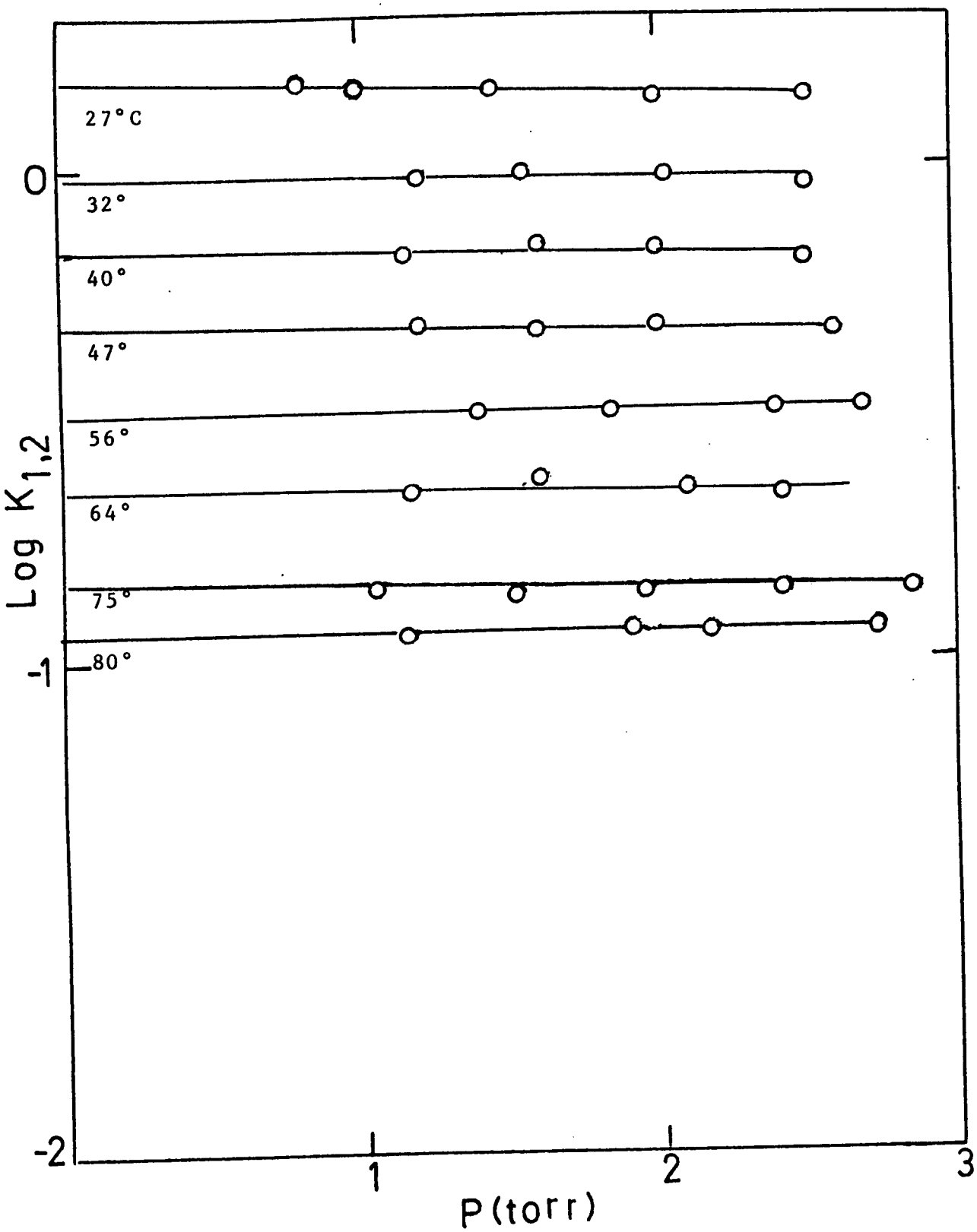

Figure 4-15: Plots of Log $K_{1,2}$ for the Gas Phase Hydration of I^-, at Various Temperatures, Versus Pressure of H_2O.

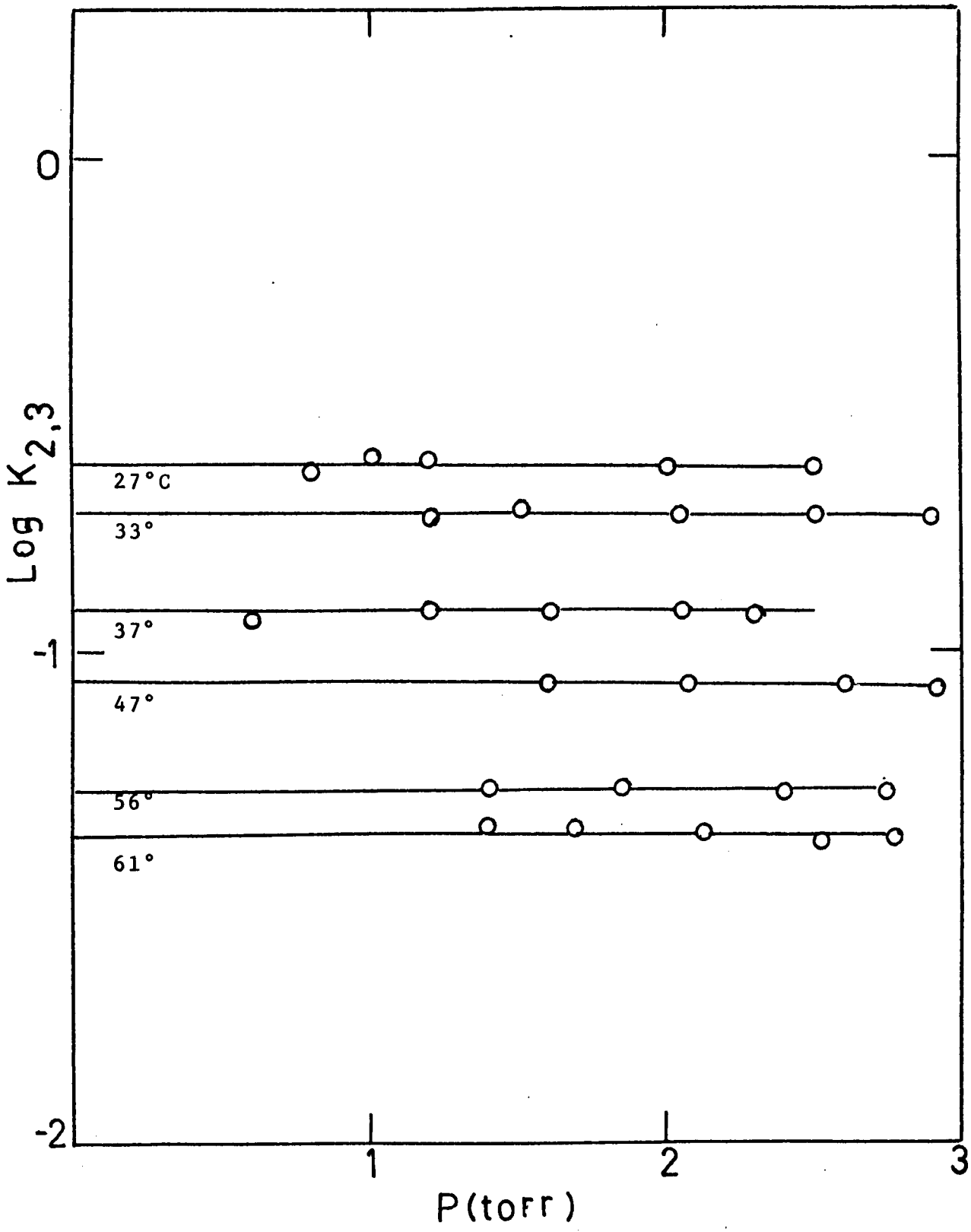

Figure 4-16: Plots of Log $K_{2,3}$ for the Gas Phase Hydration of I^-, at Various Temperatures, Versus Pressure of H_2O.

The Van't Hoff plots of the equilibrium constants are shown in figures (4-17) to (4-20). The equilibrium constants presented in these figures are, $K_{0,1}$ to $K_{4,5}$ for fluoride, $K_{0,1}$ to $K_{3,4}$ for chloride and bromide, and $K_{0,1}$ to $K_{2,3}$ for iodide ion clusters. From the least squares treatment of the values of $K_{n-1,n}$ measured at various pressures and temperatures, the slope of Van't Hoff line and, consequently, the change of enthalpy for the reaction

$$X^-(H_2O)_{n-1} + H_2O \rightleftharpoons X^-(H_2O)_n$$

was obtained. These values of $\Delta H^\circ_{n-1,n}$ as well as values of $\Delta G^\circ_{n-1,n}$ and $\Delta S^\circ_{n-1,n}$ at 298°K are presented in tables(4-1) to(4-4). In figure (4-21) the relative abundance of the cluster $X^-(H_2O)_n$, at the temperature of 292°K and one torr pressure, is plotted for F^-, Cl^-, Br^- and I^- ion clusters. This figure illustrates the effect of the ionic size on the extent of the gas phase hydration. As can be seen from this figure, as the size of the negative ion increases the number of water molecules attached to the halide ion decreases. Thus while it is possible to observe the cluster $F^-(H_2O)_5$ at room temperature and one torr water pressure; in order to be able to observe the cluster $I^-(H_2O)_5$, the ion source has to be cooled to about 250°K.

4.3 Calculation of Electrostatic Potential Energy of The Negative Ion Clusters

Theoretical electrostatic calculations of potential

Table 4-1

Experimental Thermodynamic Values for the Gas Phase Reaction

$$F^-(D_2O)_{n-1} + D_2O \rightleftharpoons F^-(D_2O)_n$$

Reaction	$-\Delta H_{n-1,n}$	$-\Delta G°_{n-1,n}(298°)$	$-\Delta S°^*_{n-1,n}$
n-1,n	Kcal/mole	Kcal/mole	e.u.
0,1	23.3	18.1	17.4
1,2	16.6	11.0	18.7
2,3	13.7	7.64	20.4
3.4	13.5	5.46	26.9
4.5	13.2	4.07	30.68

*Calculated for 298°K

Table 4-2

Experimental Thermodynamic Values for the Gas Phase Reactions

$$CI^-(H_2O)_{n-1} + H_2O \rightleftharpoons CI^-(H_2O)_n$$

Reaction	$-\Delta H_{n-1,n}$	$-\Delta G^\circ_{n-1,n}(298^\circ)$	$-\Delta S^{\circ *}_{n-1,n}$
n-1,n	Kcal/mole	Kcal/mole	e.u.
0,1	13.1	8.17	16.5
1,2	12.7	6.49	20.8
2,3	11.7	4.84	23.2
3,4	11.1	3.42	25.8

*Calculated for 298°K

Table 4-3

Experimental Thermodynamic Values for the Gas Phase Reaction

$$Br^-(H_2O)_{n-1} + H_2O \rightleftharpoons Br^-(H_2O)_n$$

Reaction	$-\Delta H_{n-1,n}$	$-\Delta G^\circ_{n-1,n}(298^\circ)$	$-\Delta S^{\circ *}_{n-1,n}$
n-1,n	Kcal/mole	Kcal/mole	e.u.
0,1	12.6	6.98	18.4
1,2	12.3	5.48	22.9
2,3	11.5	4.09	24.8
3,4	10.9	2.91	26.8

*Calculated for 298°K

Table 4-4

Experimental Thermodynamic Values for the Gas phase Reaction

$$I^-(H_2O)_{n-1} + H_2O \rightleftharpoons I^-(H_2O)_n$$

Reaction n-1,n	$-\Delta H_{n-1,n}$ Kcal/mole	$-\Delta G^\circ_{n-1,n}(298)$ Kcal/mole	$-\Delta S^{\circ *}_{n-1,n}$ e.u.
0,1	10.2	5.4	16.3
1,2	9.85	4.20	19.0
2,3	9.40	3.08	21.3

*Calculated for 298°K

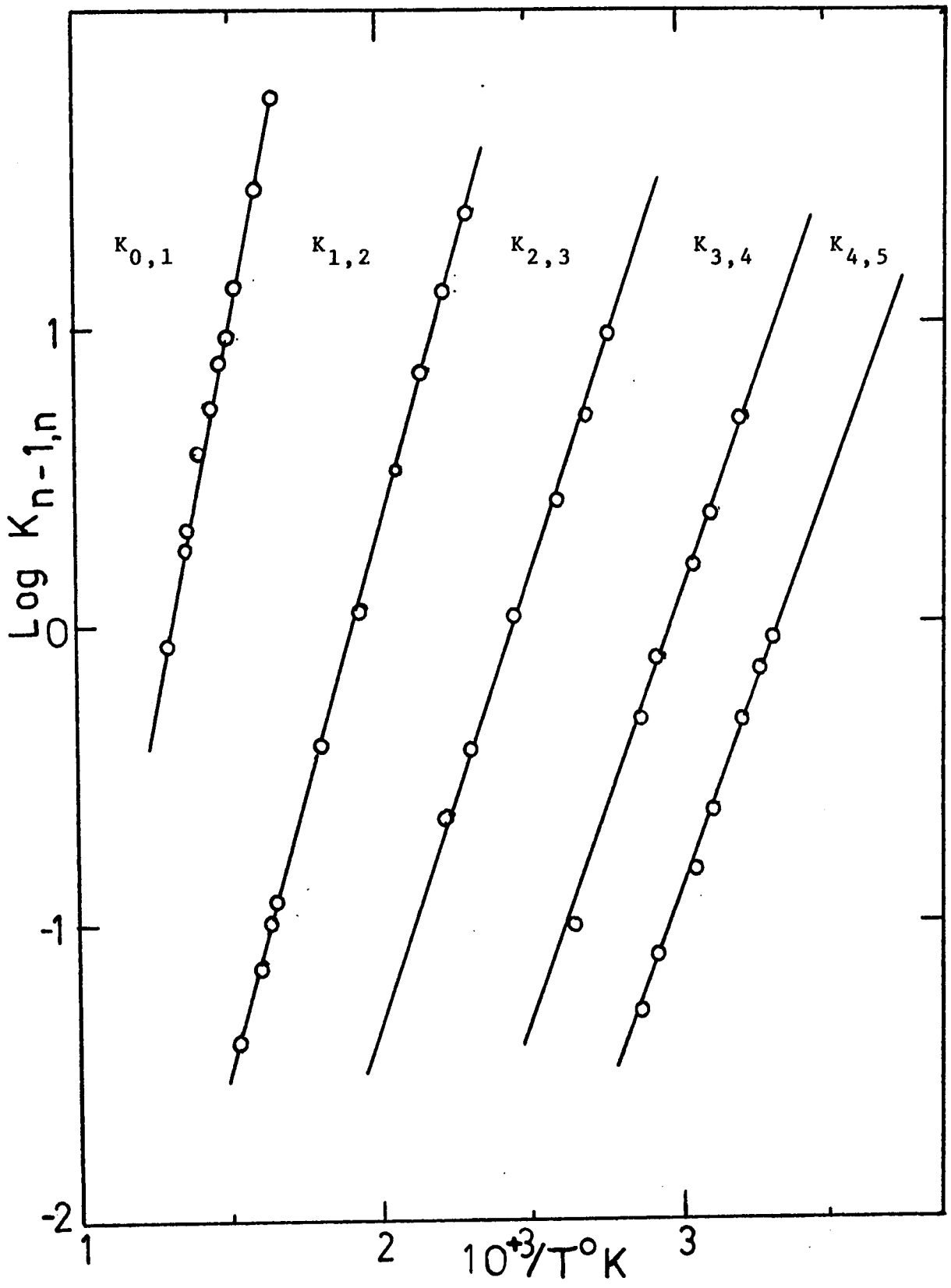

Figure 4-17: Van't Hoff-Type Plots of the Equilibrium Constants for the Gas Phase Hydration of F^-.

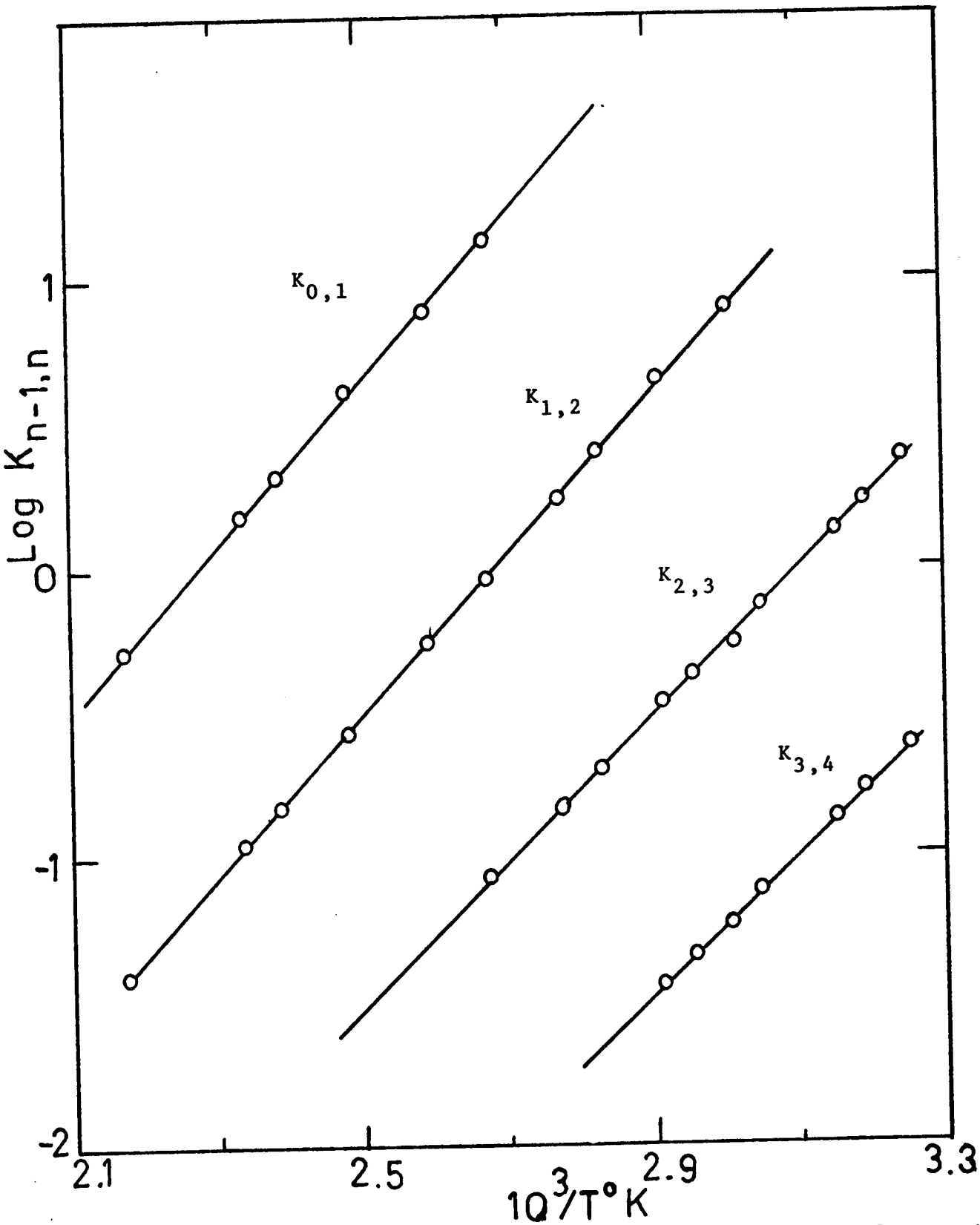

Figure 4-18: Van't Hoff-Type plots of the Equilibrium Constants, $K_{n-1,n}$ for the Gas Phase Hydration of Cl^-.

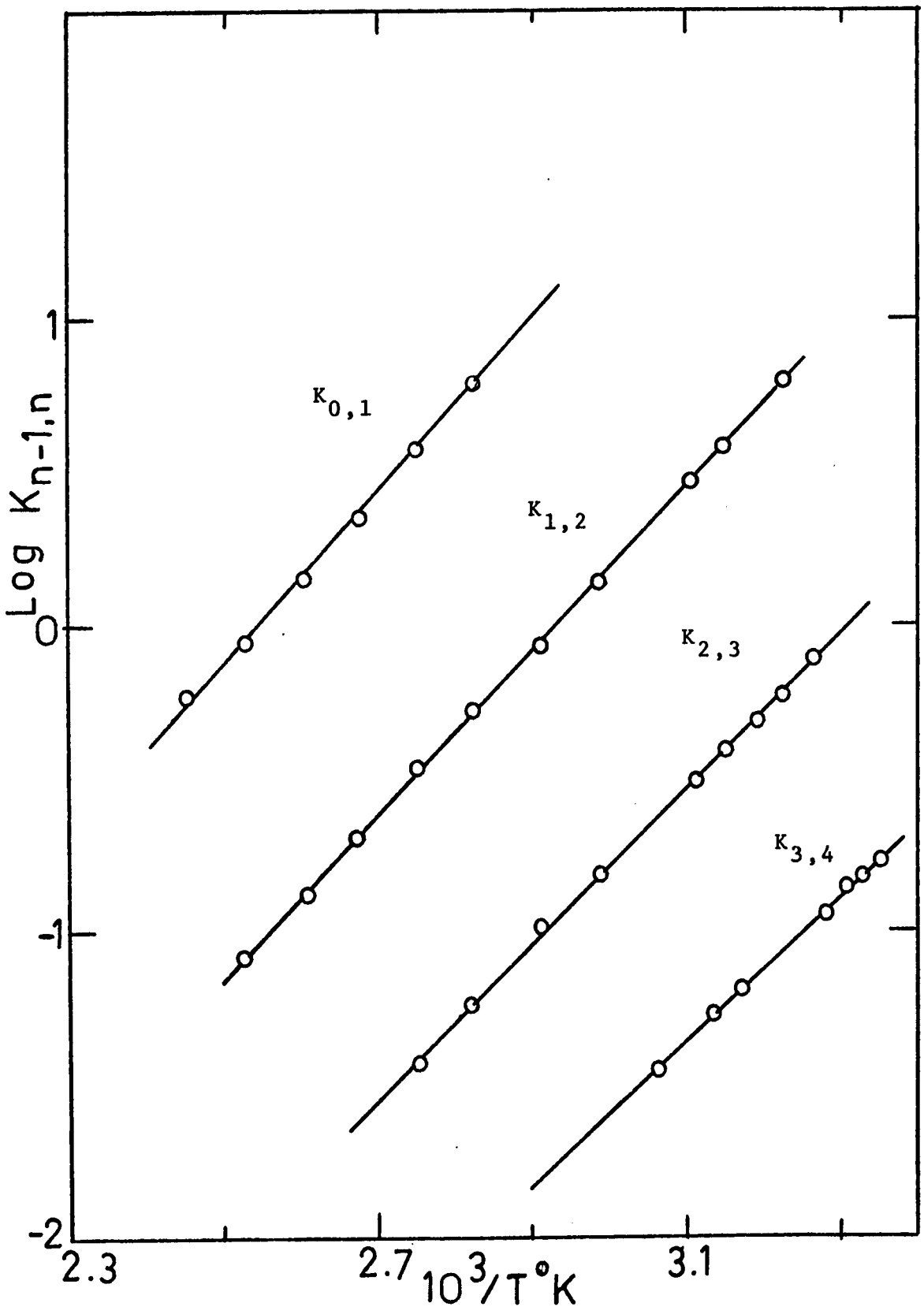

Figure 4-19: Van't Hoff-Type plots of the Equilibrium Constants, $K_{n-1,n}$ for the Gas Phase Hydration of Br^-.

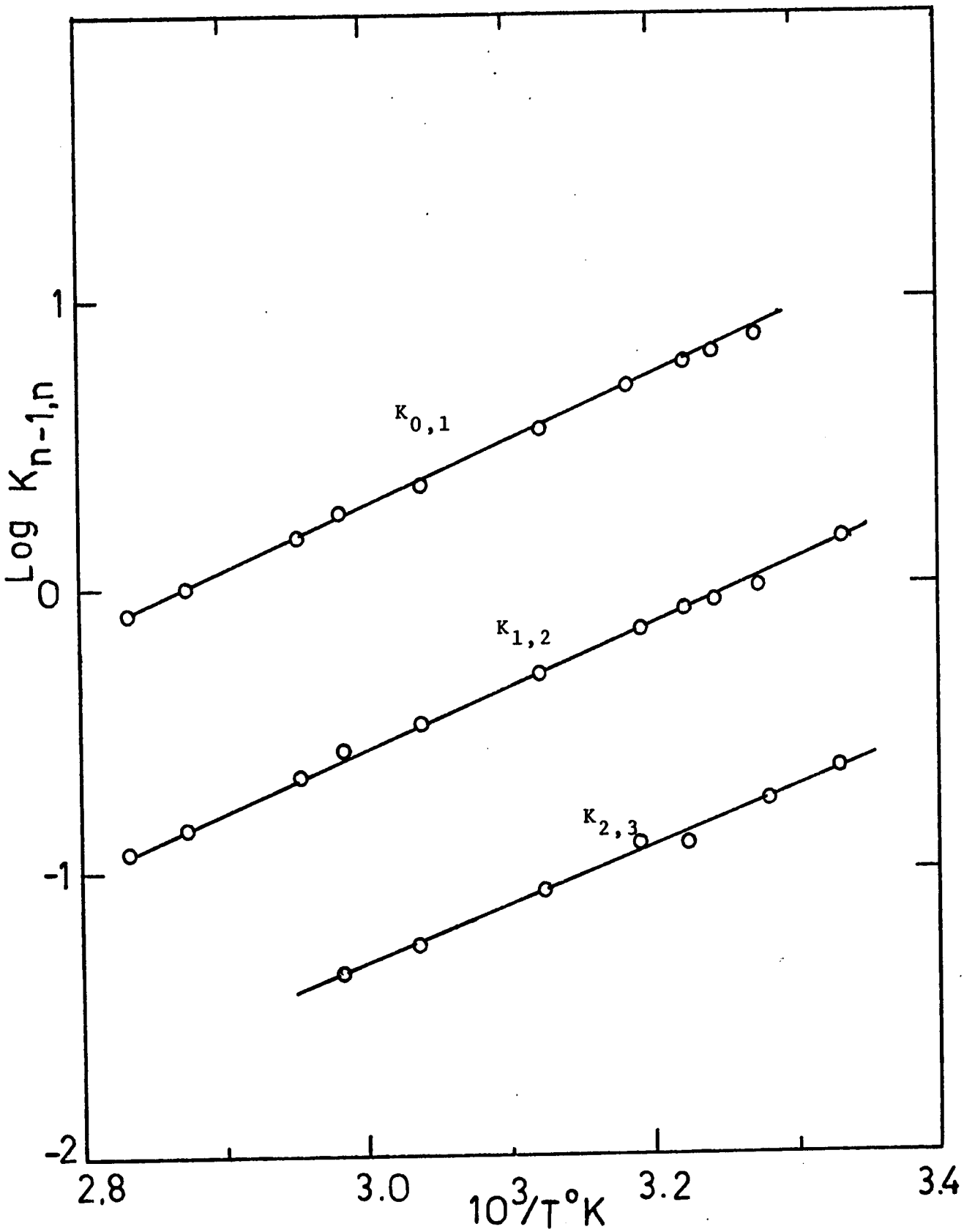

Figure 4-20: Van't Hoff-Type Plots of the Equilibrium Constants $K_{n-1,n}$ for the Gas Phase Hydration of I^-.

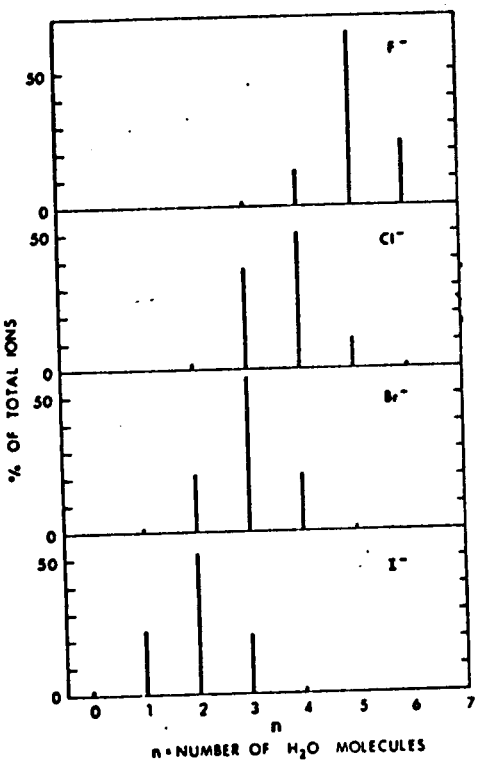

Figure 4-21: Experimentally Measured Equilibrium Distribution of Hydrates $X^-(H_2O)_n$ at one torr Water Pressure and 292°K, Showing Shift to Lower Hydration Number with Increase of Ionic Size.

energy of ion clusters have been carried out by a number of authors (34),(42),(43). Doyle and Caldwell (34) have applied this method to the system $H_3O^+(H_2O)_n$. Their calculation is based on a "point charge" model for water molecules. Thus they have assumed the electrostatic charges to be centered on the atomic nuclei of the water molecule, as it is shown in the figure (4-22). S. K. Searles (35) and I. Dzidic and P. Kebarle (24) have applied the same technique to calculate the potential energy of hydration of alkali positive ions. In the present work, Searles, Dzidic and Kebarle's method has been adopted for the calculation of potential energy of halide negative ions. It should be pointed out that these calculations are only approximations to the real bonding conditions and can not be expected to give accurate values of the actual energies involved. Nevertheless, reasonable conclusions can be drawn from a comparison of the results of this calculation with the experimental hydration energies.

In order to perform these calculation for negative ion hydration, we must select a reasonable "negative ion, water" configuration. There are two such configurations possible. In one, the negative ion, X^-, is located on the bisector of HOH angle (X^-——O^H_H) and in the other model, the negative ion is on the O-H bond axis (X^-——H—O^H).

The potential energy, E, relative to that of the

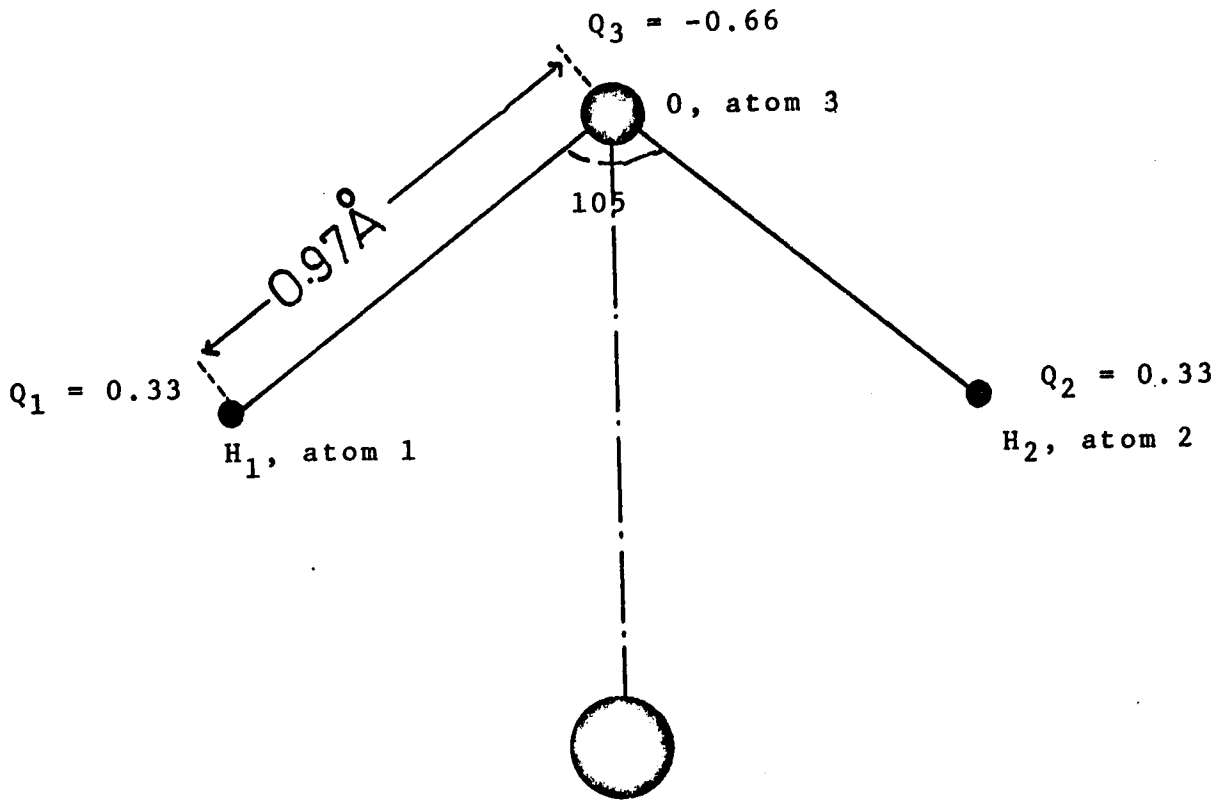

Figure 4-22: H_2O "Point Charge" Model used in Theoretical Calculation.

halide and water molecules at infinity, of an ion cluster, can be written as

$$(4\text{-}4) \quad E = E_{ID} + E_{IP} + E_{DD} + E_{DS} + E_{RP}$$

Here E_{ID} represents the attraction energy between the central ion and the permanent dipole of the ligand molecules, E_{IP} represents the attraction energy due to the polarization of the ligand molecules by central ion, E_{DD} represents the dipole-dipole repulsion energy between the ligand molecules, E_{DS} represent the dispersion energy between the central ion and ligands as well as the dispersion energy between the various ligands, and finally, E_{RP} represents the ion-ligand repulsion energy. The dipole-dipole repulsion energy can be further divided into three components: permanent dipole-permanent dipole repulsion, induced dipole-induced dipole repulsion, and induced dipole-permanent dipole repulsion. The following equations were used (35), (37) to calculate the various contribution to the total energy:

Ion-Dipole

$$(4\text{-}5) \quad E_{ID} = \sum_{j=1}^{n} \sum_{i=1}^{p} \frac{(334)(Q_{ion})(Q_{i,j})}{R_{i,j}}$$

Ion Polarizability

$$(4\text{-}6) \quad E_{IP} = - \sum_{j=1}^{n} \sum_{i=1}^{p} \frac{(167)(Q_{ion})^2 \alpha_{i,j}}{R_{i,j}^4}$$

Permanent Dipole - Permanent Dipole

$$(4\text{-}7) \quad E_{PD} = \sum_{l=2}^{n} \sum_{i=1}^{p} \sum_{j=1}^{l-1} \sum_{k=1}^{p} \frac{(334)(Q_{i,i})(Q_{k,l})}{R_{i,j,k,l}}$$

Induced Dipole - Induced Dipole

$$(4\text{-}8) \quad E_{II} = \sum_{j=1}^{n-1} \sum_{m=j+1}^{n} \frac{14.397\alpha_M^2 e^2}{R_{ion,j}^4 S_{j,m}^3} (1+\cos^2\theta_{j,m})$$

Induced Dipole - Permanent Dipole

$$(4\text{-}9) \quad E_{IPD} = \sum_{j=1}^{n-1} \sum_{m=j+1}^{n} \frac{28.794 P \alpha_M e}{R_{ion,j}^2 S_{j,m}^3} (1+\cos^2\theta_{j,m})$$

Dispersion

$$(4\text{-}10) \quad E_{DD} = \sum_{j=1}^{n-1} \sum_{m=j+1}^{n} \frac{17.28\alpha_M^2 I_{PM}}{S_{j,m}^6} + \sum_{j=1}^{n} \frac{(34.56)\alpha_{ion}\alpha_M (I_{PI} \cdot I_{PM})}{R_{ion,j}^6 (I_{PI} + I_{PM})}$$

Ion-ligand Repulsion

$$(4\text{-}11) \quad E_{rep} = \sum_{j=1}^{n} \sum_{i=1}^{p} \frac{A_{i,j}}{R_{i,j}^{12}}$$

Q_{ion} is the ionic charge, $Q_{i,j}$ is the charge on the $i^{\underline{th}}$ atom of the $j^{\underline{th}}$ molecule with p atoms per molecule and n molecules per cluster. α is the atomic polarizability and α_M the polarizability of the water molecule. $R_{i,j}$ is the ion-atom distance and $R_{i,j,k,l}$ is the distance between the $i^{\underline{th}}$ atoms of $j^{\underline{th}}$ molecule and $k^{\underline{th}}$ atom of the $i^{\underline{th}}$ molecule. $S_{j,m}$ is the distance of the $j^{\underline{th}}$ molecule from the $m^{\underline{th}}$ molecule in the cluster and $R_{ion,j}$ is the distance between the central ion and $j^{\underline{th}}$ molecule, and finally, θ is the angle between the induced dipole and the axis of the water molecule and P is the permanent dipole moment of

water (1.84 Debye). "A" is a semi-empirical constant whose evaluation will be given in the next paragraph. The numerical factors in the above equations are adjusted to give the energy in Kcal/mole for values of Q in atomic units and R and S in A°. The polarizability of oxygen, hydrogen, and the water molecule were taken as 0.60, 0.44, and 1.44$A^{\circ 3}$ respectively (35). The ionization potentials of the negative ions were taken as the electron affinities of the parent atom and are 3.57 eV for fluoride, 3.76 eV for chloride, 3.54 eV for bromide, and 3.29 eV for iodide ion (48). The value 12.56 eV was used for the ionization potential of water (43). The calculation of potential energy was done by means of an IBM 360 computer. The program used was taken from the work of S. K. Searles (35) and adapted for the negative ions calculation by Dr. R. Yamdagni, Department of Chemistry, University of Alberta.

For determination of values of the constant "A", the following procedure was adapted. The values of "A" for repulsion between two atoms of inert gases Ne, Ar, Kr and Xe were calculated by the equation

$$A = 4\varepsilon\sigma^{12} \qquad (4\text{-}12)$$

ε is the depth of potential well and σ is the inter-atomic distance for zero potential energy. The values of ε and σ taken from literature (39), (40) as well as values of "A" calculated from the equation (4-12) are presented in table

(4-5). The square root of these values of "A" for the inert gases were plotted versus the atomic radii, figure (4-23) obtained from reference (46). Using the experimental radii of the negative ions obtained by Gourary and Adrian (48) and the Bohr hydrogen radius, values of $A^{1/2}$ for halide negative ions as well as hydrogen atom were obtained from the plot of figure (4-23). The constant "A" for repulsion between individual halide negative ions and the hydrogen atom of the water molecule was then assumed to be:

$$A_{X^-,\ H} = A_H^{1/2} \cdot A_{X^-}^{1/2}$$

For the clusters with more than one water molecules many different structures are possible. For the purpose of these calculations, the most symmetrical ligands arrangements were assumed. In other words, the clusters with two water molecules were assumed to be linear with negative ions placed equidistant between two water molecules. Three molecular clusters were assumed to have trigonal structure with negative ions in the centre, four molecular clusters have tetrahedral structure, clusters with five water molecules were considered to have bipyramidal and those with six water molecules were assumed to be octahedral. The final results of the classical electrostatic calculations for different halide negative ions and for two different arrangements, symmetric $X^-\!\!-\!\!\begin{smallmatrix}H\\H\end{smallmatrix}\!\!>\!O$ and asymmetric $X^-\!\!-\!\!H\!-\!\!O\!\!<^{H}$, are given in table (4-6).

Table 4-5

The Coefficient "A" for Repulsion Term (A/R^{12}) between Two atoms of the Inert Gases from Equation $A=4\varepsilon\sigma^{12}$

	ε Electron-Volt	σ A°	A KCal-A°12
Neon-Neon	$3.129X10^{-3}$	2.82	$7.30X10^{5}$
Argon-Argon	$1.036X10^{-2}$	3.44	$2.62X10^{6}$
Krypton-Krypton	$1.41X10^{-2}$	3.827	$1.29X10^{7}$
Xenon-Xenon	$1.84X10^{-2}$	4.22	$5.93X10^{7}$

ε is the depth of the potential well

σ is the inter-atomic distance for zero potential energy

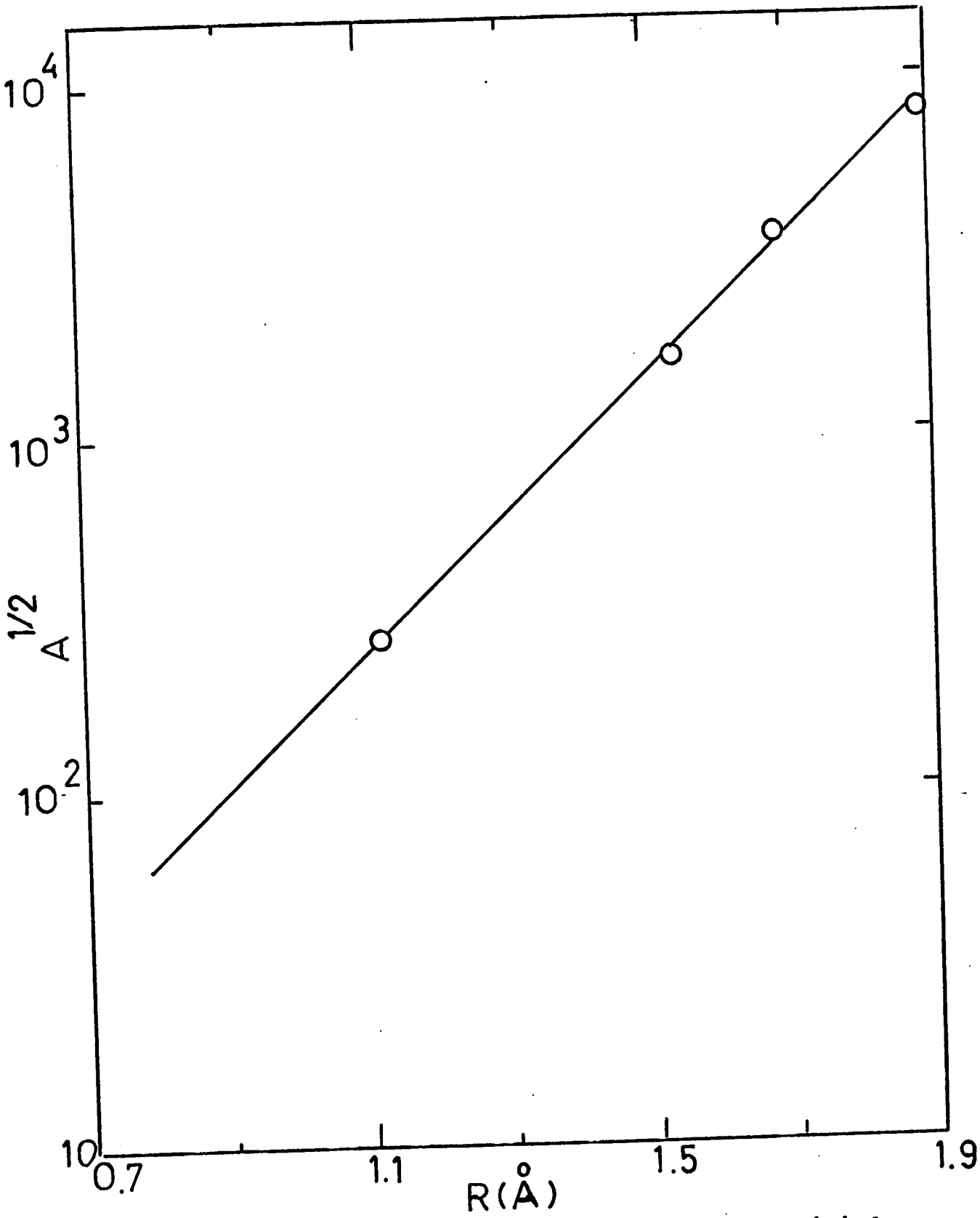

Figure 4-23: Square Root of Repulsion Coefficient 'A' for Noble Gases as a Function of Atomic Radii.

4.4 Comparison of Calculated and Experimental Hydration Energies

The theoretical $\Delta E_{n-1,n}$ calculated from equation (4-4) along with the experimentally determined $\Delta H_{n-1,n}$ for halide negative ions are plotted in figures (4-24) to (4-31). Comparison between the calculated values of $\Delta E_{n-1,n}$ based on the two different arrangements of the water molecules around the negative ion indicates that initially the symmetric arrangement is more favorable but the asymmetric arrangement becomes more favorable for the clusters with more than about three water molecules. This is due to the closeness of the ligand molecules in the symmetric arrangement, and thus, a larger contribution from the dipole-dipole repulsion terms (equations 4-7, 4-8, 4-9). The dipole-dipole repulsion term, of course, does not exist in the cluster $X^-(H_2O)$, but as more water molecules are added, the effect of dipole-dipole repulsion energy becomes more pronounced. Evidently, when the fourth water molecule is added the dipole repulsion energy becomes strong enough to cause a change from a symmetrical to an asymmetrical arrangement of the water molecules in the complex. Table (4-6) shows that the absolute values of $\Delta E_{0,1}$ calculated on the basis of the symmetric arrangements, are higher than $\Delta H_{0,1}$, determined experimentally, by about 20 to 30% depending on the halogen under consideration. Of course the possibility

Table 4-6

Calculated and Experimental Values of Energy Change for Reaction

$$X^-(H_2O)_{n-1} + H_2O \rightleftharpoons X^-(H_2O)_n$$

	$-\Delta E_{0,1}$ Kcal/mole		$-\Delta H_{0,1}$ Kcal/mole	$-\Delta E_{1,2}$ Kcal/mole		$-\Delta H_{1,2}$ Kcal/mole	$-\Delta E_{2,3}$ Kcal/mole		$-\Delta H_{2,3}$ Kcal/mole	$-\Delta E_{3,4}$ Kcal/mole		$-\Delta H_{3,4}$ Kcal/mole	$-\Delta E_{4,5}$ Kcal/mole		$-\Delta H_{4,5}$ Kcal/mole	$-\Delta E_{5,6}$ Kcal/mole		$-\Delta H_{5,6}$ Kcal/mole
	Symm	Asym	Expt	Symm	Asym	Expt	Symm	Asym	Expt	Symm	Asym	Expt	Symm	Asym	Expt	Symm	Asym	Expt
F^-	29.8	19.1	23.3	25.4	18.6	16.6	17.8	16.1	13.7	11.9	14.4	13.5	4.21	13.1	13.2		11.7	
Cl^-	18.6	12.0	13.1	17.0	11.6	12.7	13.9	10.5	11.7	11.6	9.80	11.1	7.25	9.22		2.36	8.42	
Br^-	16.0	10.4	12.6	14.8	10.0	12.3	12.5	9.2	11.5	10.8	8.62	10.9	7.25	8.28		2.60	7.58	
I^-	12.3	8.0	10.2	11.5	7.9	9.85	10.2	7.3	9.40	9.12	6.92		6.65	6.66		3.88	6.21	

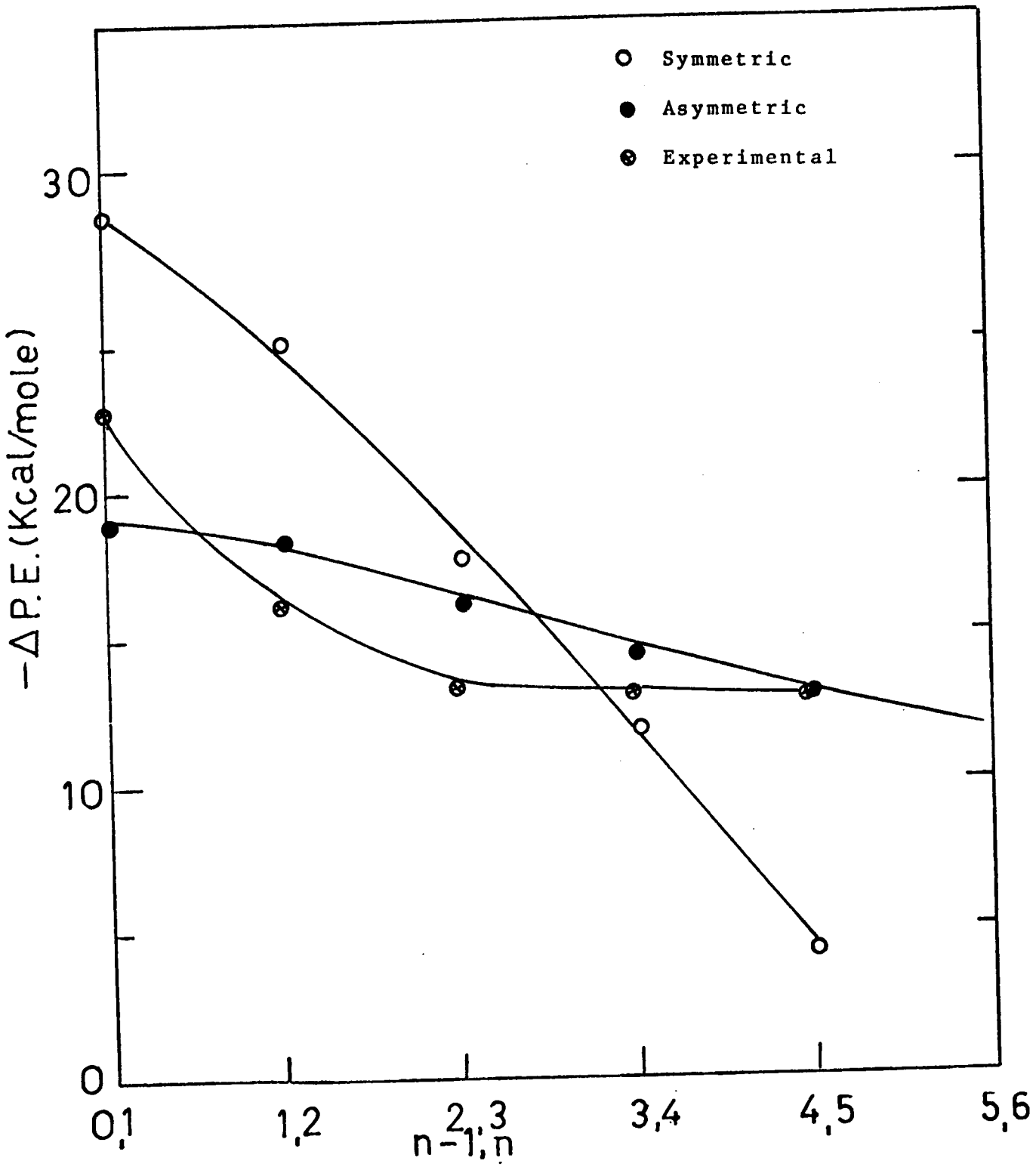

Figure 4-24: Plots of Change of Potential Energy for Cluster $F^-(D_2O)_{n-1,n}$ Versus n-1,n.

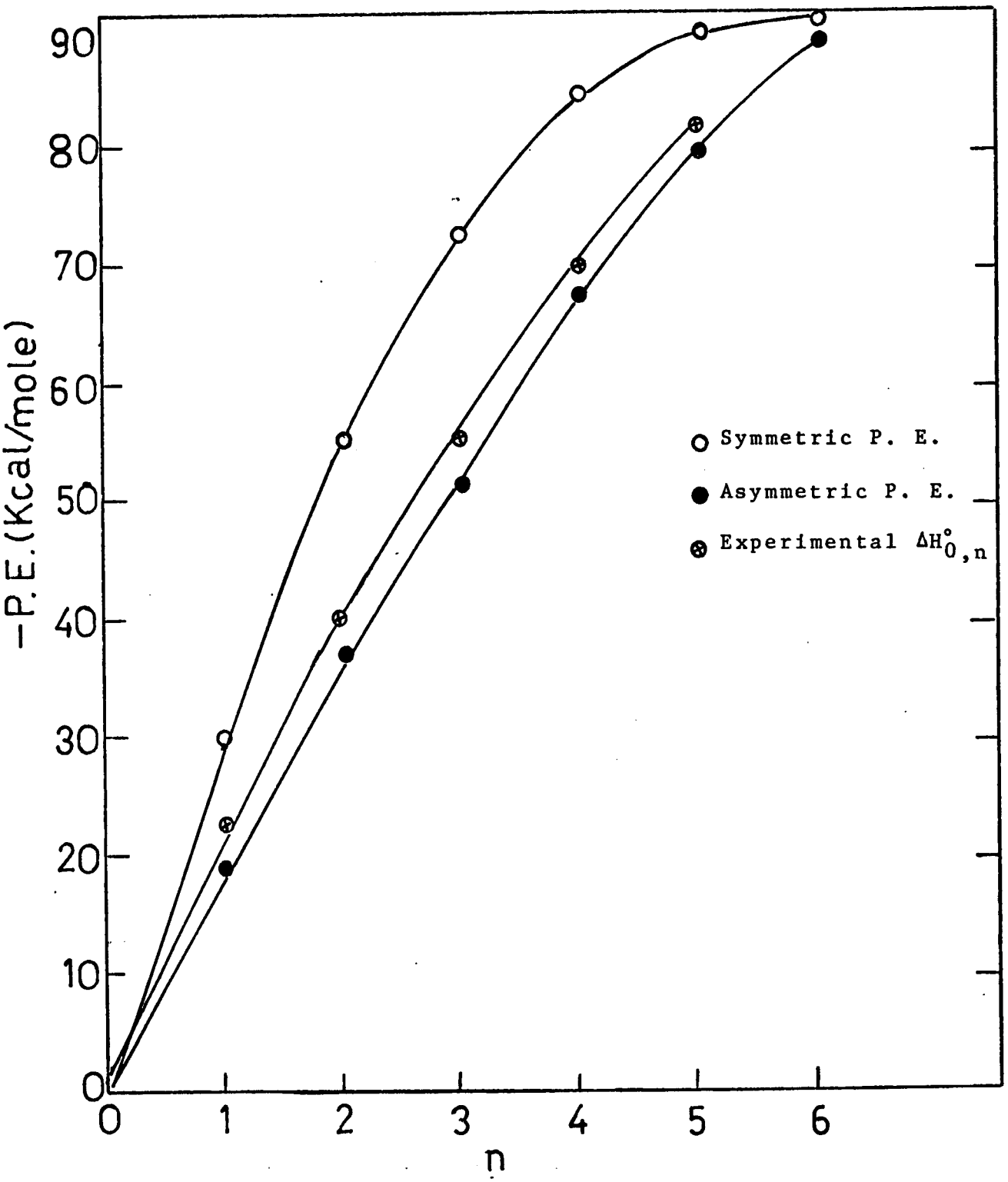

Figure 4-25: Plots of Potential Energy for Cluster $F^{-}(D_2O)_n$ Versus n.

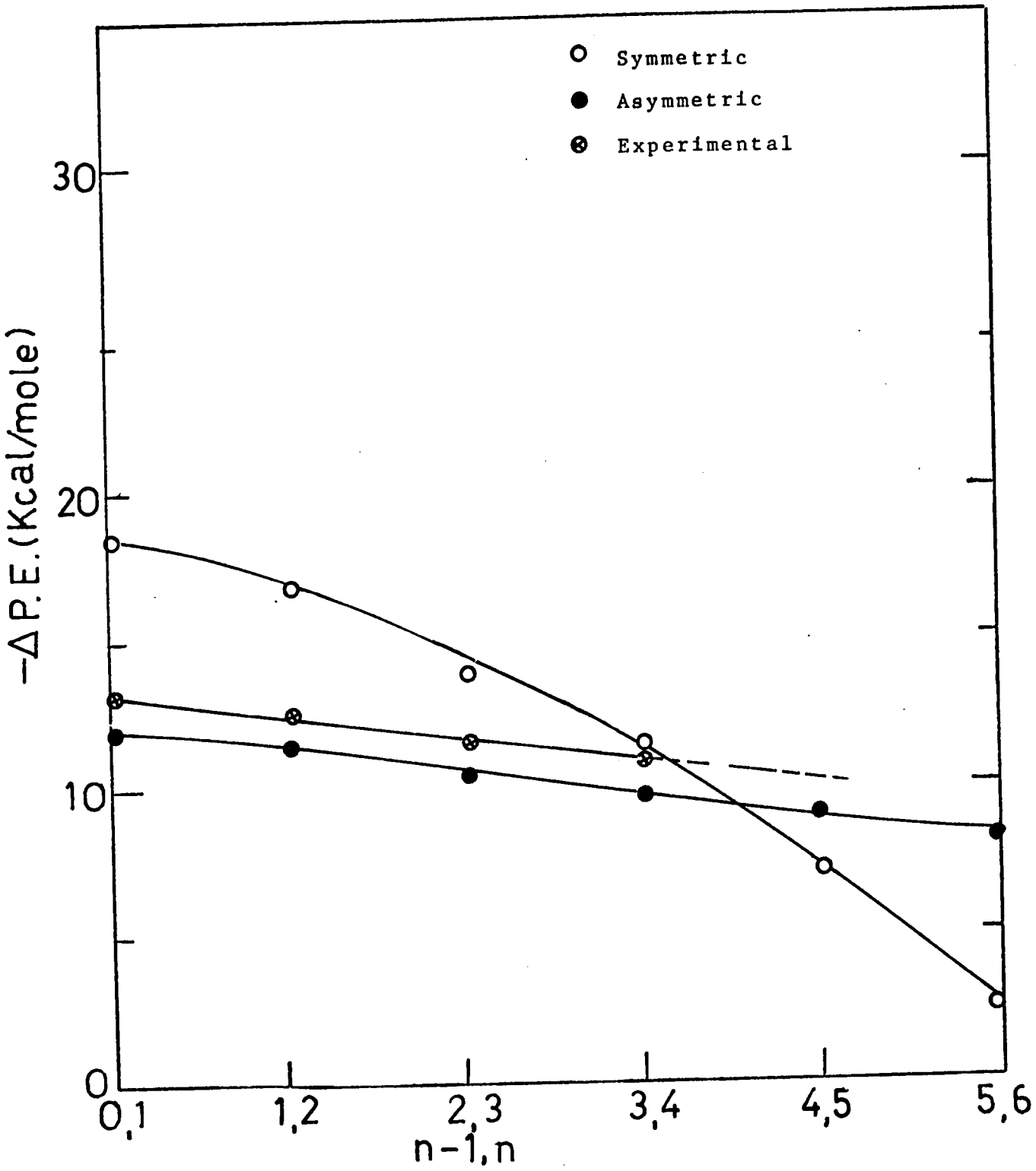

Figure 4-26: Plots of the Change of Potential Energy for Cluster $Cl^-(H_2O)_{n-1,n}$ Versus n-1,n.

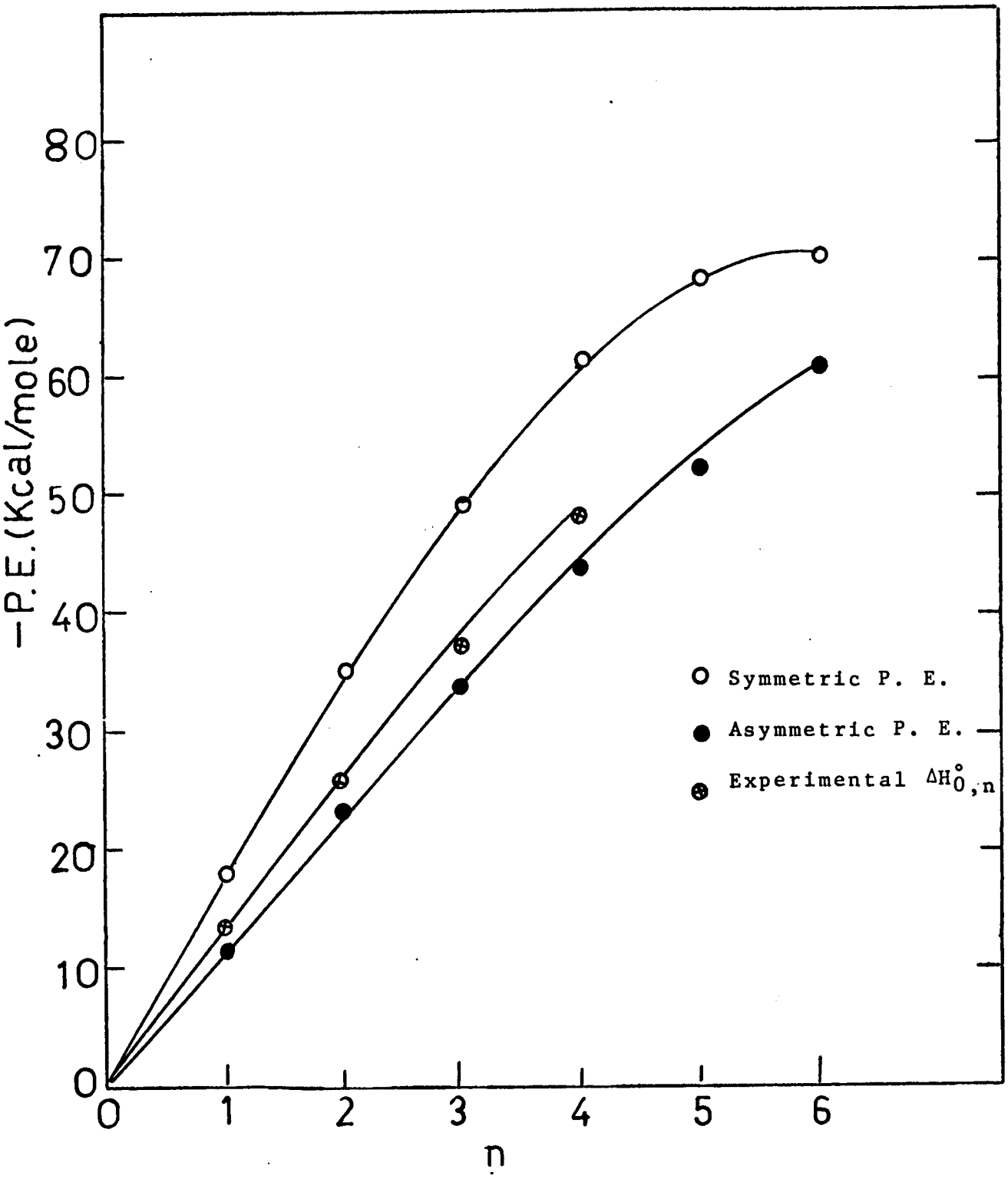

Figure 4-27: Plots of Potential Energy for Cluster $Cl^{-}(H_2O)_n$ Versus n.

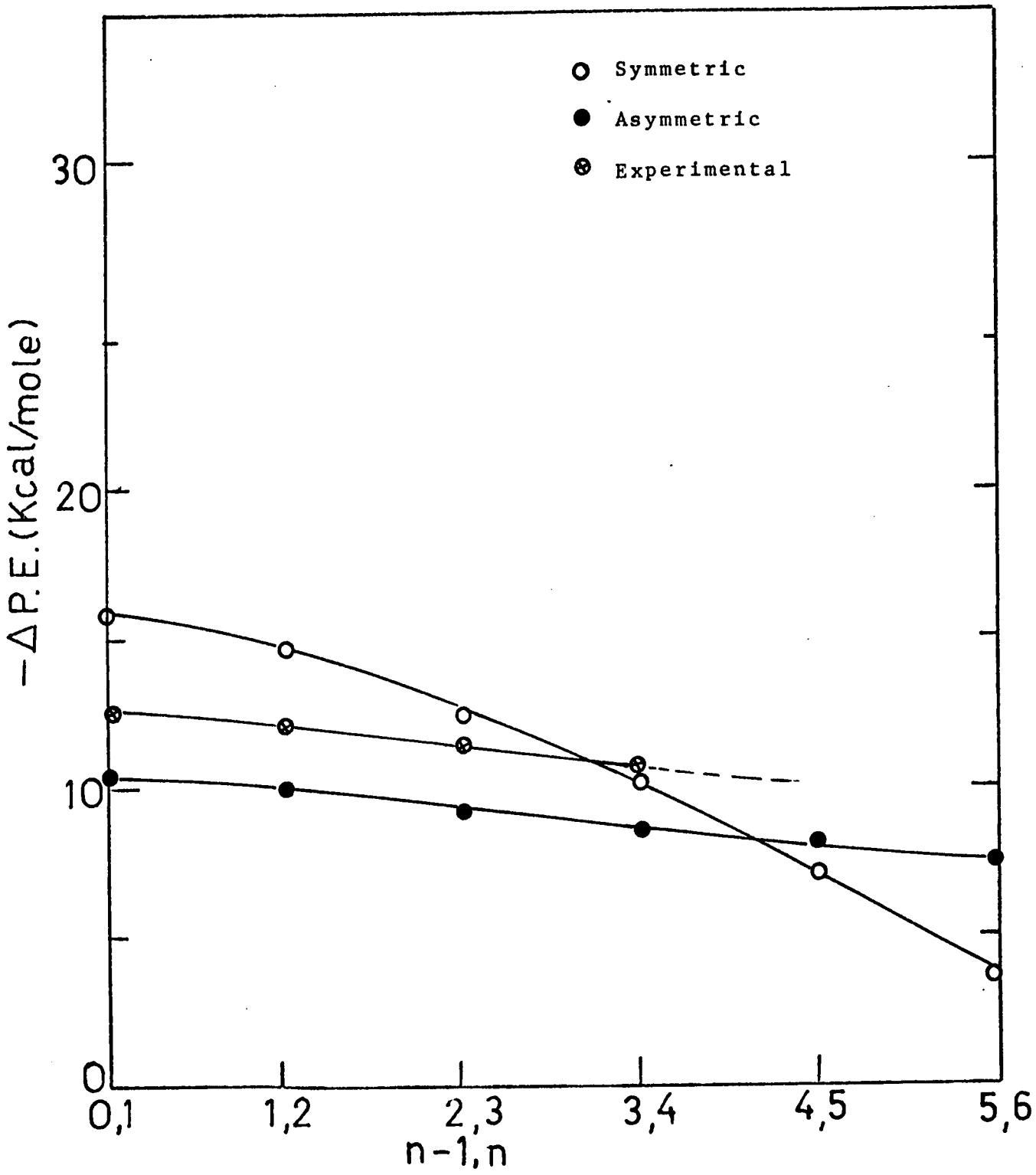

Figure 4-28: Plots of Change of Potential Energy for Cluster $Br^-(H_2O)_{n-1,n}$ Versus n-1,n.

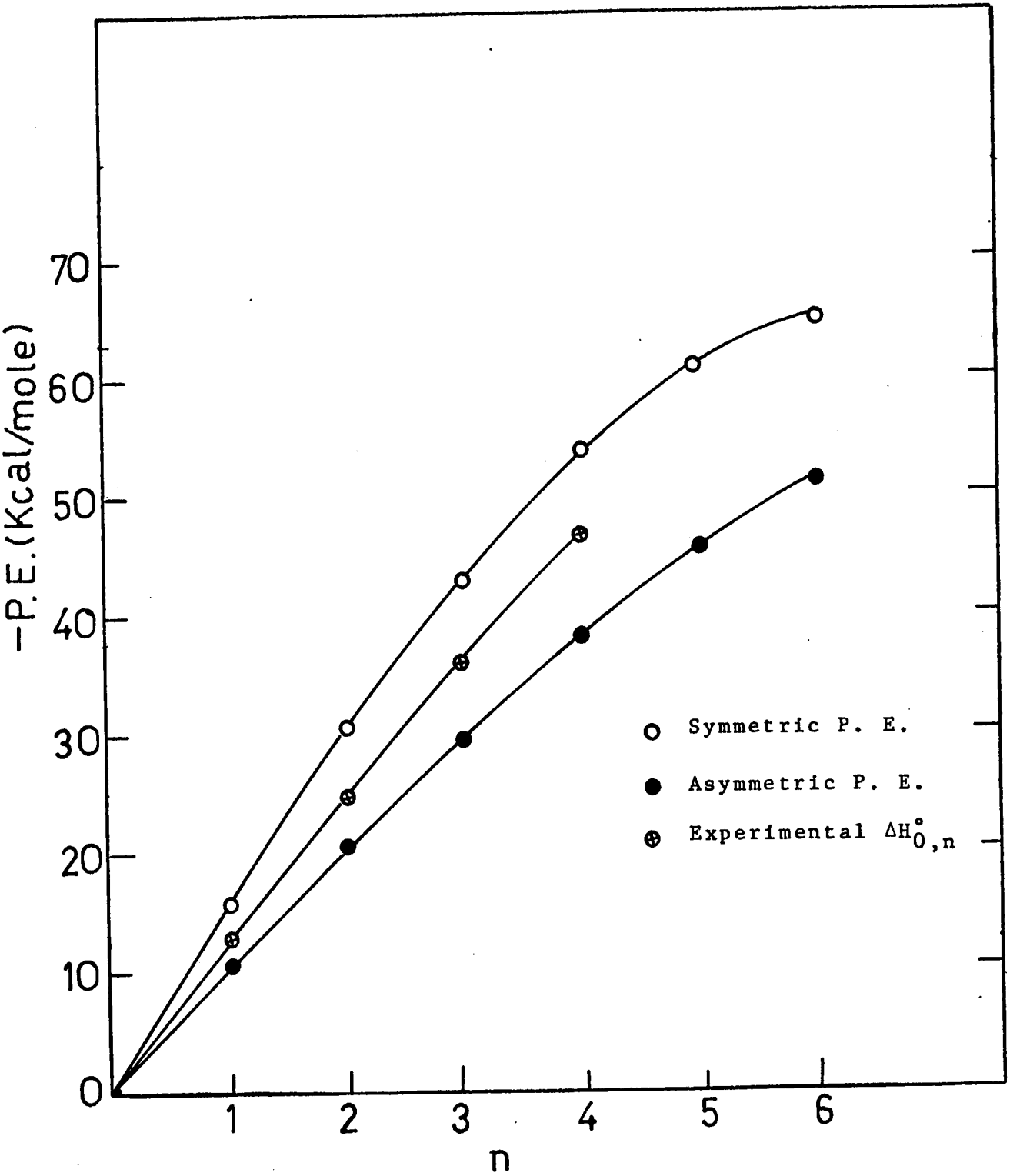

Figure 4-29: Plots of Potential Energy for Cluster $Br^{-}(H_2O)_n$ Versus n.

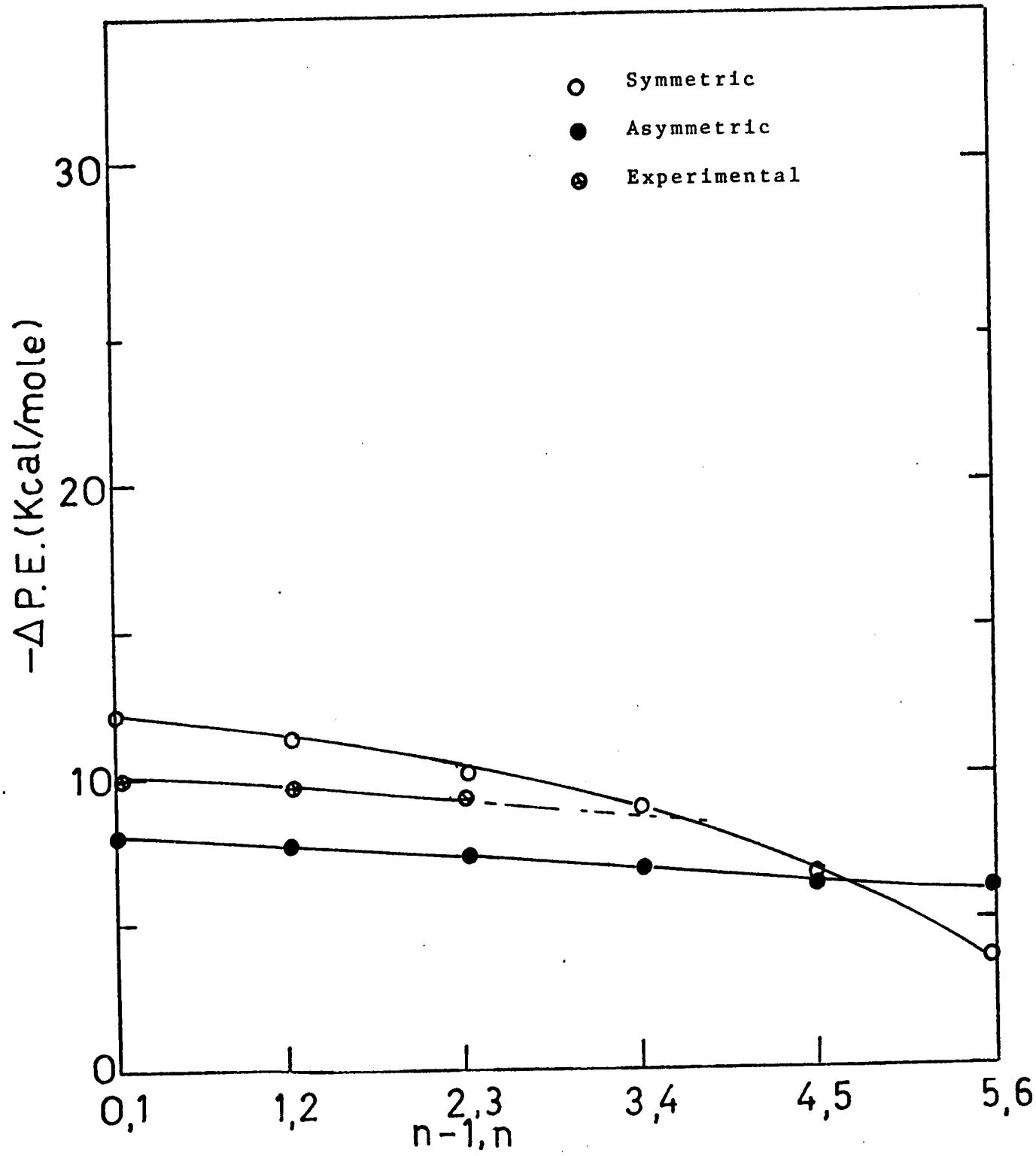

Figure 4-30: Plots of Change of Potential Energy for Cluster $I^-(H_2O)_{n-1,n}$ Versus n-1,n.

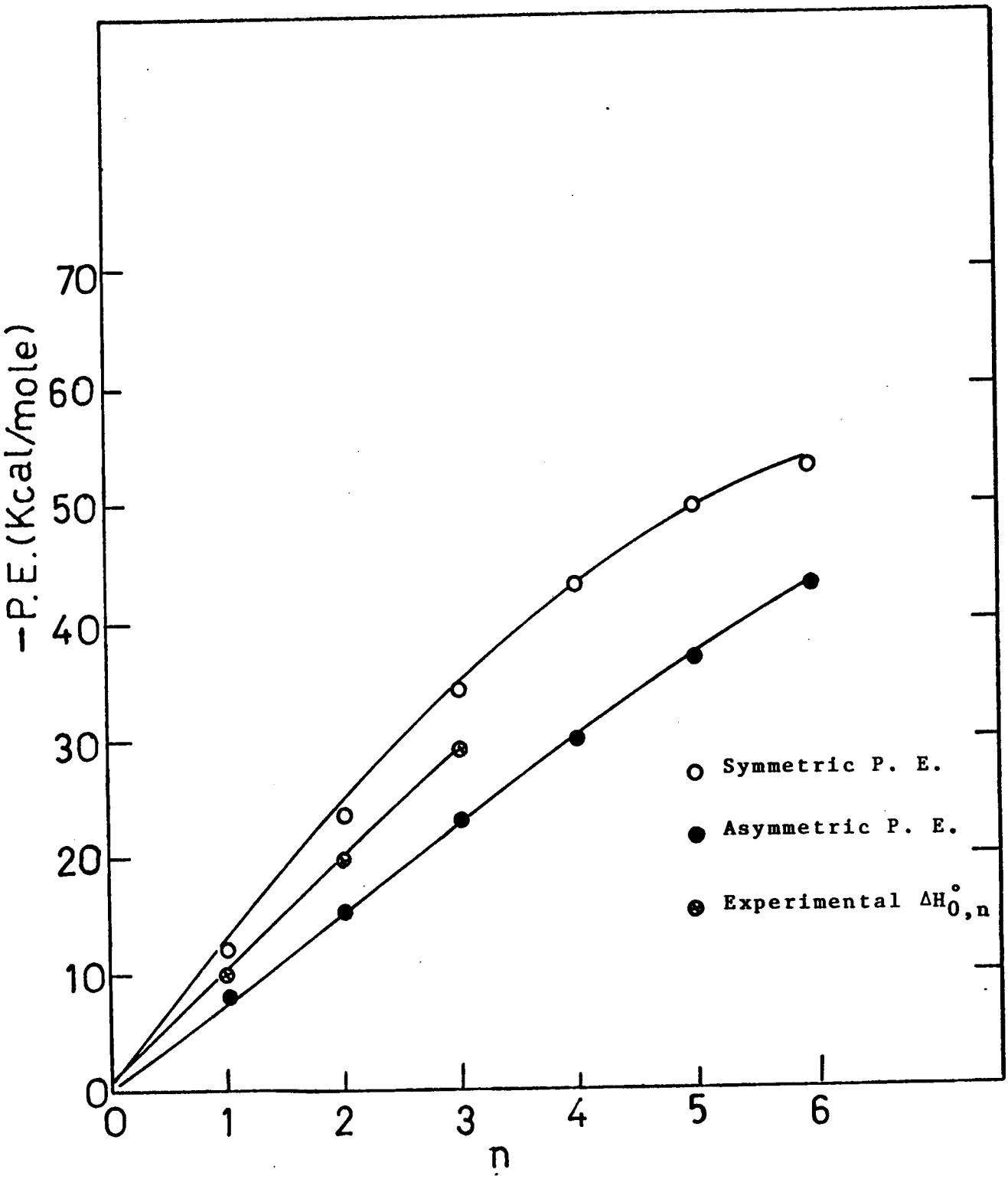

Figure 4-31: Plots of Potential Energy for Cluster $I^{-}(H_2O)_n$ Versus n.

that our experimental values are in error cannot be entirely ruled out, but the internal consistency of the data represented by the Van't Hoff's plots of figures (4-17) to (4-20) makes the existence of an error of 20 to 30% very unlikely. Perhaps the most significant factor contributing to the lack of better agreement between the experimental and calculated values is the method used and the approximations made in the evaluation of the constant "A" in the ion-ligand repulsion term (equation 8-4). Aside from the question of the reliability of method, the uncertainty in the radii of the negative ions, used in evaluating "A" could be a major source of error. To illustrate the effect of the uncertainty of the ionic radii on the ultimate values of $\Delta E_{0,1}$ the ionic radii of Gourary and Adrian were increased by 5% and the total electrostatic energies of the cluster $X^-(H_2O)_n$ were recalculated. The new values of $\Delta E_{0,1}$ for all the halide ions are compared with the old ones in table (4-7). This table shows that a 5% increase in ionic radii will result in a 7.4 to 14% decrease in the absolute value of $\Delta E_{0,1}$. Thus, one may conclude that perhaps the values of the ionic radii used in this calculation are too low. This becomes more obvious when the Na^+ radius obtained by Gourary and Adrian is compared with the atomic radius of neon ($r_{Na^+} = 1.17$ and $r_{Ne} = 1.12$ A°). This of course is not acceptable, and shows that the Gourary and Adrian ionic radii are too low

Table 4-7

Decrease in Absolute Values of $(-\Delta E_{0,1})_{sym}$ as a Result of 5% Increase in Ionic Radii of the Halide Negative Ions

Ion	$(-\Delta E_{0,1})^{**}_{sym.}$ Based on G and A*	$(-\Delta E_{0,1})^{**}_{sym.}$ with 5% increase in r_{ion}	per cent Decrease
F^-	29.8	27.6	7.4
Cl^-	18.6	16.9	9.2
Br^-	16.0	14.3	10.6
I^-	12.3	10.6	14.0

*Reference (47)

**Unit; Kcal/mole

for negative ions and too high for positive ions by approximately 10%.

It has been suggested (71) that the Van der Waals radii should be used, instead of the ionic radii, in electrostatic calculations such as those in this work. It would be of interest, in future studies, to make some calculations similar to the ones which were performed in this work but with values of "A" based on Van der Waals' radii.

In conclusion, it should be emphasized that in view of the approximations which had to be made and the simple models used,the calculated values could only support our experimental results qualitatively.

4.5 Calculation of The Entropy Change $\Delta S^\circ_{0,1}$

The entropy change for a reaction such as

(4-13) $$X^- + H_2O \longrightarrow X^-(H_2O)$$

can be calculated theoretically by means of statistical mechanics. In such calculations, the assumption is made that the change of the entropy can be represented simply as the sum of translational, rotational, and vibration contributions

(4-14) $$\Delta S = \Delta S_t + \Delta S_r + \Delta S_v$$

Each individual part of the right hand side of equation (4-14) is then evaluated separately. The translational

contribution can be calculated from Sackur-Tetrode equation (49). The application of Sackur-Tetrode equation to the chemical reaction represented by equation (4-13) is

$$\Delta S_t = \frac{3}{2} R \ln \frac{M_{X^-(H_2O)}}{(M_{X^-})(M_{H_2O})} - \frac{5}{2} R \ln T + 2.311$$

here $M_{X^-(H_2O)}$, M_{X^-} and M_{H_2O} are molecular weight of $X^-(H_2O)$, X^- and H_2O respectively. T is the absolute temperature in degrees K; the gas constant, R, is taken as 1.987 cal. deg.$^{-1}$; and ΔS_t comes out in entropy units, e.u. The rotational contribution to the entropy of one mole of gas is given (49) by the equation

$$(4\text{-}15) \qquad S^\circ_{rot} = R(\ln Q_{rot} + 1)$$

Q_{rot}, the rotational partition function is

$$(4\text{-}16) \quad Q_{rot} = \frac{(8\ )^{5/2}(KT)^{3/2}(I_x\ I_y\ I_z)^{1/2}}{a\ h^3}$$

where I_x, I_y and I_z are the three moments of interia about the three principal axes and "a" is the symmetry number. When the equation (4-15) is applied to calculate the change of entropy for reaction (4-13), the following equation will be obtained

$$(4\text{-}17) \qquad \Delta S^\circ_{rot} = R \ln \frac{[Q_{rot}]_{X^-(H_2O)}}{[Q_{rot}]_{H_2O}}$$

When the proper values of the partition functions are substituted in equation (4-17) and the appropriate simplification has been made, the ΔS°_{rot} will be

$$(4\text{-}18) \qquad \Delta S^{\circ}_{rot} = \frac{R}{2} \ln \frac{[I_x I_y I_z]_{X^-(H_2O)}}{[I_x I_y I_z]_{.H_2O}}$$

For the evaluation of ΔS°_{rot} from equation (4-18), the moments of inertia of the cluster $X^-(H_2O)$ as well as the moments of inertia of H_2O molecule are required. The moments of inertia of H_2O are (51): $I_x = 1.92$, $I_y = 1.02$ and $I_z = 2.95 \times 10^{-40}$ g-cm^2. The moments of inertia for the cluster $X^-(H_2O)$ are based on the $X^- - OH_2$ equilibrium distances obtained from the electrostatic calculations in the previous section and the bond distances and the bond angle of the water molecule. These moments of inertia as well as the X^-——OH_2 equilibrium distances are given in table (4-8). The moments of inertia of D_2O, used for the calculation of $F^-(D_2O)$ also taken from reference (51), are: I_x=3.81, I_y=1.79 and I_z=5.75 X 10^{-40} g-cm^2. The principal axes of D_2O and $F^-(D_2O)$ used to calculate the moments of inertia are shown in figure (4-32). Similar types of arrangements were used to calculate the moments of inertia of the other halide negative ion clusters $X^-(H_2O)$.

To calculate the vibrational contribution to the entropy change of the reaction (4-9), it was assumed that the fundamental vibrations of water molecule remain the same before and after the formation of the cluster $X^-(H_2O)$. Accordingly, the vibrational entropy change is due to three new vibrations in the complex. These are the stretching vibration along the oxygen, halide ion axis, and two rocking

Talbe 4-8

Moments of Inertia and X^--OH_2 Equilibrium Distances

Cluster	X^--OH_2 Distance A°	$IX10^{40}$ g-cm^2		
		I_x	I_y	I_z
$F^-(D_2O)$	2.320	3.94	80.30	83.24
$Cl^-(H_2O)$	2.810	1.97	149.7	151.7
$Br^-(H_2O)$	2.990	1.97	241.0	243.
$I^-(H_2O)$	3.330	1.97	280.0	282.0

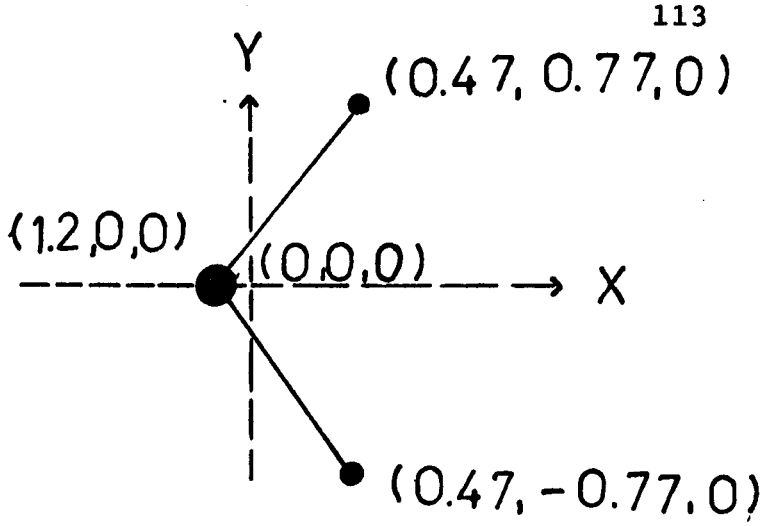

Principal Axes of D_2O. The Z axis is Perpendicular to the Plane of Paper.

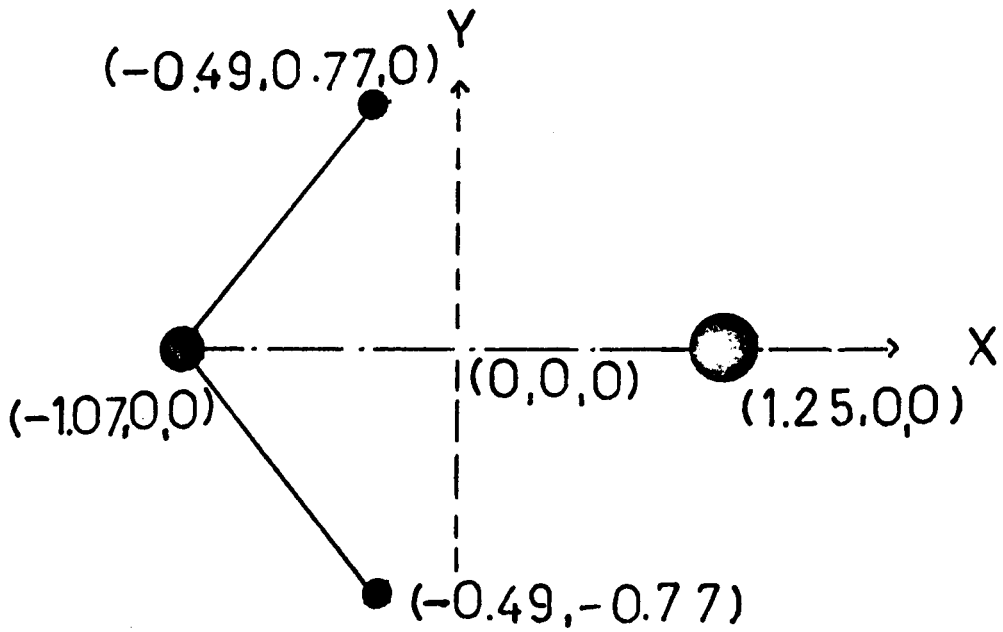

Principal Axes of $F^-(D_2O)$. The Z Axis is perpendicular to the Plane of Paper.

Figure 4-32: Principal Axes of D_2O and $F^-(D_2O)$ used in the Calculation of Moments of Inertia.

vibrations of the water molecule around its centre of mass. One of these rocking vibrations occurs in the plane of the molecule $X^-(H_2O)$, figure (4-34), and the other one perpendicular to this plane.

In the calculation of the stretching vibrational frequency, the water molecule and the negative ion were treated as two mass points. The force constant for this vibration was estimated by fitting an equation of parabola to the bottom portion of the potential energy curves of figure (4-33). These curves were obtained by plotting the total electrostatic potential of the previous section versus water molecule-negative ion distance. The frequency, v then, can be calculated from the equation

$$v = \frac{1}{2\pi} \left(\frac{K}{u}\right)^{1/2}$$

where the u is the reduced mass of water-negative ion system and K is the force constant.

The two rocking vibrational frequencies were obtained by first calculating the total electrostatic potential energy of the complex $X^-(H_2O)$ as a function of angle θ, figure (4-34). Then the equation of a parabola, in the form of (4-19), was fitted to the bottom portion of the potential energy curve as in stretching frequency calculation.

$$E = \frac{1}{2} K_{roc} \theta^2 \qquad (4\text{-}19)$$